ENERGY CONSERVATION

ORNL/Sub/84-05907/1

Preliminary Design of Linear Alternator Dynamometer for Free Piston Stirling Engines

Final Report

FILE COPY
DO NOT
REMOVE

Report Prepared by

ASPEN SYSTEMS, INC.
275 Boston Post Road
Marlborough, MA 01752

under
Subcontract 62X-05907V

for

OAK RIDGE NATIONAL LABORATORY
operated by
MARTIN MARIETTA ENERGY SYSTEMS, INC.
for the

U.S. DEPARTMENT OF ENERGY

OFFICE OF BUILDINGS ENERGY
RESEARCH AND DEVELOPMENT

Printed in the United States of America. Available from
National Technical Information Service
U.S. Department of Commerce
5285 Port Royal Road, Springfield, Virginia 22161
NTIS price codes—Printed Copy: A08 Microfiche A01

This report was prepared as an account of work sponsored by an agency of the United States Government. Neither the United States Government nor any agency thereof, nor any of their employees, makes any warranty, express or implied, or assumes any legal liability or responsibility for the accuracy, completeness, or usefulness of any information, apparatus, product, or process disclosed, or represents that its use would not infringe privately owned rights. Reference herein to any specific commercial product, process, or service by trade name, trademark, manufacturer, or otherwise, does not necessarily constitute or imply its endorsement, recommendation, or favoring by the United States Government or any agency thereof. The views and opinions of authors expressed herein do not necessarily state or reflect those of the United States Government or any agency thereof.

ORNL/Sub/84-05907/1
Dist. Category UC-95d

Preliminary Design of Linear Alternator Dynamometer for Free Piston Stirling Engines

Final Report

Date Published - June 1985

Report Prepared by

K. P. Lee
W. M. Toscano

Aspen Systems, Inc.
275 Boston Post Road
Marlborough, MA 01752

under

Subcontract 62X-05907V

for

Oak Ridge National Laboratory
Oak Ridge, Tennessee 37831
operated by
MARTIN MARIETTA ENERGY SYSTEMS, INC.
for the
U.S. DEPARTMENT OF ENERGY
Under Contract No. DE-AC05-84OR21400

FOREWORD

This Phase I Final Report is prepared by Aspen Systems, Inc. for Oak Ridge National Laboratory. The report presents results of the effort to prepare a preliminary design of a general-purpose linear alternator type dynamometer for Free Piston Stirling Engines.

The work was performed under the following three separate contracts:

ORFMA Oak Ridge, TN	Union Carbide Corp. Subcontract No. ORNL 62X03-4998
L. F. GOLDBERG U. of Minn.	Martin Marietta Energy Systems, Inc. Subcontract No. 11X-39005V
ASPEN SYSTEMS Marlborough, MA	Martin Marietta Energy Systems, Inc. Subcontract No. ORNL 62X-05907V

Professor L. F. Goldberg's work was in the area of control system analysis and design and is reported in Subsection 2.3 and Appendix B.

ABSTRACT

A preliminary design of a linear alternator type dynamometer for testing free piston Stirling engines (FPSE's) in the output power range up to 3.0 kW and operating frequency range of up to 60 Hz is prepared. The purpose of the dynamometer is to provide the FPSE's with simulated loads such as double-acting inertia compressors for heat pumps, hydraulic pumps, and linear alternators.

The dynamometer has two major components: the electromechanical transducer and the control system. The electromechanical transducer consists of a light-weight armature coil tube plunger moving in a permanent magnet field provided by cylindrical magnets made of Samarium Cobalt. The electrical connection to the moving armature coil is accomplished using flexible leads made of thin Beryllium Copper strips on thin high-temperature polyamid ribbons and bent in a U shape.

The dynamometer control system utilizes active force control scheme and consists of a microprocessor based negative feedback control system and the power supply capable of supplying to and absorbing power from the electromechanical transducer. The control system operates in two modes simultaneously: the foreground mode and the background mode. The foreground mode instantaneously regulates the current to the armature coil according to the predetermined load force profile. The background mode continually refines the load force profile and upgrades the foreground mode load force profile until convergence is reached.

The digital simulation of the entire system including the control system, the dynamometer, and the RE-1000 FPSE showed that the dynamometer is capable of simulating various loads very accurately and fast. For example, a convergence within 0.5 percent over the entire cycle was reached within a maximum of 50 engine cycles.

It is expected that experimental investigations of FPSE's operating with the dynamometer simulated loads will help to accurately predict the FPSE's performance characteristics under actual load conditions. The dynamometer would also help to design a more suitable load device for a particular application.

ACKNOWLEDGEMENT

The authors would like to express deep gratitude to Messrs. James L. Crowley (Technical Program Monitor), George T. Privon and Dr. Colin D. West of Oak Ridge National Laboratory for considerable technical and management support.

The authors also acknowledge the technical services of Professors James L. Kirtley, Jr. and Joseph L. Smith, Jr., of the Massachusetts Institute of Technology, Mr. David Gedeon of Gedeon Associates, Ohio, and especially Professor Louis F. Goldberg of the University of Minnesota for his excellent work in the control system design.

TABLE OF CONTENTS

		Page
	FOREWORD	iii
	ABSTRACT	v
	ACKNOWLEDGEMENTS	vii
	TABLE OF CONTENTS	ix
	LIST OF FIGURES	xi
	LIST OF TABLES	xiii
	EXECUTIVE SUMMARY	ES-1
1.	INTRODUCTION	1-1
2.	PRELIMINARY DESIGN OF A LINEAR ALTERNATOR DYNAMOMETER	2-1
	2.1 PRELIMINARY DESIGN PROCESS	2-1
	2.2 ELECTROMECHANICAL TRANSDUCER	2-1
	2.2.1 Preliminary Design Concepts	2-1
	2.2.2 Comparison and Selection	2-6
	2.2.3 Magnetic Field Analysis of the Selected Concept	2-9
	2.2.4 Transducer Preliminary Design	2-13
	2.3 CONTROL SYSTEM DESIGN AND ANALYSIS	2-31
	2.3.1 Preliminary Design Concepts and Selection	2-31
	2.3.2 Selected Control System for the Linear Alternator Dynamometer	2-31
	2.3.3 A Simulation Assessment of the Stability, Accuracy, and Convergence of the Selected Linear Alternator Dynamometer Control System	2-34
	2.4 FREE PISTON STIRLING ENGINE/LOAD ANALYSIS AND SIMULATION	2-50
	2.4.1 Modeling and Simulation of the Double-Acting Inertia Compressor Load	2-51
	2.4.2 Unconstrained Simulation of Compressor and Engine System	2-56
3.	PHASE II COST ESTIMATE	3-1
	3.1 PHASE II PROGRAM PLAN	3-1
	3.2 PHASE II COST ESTIMATE	3-3

TABLE OF CONTENTS (continued)

	Page
4. SUMMARY AND RECOMMENDATIONS	4-1
REFERENCES	REF-1
APPENDIX A - MAGNETIC FIELD ANALYSIS FOR THE LINEAR ALTERNATOR DYNAMOMETER	A-1
APPENDIX B - DIGITAL SIMULATION OF THE CONTROL SYSTEM	B-1
APPENDIX C - DIGITAL SIMULATION OF A DOUBLE-ACTING INERTIA COMPRESSOR AS A LOAD FOR THE RE-1000 FPSE	C-1
APPENDIX D - DESIGN CALCULATIONS	D-1

LIST OF FIGURES

Figure No.	Description	Page
ES.1	Normalized Average Magnetic Flux Density Experienced by the Coil Versus Coil Tube Displacement	ES-6
ES.2	Preliminary Assembly Drawing for the Linear Alternator Dynamometer for Free Piston Stirling Engine	ES-8
ES.3	Block Diagram of the Dynamometer Control System . .	ES-12
ES.4	Schematic of a Double-Acting Inertia Compressor . .	ES-18
ES.5	Phase II Project Schedule	ES-22
2.1	Preliminary Design Process	2-2
2.2	Moving Iron Plunger Reciprocating Transducer . . .	2-4
2.3	Moving Pole Reciprocating Transducer	2-4
2.4	Moving Permanent Magnet Reciprocating Transducer .	2-5
2.5	Moving Field Coil Reciprocating Transducer . . .	2-5
2.6	Moving Armature Coil/Electromagnetic Field Reciprocating Transducer	2-7
2.7	Moving Armature Coil/Permanent Magnet Field Reciprocating Transducer	2-7
2.8	Moving Conductor Ring Reciprocating Transducer . .	2-8
2.9	Normalized Average Magnetic Flux Density Experienced by the Coil Versus Coil Tube Displacement	2-12
2.10	Preliminary Assembly Drawing for the Linear Alternator Dynamometer for Free Piston Stirling Engines	2-14
2.11	Inner Magnet	2-17
2.12	Outer Magnet	2-18
2.13	Inner Iron Cylinder Assembly	2-19
2.14	Outer Iron Cylinder Assembly	2-20
2.15	Lower Mounting Cylinder	2-22
2.16	Non-Magnetic Cap for Iron Cylinders	2-23

LIST OF FIGURES (continued)

Figure No.	Description	Page
2.17	Coil Tube Assembly	2-24
2.18	Center Shaft Assembly	2-25
2.19	Lower Bearing Assembly	2-26
2.20	Upper Bearing Assembly	2-27
2.21	Flexible Connection Ribbon	2-30
2.22	Block Diagram of the Dynamometer Control System . .	2-32
2.23	Schematic of a Double-Acting Inertia Compressor . .	2-52
3.1	Phase II Project Schedule	3-4
A.1	Geometry and Parameter Definitions for the Magnetic Field Analysis	A-2
A.2	Voltage Phasor Diagram	A-6
B.1	Simulation Algorithm Main Routine Flowchart . . .	B-2
B.2	Displacement Driven Integration Subroutine Flowchart	B-5
B.3	Differential Equation Subroutine Flowchart . . .	B-7
C.1	Pressure Versus Piston Position for Compressor Spaces and Gas Springs	C-3
C.2	Gas Temperature Versus Piston Position for Compressor Spaces and Gas Springs	C-4

LIST OF TABLES

Table No.	Description	Page
ES.1	Comparison of Linear Alternator Type Dynamometer Configurations	ES-4
ES.2	Electromechanical Transducer Preliminary Design Summary	ES-7
ES.3	Flexible Electrical Connection Design Summary	ES-10
ES.4	Phase II Cost Estimate	ES-23
2.1	Comparison of Linear Alternator Type Dynamometer Configurations	2-10
2.2	List of Component Drawings	2-15
2.3	Electromechanical Transducer Preliminary Design Summary	2-16
2.4	Flexible Electrical Connection Design Summary	2-28
2.5	Simulation Test Sequence Baseline Parameter Set	2-41
2.6	Dynamometer Simulation Results	2-45
3.1	Phase II Cost Estimate	3-3
3.2	Direct Material Cost Breakdown	3-5
C.1	Double-Acting Inertia Compressor Simulation Summary.	C-2

EXECUTIVE SUMMARY

1. INTRODUCTION

Free Piston Stirling Engines (FPSE's) have many favorable characteristics suitable for energy conversion. These include high reliability, low noise, and expected high energy efficiency for converting thermal energy into mechanical power. The FPSE's power can then be used to drive output devices such as inertia compressors for heat pumps, hydraulic pumps, and linear alternators.

To date, the full commercialization of FPSE's has been advancing slowly. One of the difficulties arises from the close interaction between thermodynamics of the working gas and dynamics of the moving parts. The close intereaction makes it difficult to analyze the performance of FPSE's under various load conditions. The resulting mismatch between a FPSE and the load can render the combined FPSE/Load System unsuitable for the original intended application.

The analytic difficulties and FPSE/Load mismatches can be avoided if one can test the FPSE with a dynamometer that can accurately simulate various load devices before a load device is designed and fabricated.

The objectives of the program are:

- preparation of a preliminary design of a dynamometer for FPSE's capable of detailed simulation of a double-acting inertia piston compressor and other loads;
- preparation of cost estimate for Phase II, Final Engineering Design and Fabrication of Prototype Linear Alternator Dynamometer.

The design requirements are the following:

- Compatibility with RE-1000 FPSE (manufactured by Sunpower, Inc., Ohio) - no changes in the engine working gas space should be required.
- Load simulation capacity - 0.5 ~ 3.0 kW
- Engine Frequency - up to 60 Hz
- Power piston stroke - up to 5 cm peak to peak.

2. PRELIMINARY DESIGN OF A LINEAR ALTERNATOR DYNAMOMETER

In this section, candidate dynamometer systems are investigated and selected. Necessary design effort and analyses are performed for the preliminary design.

2.1 Preliminary Design Process

There are two major components of a linear alternator dynamometer system: electromechanical transducer and control system. The elctro-mechanical transducer generally consists of an armature coil, a stator, and other structural elements. The control system generally consists of switching devices, microprocessors, power supplies, and instrumentation.

The approach taken for the Preliminary Design Process is as follows. First, preliminary design concepts for the electromechanical transducer and the control system are generated. These design concepts are then investi-gated and compared with one another in order to select the best concepts for the particular application. Once the design concepts are selected, the effort is subdivided into three areas:

- Electromechanical Transducer Analysis and Design
- Dynamics and Thermodynamics Analyses of FPSE/LOAD, and
- Control System Design and Analysis.

Finally, the design integration of the elctromechanical transducer, control system, and RE-1000 FPSE is performed.

2.2 Electromechanical Transducer

In this section, seven preliminary design concepts for the Electromechanical Transducer for the dynamometer are compared with one another. A moving armature coil type with a permanent magnet field proves to be the most suitable for the dynamometer. A detailed magnetic field analysis is performed to arrive at a transducer preliminary design.

2.2.1 Preliminary Design Concepts

Candidate configurations of linear motion electromechanical transducers include the following:

a. moving iron plunger (stationary armature and field coils)

b. stationary iron core (moving pole plunger, stationary armature and field coils)

c. moving permanent magnet (stationary armature and field coils)

d. moving field coil plunger (stationary armature coil)

e. moving armature coil plunger (stationary electromagnet field)

f. moving armature coil plunger (stationary permanent magnet field)

g. moving conductor ring (stationary armature and field coil).

Each of these candidate configurations has advantages and disadvantages for the proposed dynamometer application.

Comparison and Selection

The important selection criteria for a linear alternator dynamometer transducer include low mass, low reactance, and low internal losses, such as magnetic hysterises loss, eddy current loss, and flux leakage loss.

Table ES.1 summarizes the relevant characteristics of the various types of the electromechanical transducers for the dynamometer. The moving iron plunger and the moving field coil configurations are eliminated from further consideration due to the heavy plunger mass. The stationary iron core/moving pole configuration was eliminated due to its relatively high reactance and the difficulty of analyzing its internal losses. The moving permanent magnet required a relatively heavy plunger mass and was eliminated. The moving conductor ring configuration has a favorable combination of characteristics except that its internal losses and magnet field are relatively difficult to analyze.

Of the remaining two moving armature coil configurations, the one with the electromagnet field was discarded because the iron core magnetic saturation will make the overall dynamometer size larger and the plunger mass heavier than the one with the permanent magnet field.

The moving armature coil with permanent magnet field was the best choice of the seven configurations. It has the following salient characteristics:

- the lowest reciprocating mass,
- the lowest dynamometer reactance,
- almost uniform magnetic field, which is easy to analyze,
- very low internal losses due to eddy current, flux leakage, and almost no magnetic hysteresis loss due to nearly constant magnetic field,
- very close to a linear electromechanical transducer, which is easy to analyze and model,
- reasonably high power density, and
- the flexible electrical connection, required in this configuration, can easily be designed.

Table ES.1: Comparison of Linear Alternator Type Dynamometer Configurations

Linear Alternator Dynamometer Configuration	Plunger Mass	Internal Losses (very low and easy to analyze)	Alternator Reactance	Magnetic Field Strength Control	Flexible Connection Required	Recommendation
Moving Iron Plunger	Heavy	No	High	Yes	No	No
Stationary Iron Core/ Moving Pole	Light	No	High	Yes	No	No
Moving Permanent Magnet	Light	Yes	Very Low	NO	No	No
Moving Field Coil	Heavy	No	High	Yes	Yes	No
Moving Armature Coil/ Electromagnet Field	Very Light	Yes	Very Low	Yes	Yes	No
Moving Armature Coil/ Permanent Magnet Field	Extremely Light	Yes	Very Low	No	Yes	Yes
Moving Conductor Ring	Very Light	No	Moderate	Yes	No	No

Magnetic Field Analysis

A three-dimensional magnetic field analysis was performed for the selected design concept. The magnetic field analysis is presented in detail in Appendix A.

The electromagnetic force exerted on a circumferentially wound coil of length l, carrying a current i, and moving axially in a concentric gap with radial magnetic flux of density B, is given by

$$F = B\,i\,l \tag{2-1}$$

In order to design a dynamometer with accurate force simulation capability, the above relationship has to be known accurately. In particular, the distribution of the magnetic flux density along the axial travel length of the coils is of primary interest.

Figure ES.1 illustrates the normalized average magnetic flux density, B_{av}, predicted by the magnetic analysis, as a function of the coil tube location. It shows that the coils, averaged over the axial length of the windings, experience nearly constant magnetic field along the travel distance. It is only at the maximum travel positions of coils (2.5 cm from the midstroke position) that there is an appreciable drop of approximately 5.8 percent in magnetic flux density. It is shown that as long as the coil tube travels within 75 percent of the maximum allowable stroke, the force exerted on the coil tube will be directly proportional to the current, i. The near linear force-current relationship is advantageous in achieving an accurate force simulation.

Based on the above magnetic analysis, a Magnetic Field Analysis Computer program was written to assist in the preliminary design of the dynamometer. The listing of this computer program is given in Appendix A. The input variables include: magnet characteristics, number of poles, overall dimensions of coil tube, air gap distance, coil dimensions, operating frequency, stroke, etc. The output of the program gives power, peak force, power dissipation, voltage, current required, etc. The program can be run interactively. A preliminary design obtained using the program for an electromechanical transducer is summarized in Table ES.2. The average power rating and operating points are 3kW, 30 Hz, and 5 cm, respectively.

Transducer Preliminary Design

Figure ES.2 represents a schematic of the preliminary design of the selected electromechanical transducer. The design shown is the culmination of a design effort that included a detailed magnetic field analysis described in Section 2.2.3, and summarized in Table ES.2. Brief discussions on salient features of the preliminary design are given below.

The coils are carried on an epoxy tube and located between the two rows of concentric permanent magnets. The magnets, made of Samarium Cobalt, are arranged in a four-pole configuration with the magnetic flux alternating radially outward and inward. There are also two sets of half-length magnets at both ends. The end magnets provide one of the two magnetic return paths for the adjacent full-length magnets in order to reduce the thickness of the

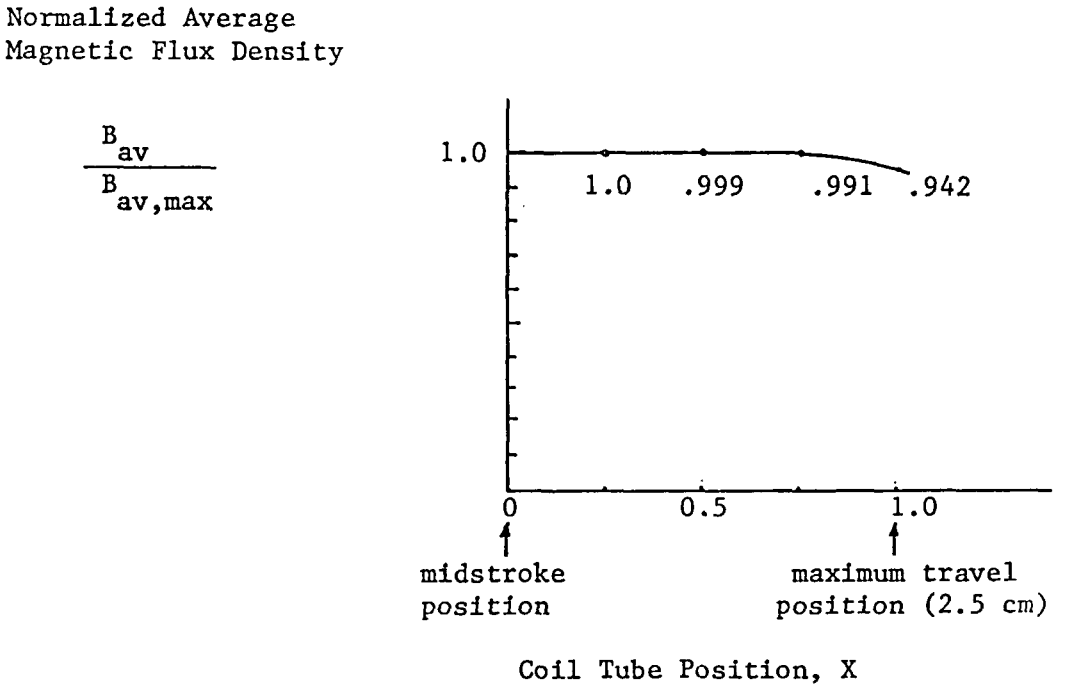

Figure ES.1: Normalized Average Magnetic Flux Density Experienced by the Coil Versus Coil Tube Displacement

Table ES.2: Electromechanical Transducer Preliminary Design Summary

	Value	Input/Output
Operating Point		
Frequency	30 Hz	I
Stroke	5 cm	I
Rating		
Average Power	2999 W	O
Peak Force	3440 N	O
Mechanical Power Factor	0.37	I
Dissipation	845 W	O
Voltage	127 V	O
Current	133 A	O
Coil (Copper)		
Resistance	0.0954 Ohms	O
Reactive Impedance	0.000196 Ohms	O
Number of Pole Pairs	2	I
Space Factor	0.6	I
Temperature Rise	31 C	O
Magnets (Samarium Cobalt)		
Residual Flux Density	1.05 T	I
Working Flux Density	0.72 T	O
Dimensions & Weights		
Inner Iron Cylinder	37.3 kg	O
Outer Iron Cylinder	37.3 kg	O
Coils	1.8 kg	O
Magnets	21.4 kg	O
Coil Tube	0.411 kg	O
Pressure Vessel	22 cm (i.d.)	
	125 cm (length)	I
Air Gap	0.1 cm	I

LEGEND:
1. Inner Magnets
2. Outer Magnets
3. Inner Iron Cylinder
4. Outer Iron Cylinder
5. Lower Mounting Cylinder
6. Non-Magnetic Support for Iron Cylinders
7. Coil Tube Assembly
8. Center Shaft Assembly
9. Lower Bearing Assembly
10. Upper Bearing Assembly
11. Flexible Connection Ribbon

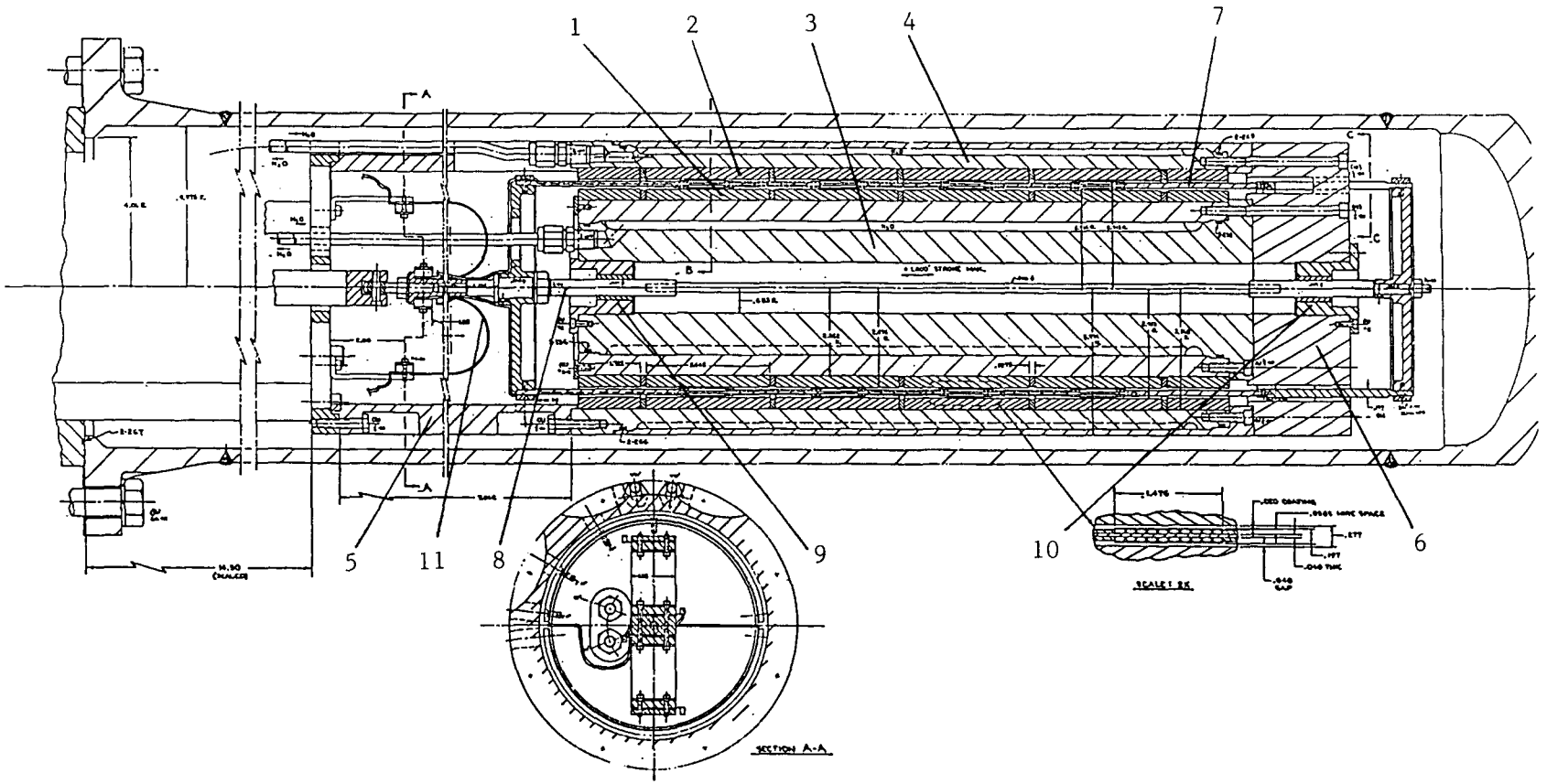

Figure ES.2: Preliminary Assembly Drawing for Linear Alternator Dynamometer for Free Piston Stirling Engines

iron cylinders. The length of the magnets is designed to allow the maximum stroke requirement of 5 cm.

There are two iron cylinders that make up the magnetic return circuit: the inner iron cylinder and the outer iron cylinder. The inner and outer iron cylinders also have water coolant passages to remove the heat from the coil.

The major structure of the moving coil assembly is the tube of fiber-reinforced epoxy. The coils are to be bonded to the tube using an impregnation process to ensure a tight bond.

The lower rim of the epoxy tube is inserted into the groove of the lower disk and fastened by screws. The lower disk is connected to the engine piston via rod end bearings and force transducer. The upper rim of the epoxy tube is reinforced by a stainless steel ring with a circumferential groove for holding and fastening the tube. The ring has six legs that are attached to the upper disk. The six legs move back and forth inside six slots in the non-magnetic cap. These legs support the plastic tube in the radial direction.

The lower disk and the upper disk are connected by the center shaft assembly. At both ends of the center shaft, there are clearance bearings and positive stop dampers made of nylon blocks.

The coil winding direction at the four pole locations alternates from right helix to left helix. The alternately wound coils move between the alternately arranged magnets. This makes forces acting on the individual coils point in the same direction; the total force is the algebraic sum of all the forces.

There are two flexible connections to be made to the moving coil: one to the lead wire for the four coil windings glued to the inside of the epoxy tube, and the other to the lead wire for the four coil windings glued to the outside of the epoxy tube. The electrical connections are accomplished using flexible leads specifically designed for this purpose.

Table ES.3 presents the design summary. The flexible leads are made of 0.1 mm thick, 2.5 mm wide, 15.6 cm long Beryllium copper strips glued to 0.075 mm thick, 3.18 cm wide, 18.14 cm long ribbons of high-temperature, high-strength polyamid. As shown in Figure ES.2, these flexible leads are bent in U shape, with a half circle in the middle, one flat section attached to the stationary post, the other flat section attached to the plunger rod.

Beryllium Copper has a moderate electrical resistivity. At 133 A peak current in the flexible connections, Joulean heating loss is 60 Watts. The maximum allowable strip tempereature is about 200 C, which is the temperature limit imposed by the glue used to attach Beryllium Copper strips to the polyamid ribbon. The metal strips will experience heat transfer with the ambient gas. The temperature of the metal strips will not be more than 68 C above the ambient helium gas temperature.

Table ES.3: Flexible Electrical Connection Design Summary

Shape	Thin Metal Strips Glued on Polyamid Ribbon Bent in a U Shape
Number of Ribbons	2
Overall Size of Ribbons	0.075 mm Thick, 3.18 cm Wide, 18.14 cm Long
Mean Radius of Circular Section	2.54 cm
Electrical Conductors	
Material	Beryllium Copper
Dimension	0.1 mm Thick, 2.5 mm Wide, 15.6 cm Long
Number	20 (10 for each side)
Resistance	0.00395 Ohms
Buckling Stress	738 MPa
Yield Point	965 MPa
Endurance Stress	276 MPa
Maximum Bending Stress	258 MPa
Maximum Dynamic and Fluid Dynamic Stress	4 MPa
Maximum Operating Stress	262 MPa
Heat Dissipation	60 Watts at 133 A Peak Current
Temperature Rise	Less Than 68 Degrees C Above Helium Gas Temperature
Maximum Allowable Strip Temperature	200 Degrees C (Limited by the Glue Used to Attach Metal Strips to the Polyamid Ribbon)

Beryllium Copper is a precipitation hardening alloy and is often used in bellows construction. It has excellent strength characteristics: yield point stress of 965 MPa and endurance stress of 276 MPa. Because the metal strips are very thin and narrow, the dynamic stress, of 3.7 MPa, due to the inertia of the metal strips, is quite negligible. The buckling stress for the flat section of the metal strips is about 738 MPa.

The maximum operating stress is designed below the endurance stress of 276 MPa. With the moderate temperature rise of 68C and the relatively low operating stress, the flexible leads are expected to endure indefinitely.

2.3 Control System Design and Analysis

In this subsection, preliminary design concepts of the control system for the linear alternator dynamometer are investigated. A Control System based on the Active Force Simulation is selected for its predicted simulation accuracy and flexibility in simulating various load forces. The algorithm for the dynamometer control system is described by block diagrams. The control system is digitally simulated to demonstrate its fast convergence and accurate load simulation capability.

2.3.1 Preliminary Design Concepts and Selection

Two methods of load force simulation were examined: Passive Force Simulation and Active Force Simulation

Passive Force Simulation

In Passive Force Simulation, load forces are simulated by connecting passive electrical elements, such as resistance, inductance, and capacitance, to the transducer output terminals. In order to simulate complicated load forces, this method will require a "library" of force elements to be switched on or off and probably to be modulated at the same time. This probably requires a microprocessor-based control system.

Active Force Simulation

In Active Force Simulation, load forces are simulated by modulating the transducer terminal current. The current will be supplied by a power supply that can supply power and absorb power. The control system will definitely be based on microprocessors. The control system algorithm will contain the digital simulation of different load forces.

Of the two force simulation concepts, the Active Force Simulation method was selected for its perceived advantages in simulation accuracy and versatility.

2.3.2 Selected Control System for the Linear Alternator Dynamometer

In Figure ES.3 is presented the block diagram of the dynamometer control system based on the Active Force Simulation principle.

The control system operates in two modes simultaneously: the foreground mode and the background mode. In the foreground mode, the current cycle table in the Control D/A Converter sends the control voltage to the power supply. The power supply, in turn, supplies the corresponding current to the dynamometer. There is no computation requirement in this mode, and the current cycle block simply sends out prescribed control voltage corresponding to the displacement communicated by the address bus. Therefore, there is practically no time delay in the dynamometer force simulation operating in the foreground mode.

While the dynamometer simulates FPSE load forces using the foreground mode, in the background mode, the load device characteristics block calculates the force desired corresponding to the updated stored acceleration, velocity,

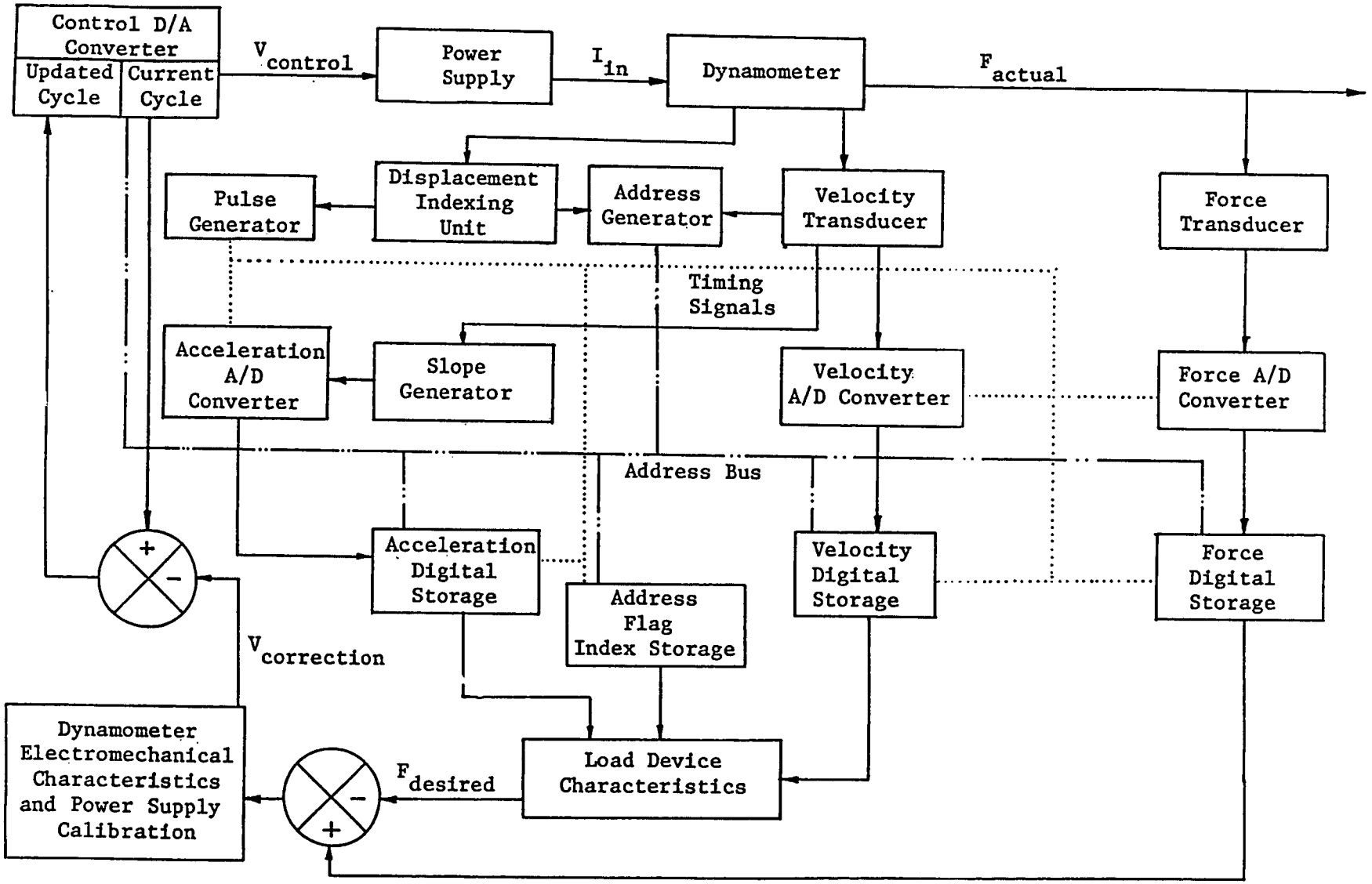

Figure ES.3: Block Diagram of the Dynamometer Control System

and address flag index. The calculated desired force profile, $F_{desired}$, is compared with the stored force profile in the force digital storage. The resulting force correction signal is transmitted to the block called "dynamometer electromechanical characteristics and power supply calibration," which in turn generates voltage correction information $V_{correction}$. $V_{correction}$ is then applied to the control voltage profile in Current Cycle Table of the Control D/A Converter to generate the Updated Cycle Table.

When the updating is completed, the updated force values will be transferred to "current cycle" to be used in the foreground mode. A new updating process will begin in the background mode. The updating process will continue until the FPSE/Dynamometer system reaches a converged state.

The convergence characteristics of the control system described above will be digitally simulated in Section 2.3.3.

2.3.3 A Simulation Assessment of the Stability, Accuracy, and Convergence of the Selected Linear Alternator Dynamometer Control System

2.3.3.1 Objectives

The objectives of the assessment of the linear alternator dynamometer (LAD) and its control system are as follows:

a. To determine whether the control system is convergent and, if not, what modifications are necessary to achieve convergence.

b. To investigate the effect (if any) of various strategies for dealing with under- and over-stroking occurring as a result of dynamic changes in the load/displacement profile.

c. To determine the minimum resolution of the displacement indexing unit necessary for convergence (that is, the number of pulses per unit length).

d. To check the control system convergence for a variety of arabitrary driving and loading devices in any combination.

2.3.3.2 Research Approach

In order to fully meet the specified objectives, the dynamometer and its control system need to be tested in a realistic engine operating environment.

The only suitable method of providing a realistic simulation environment is to implement a coupled dynamic/gas dynamic simulation of the RE-1000 free piston Stirling engine in which all the dynamic characteristics (frequency, amplitude, and phase angle) are treated as dependent variables.

A completely stable and convergent algorithm for simulating a free piston Stirling engine as a combined dynamic/gas dynamic system with arbitrarily complex mathematical descriptions of the dynamics and gas dynamics has been developed and validated. This algorithm provides the physically realistic representation of a free piston Stirling engine which enables the

dynamometer and its control system to be tested in such a way that the stated objectives may be met.

2.3.3.3 Engine Stability Considerations

Within the context of the combined dynamic/gas dynamic simulation algorithm, there is complete freedom to choose any model to represent the gas dynamics of the engine. Due to budgetary and temporal constraints of this project, the choice of models were limited to either an assumption of isothermal or adiabatic working spaces coupled to an isothermal heat exchanger assembly. Neither method has a clear advantage from a stability perspective and, hence, the isothermal model is chosen owing to its greater simplicity and ease of programming.

An engine which has theoretically isothermal working spaces has an extremely narrow stability bandwidth. Although the isothermal engine model used as the simulation test bench for evaluating the dynamometer does not possess the stability band of a real engine, the model provides a completely adequate test environment. Not only does the engine model fall within the definition of the "arbitrary" driving device specified, but also it results in a more severe operating environment for the dynamometer than can be reasonably expected in reality. Hence, the findings and conclusions with regard to the dynamometer convergence, stability, and accuracy apply without qualification to any likely free piston Stirling engine operating environment.

2.3.3.4 Overstroke Control

There are two prime reasons to be concerned with over-stroking in particular. These are:

- to prevent physical damage to the engine and dynamometer, and
- to accelerate the convergence process.

After some investigation, it was realized that the implementation of piston over-stroke control via the dynamometer control system is irreconcilable in rigorous terms with the goal of having the dynamometer duplicate the characteristics of any desired loading as accurately as possible. The introduction of this piston over-stroke control results in predictable hunting as the control system begins to converge to a set of currents corresponding to the over-stroke control load and then switches to converging towards the desired load currents. Hence, it is concluded that over-stroke control should be completely excluded from the dynamometer control loop.

2.3.3.5 Discussion of Results

During the course of the investigation into the performance of the dynamometer and its control system, several dozen simulation runs were performed.

When viewed as a whole, the simulation runs performed demonstrate the convergence, stability, and accuracy of the dynamometer control system without the incorporation of any over-stroke control mechanisms. The dynamometer armature currents required were at most 50A, well below the capability of the

power supply, 150A. This leaves considerable room for applying much greater loads to the engine. In all cases, convergence at the 0.5 percent error level is achieved within 50 machine cycles at a nominal 30 Hz. This corresponds to a real convergence time of two seconds using a control computer that can complete the armature current updating process within 30 ms which is within the capabilities of an IBM Personal Computer.

2.3.3.6 Findings and Conclusions

a. Conclusions about the dynamometer control system stability may only be inferred from the dynamometer/free piston Stirling engine system behavior if the engine itself is known to be stable when subjected to the desired loading.

b. A free piston Stirling engine modelled with isothermal working spaces has a narrow stability band in comparison with the broad stability band of an actual engine. Hence, if the control system exhibits stability and convergence under such conditions, it will also exhibit similar properties in less severe conditions. Therefore, use of the isothermal engine model provides an adequate simulation environment to test the dynamometer control system stability and convergence.

c. The dynamometer control system is capable of tracking intra- and extra-cyclic transient load changes such that the convergence process may be executed continuously without the necessity of waiting for intermediate equilibrium to be reached.

d. Precise knowledge of the dynamometer armature dynamic and electrical characteristics as well as the power supply calibration is not required, as the control system automatically compensates for all the effects.

e. Displacer over-stroke control cannot be implemented without reducing the accuracy of the system in duplicating the desired loading characteristics.

f. When the dynamometer is coupled to engines with a broad stability band, which typify real hardware, the convergence and accuracy of the control system would in all probability make the piston over-stroke control redundant.

g. In the operating environment of an isothermal engine, piston over-stroke control strategies were demonstrated to be ineffective. Such strategies caused the rate of convergence to be significantly reduced.

h. In the operating environment of an isothermal engine, piston over-stroke control strategies based upon the imposition of arbitrary end stroke load profiles which are unrelated to the characteristics of the desired load prevent convergence from being achieved due to inherent feedback instability.

i. Piston over-stroke control is optimally implemented by incorporating dashpot dampers or similar mechanical devices into the dynamometer hardware.

j. Explicit piston under-stroke control is unnecessary as it is implemented by the negative feedback process.

k. Using a nominal Sunpower RE-1000 free piston Stirling engine configuration parameter set, the simulated dynamometer/engine system exhibited the following performance:

   - The maximum force error over an entire cycle at convergence is less than 0.5 percent.

   - Convergence at the 0.5 percent maximum force error level is obtained within a maximum of 50 machine cycles from rest over the test sequence, with a mode convergence being attained in the range of 27 to 33 machine cycles.

   - The maximum armature driving currents required are below 50 A, well below the dynamometer capability.

l. During the test sequence, convergence was achieved for an overall control system resolution within the range of 200 to 331 points over a piston stroke of 42 mm. Higher resolutions are thus not necessary.

In summary, it may be concluded that all the stipulated objectives have been met and that the convergence, stability, and accuracy of the dynamometer control system have been demonstrated for a variety of arbitrary loading devices when coupled to a representative arbitrary free piston Stirling engine driving device.

2.3.3.7 Recommendations

The computer program embodying the simulation of the free piston Stirling engine and dynamometer together with the control system serves as a dynamic blueprint for any hardware design before transformed into actual hardware.

In order to confirm the piston over-stroking behavior, the simulation program should be modified to include an engine gas dynamic model incorporating momentum in the working spaces.

The high order of convergence, stability, and accuracy exhibited by the simulated control system indicates that the control system will work satisfactorily in practice. Hence, further development of the linear alternator dynamometer may be undertaken with confidence.

2.4 Free Piston Stirling Engine/Load Analysis and Simulation

This subsection describes supporting thermodynamic/dynamic analyses for the design of a linear alternator dynamometer. The analyses include:

a. A FPSE load model, specifically a double acting inertia compressor,

b. A simulation of double-acting inertia compressor with a prescribed housing motion, and

c. A combined simulation of the RE-1000 FPSE and the double-acting inertia compressor load.

2.4.1 Modeling and Simulation of the Double-Acting Inertia Compressor Load

The FPSE load device that the linear alternator dynamometer is primarily designed to simulate is a double-acting inertia compressor for heat pump applications [1]. The term "inertia compressor" indicates that the compressor has a reciprocating housing and an almost stationary heavy inertia piston inside.

Figure ES.4 represents a schematic of a double-acting inertia compressor. The housing and the power piston of a FPSE (not shown) attached together reciprocate as a unit. The inertia piston consists of two piston disks connected by a piston rod. The housing and the two piston disks of the inertia piston form the two compressor spaces. The space between the two piston disks are separated into two gas spring spaces by a dividing wall. The dividing wall has a hole at the center to accommodate the reciprocating rod of the inertia piston.

The compressor spaces have check valves for suction and discharge. In order to prevent the drifting of the mean position of the inertia piston relative to the housing, the centering port is provided as indicated in the dividing wall and the piston rod.

Based on the schematic for a Double Acting Inertia Compressor shown in Figure ES.4, a computer program was written to simulate the operation of the compressor given, as input, the housing motion specified as a truncated Fourier series. Terms up to the third harmonic are included in the specification of housing motion.

The simulation problem was set up as a system of differential equations evolving in time. Pressure (P) and Density (r) of the compressor and gas spring chambers along with inertia piston position and velocity were the solved variables in the system. Equations of continuity and energy were used to specify the time derivatives of P and r in the four Freon spaces. Equations of continuity and energy applied to each of the four spaces, together with Newton's equations of motion for the inertia piston, comprise the differential equation system for the simulation. The compressor model also included the following: cylinder heat transfer, gas spring power loss, leakages between chanbers, compressor piston-housing collision, etc.

<u>Validations</u>

A Fortran program was written based on the preceding model for the double-acting inertia compressor. The listing of the program is in Appendix C.

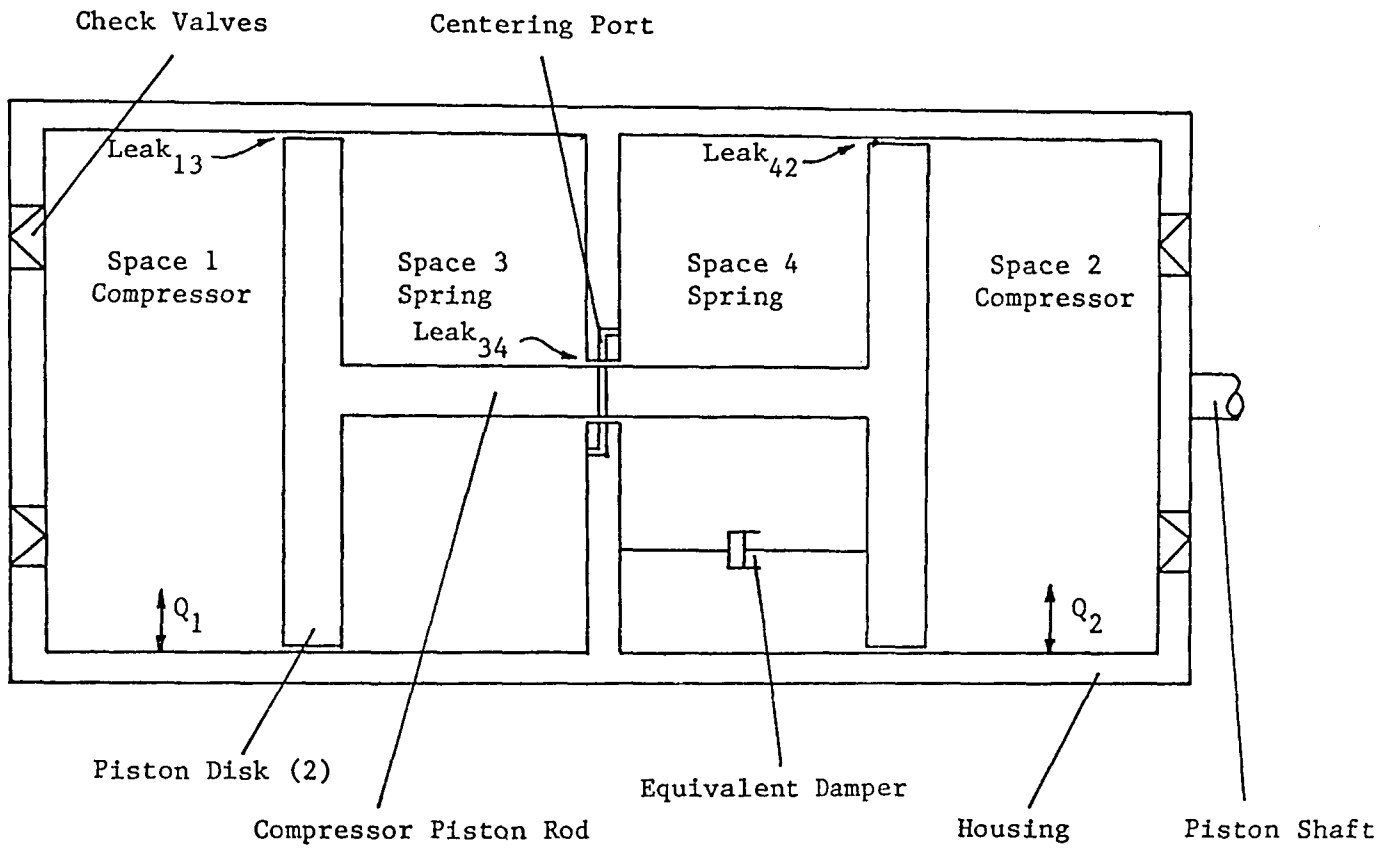

Figure ES.4: Schematic of a Double-Acting Inertia Compressor

The first test of the simulation program was to set it up to duplicate an idealized Freon compressor (based on adiabatic analysis) by setting the cylinder heat transfer to zero, using large area valves, and setting leak gaps to zero. The simulation results were compared to those expected from idealized adiabatic compressor analysis. The Fourier decomposition of the pressure waves in the compression spaces agreed with the adiabatic model quite closely. The resultant PV power absorbed was also in good agreement. The adiabatic temperature rise in the compressor cylinders also matched the theoretical values. In the spring spaces, the pressure changes were nearly those for a simple adiabatic gas spring with no leakage.

Additional tests were done to check the accuracy of some of the non-ideal components of the simulation model. They are the following:

- The heat transfer coefficients in the compressor cylinders were increased to extremely large values. As was expected, the gas temperatures in those spaces became nearly isothermal.

- The subroutines which predict leak and valve flow rates were independently checked for accuracy using several combinations of pressure ratios and relative seal velocities.

- A large interspring leak was simulated as a model for centering port. The pressure amplitudes decreased and PV losses increased in the spring spaces.

Compressor Simulations

Once the simulation model had been debugged and validated, it was necessary to define and model a more realistic compressor, sized to the Sunpower RE-1000 free piston Stirling engine. Realistic leak geometries, valve areas, and heat transfer coefficients were determined. The relative amplitude of the inertia piston with respect to the housing was arbitrarily chosen to be the same as the absolute amplitude of the housing (2.0E-2 m). After experimenting with the gas spring stiffnesses and inertia piston mass, it was possible to achieve an operating mode which matched the power output of the RE-1000 at the operating frequency and stroke. The input data and output results of this simulation are included in Appendix C.

2.4.2 Unconstrained Simulation of Compressor and Engine System

The compressor simulation that was described in the previous subsection integrated into the Sunpower nodal analysis [2] so that an unconstrained simulation could be made of the entire engine/compressor system.

A successful simulation was made of the system with an additional piston spring which ran stably in close proximity to the desired operating point.

The load model developed will be included in the control system algorithm to be developed during Phase II. The results of the unconstrained simulation can be useful to verify the actual dynamometer testing of the RE-1000 FPSE.

3. PHASE II COST ESTIMATE

In this section, the program plan and cost estimate for the Phase II--Detail Design, Fabrication, and Testing of a Linear Alternator Dynamometer--are presented.

3.1 Phase II Program Plan

Phase II is divided into four tasks:

Task 1 - Detailed Analysis and Design

Task 2 - Fabrication of Laboratory Prototype

Task 3 - Installation and Startup Testing

Task 4 - Reports

Task 1 - Detailed Analysis and Design

Task 1 is divided into four subtasks:

Subtask 1.1 Electromechanical Transducer Final Design

Subtask 1.2 Control System Software Development

Subtask 1.3 Control System Final Design

Subtask 1.4 Preparation of Manufacturing Drawings for Laboratory Prototype

In Subtask 1.1, Electromechanical Transducer Final Design, all aspects of the electromechanical transducer preliminary design performed in Phase I will be reviewed. After the review and necessary design modifications, the transducer design will be finalized.

In Subtask 1.2, Control System Software Development, the detailed control system algorithm will be developed, based on the control system structure recommended in Phase I, as illustrated in Figure ES.3.

In Subtask 1.3, Control System Final Design, the control system hardware components will be selected and necessary modifications will be specified. The control system software and hardware design will be finalized.

In Subtask 1.4, Preparation of Manufacturing Drawings for Laboratory Prototype, the manufacturing drawings for the dynamometer will be prepared based on the results of the detailed analysis and design effort.

Task 2 - Fabrication of Laboratory Prototype

Task 2 is divided into two subtasks:

Subtask 2.1 Electromechanical Transducer Fabrication

Subtask 2.2 Control System Fabrication

In Subtask 2.1, Electromechanical Transducer Fabrication, various components of the transducer will be procured or fabricated.

In Subtask 2.2, Control System Fabrication, all the control system hardware components and accompanying transducers and instrumentation will be purchased. The control system will be prepared for installation.

Task 3 - Installation and Startup Testing

Task 3 is divided into two subtasks:

Subtask 3.1 Installation

Subtask 3.2 Startup Testing

In Subtask 3.1, the fabricated components of the linear alternator dynamometer will be shipped and installed at a test facility specified by ORNL.

In Subtask 3.2, technical assistance will be given in the preparation of the startup testing.

Task 4 - Reports

The following reports will be delivered during the Phase II program:

- Project Plan and Quality Assurance Report
- Monthly Reports
- Final Report

Design Review Meetings will be held at the conclusion of Task 1 and Task 3.

Project Schedule

The project schedule that depicts the timing of initiation and completion of tasks, subtasks, various reports, and meetings is given in Figure ES.5. The estimated project duration is eighteen months.

3.2 Phase II Cost Estimate

The cost estimate for Phase II--Detail Design, Fabrication and Testing of a Linear Alternator Dynamometer is presented in this subsection.

Task No.	Task Description	Months from Start of Phase II Contract (1 2 3 4 5 6 7 8 9 10 11 12 13 14 15 16 17 18)
1.	Detailed Analysis & Design	
1.1	Electromechanical Transducer Final Design	
1.2	Control System Software Development	
1.3	Control System Final Design	
1.4	Preparation of Manufacturing Drawings for Laboratory Prototype	
2.	Fabrication of Laboratory Prototype	
	2.1 Electromechanical Transducer Fabrication	
	2.2 Control System Fabrication	
3.	Installation & Startup Testing	
	3.1 Installation	
	3.2 Startup Testing	
4.	Reports	
	• Project Plan & Quality Assurance Report	
	• Monthly Report	
	• Final Report	
	- Draft	
	- Final	
	• Review Meeting	

Figure ES.5: Phase II Project Schedule

Table ES.4 shows the breakdown of Phase II Cost Estimate. The total estimated Phase II Cost and Fixed Fee is $272,200.

Table ES.4: Phase II Cost Estimate

Direct Labor Plus Burden	$ 73,380
Travel	12,500
Other Direct Costs	15,000
Direct Material	
Dynamometer/Control System	146,580
Total Phase II Cost:	$247,460
Fee:	24,740
Total Phase II Cost and Fixed Fee:	$272,200

The direct material cost consists of the transducer and other support structure of the dynamometer cost of $44,940 and the control system cost of $101,640.

4. SUMMARY AND RECOMMENDATIONS

A Preliminary design of a linear alternator type dynamometer is completed. The dynamometer was designed to be used as a versatile load device for free piston Stirling engines with power capacities up to 3 kW, strokes up to 5 cm, and frequencies up to 60 Hz.

The dynamometer has two major components: the electromechanical transducer and the control system. The electromechanical transducer is of moving armature coil/permanent magnet field type. The microprocessor based control system modulates the current in the armature coil according to desired load characteristics.

A detailed digital simulation of the dynamometer load/FPSE system predicts that the dynamometer load simulation will be extremely accurate and fast convergent. These favorable dynamometer characteristics result from the following dynamometer design features:

- very low moving mass,
- extremely low inductance,
- almost constant, uniform magnetic field,
- almost linear current-force relationship, and
- fast convergent and very stable control system.

The proposed dynamometer will be a valuable tool for further understanding of FPSE characteristics under diverse operating conditions and loads. The dynamometer will also help the design of load devices for specific applications by reducing the number and degree of hardware modifications.

It is estimated that the next developmental step, Phase II--Detailed Analysis, Design, Prototype Fabrication and Start-up Test, will take approximately 18 months and cost approximately $272,000.

We strongly recommend that Phase II be initiated soon in order to demonstrate the predictetd capabilities of the dynamometer, and eventually to expedite the commercialization of FPSE devices.

INTRODUCTION

Free Piston Stirling Engines (FPSE's) have many favorable characteristics suitable for energy conversion. These include high reliability, low noise, and expected high energy efficiency for converting thermal energy into mechanical power. The FPSE's power can then be used to drive output devices such as inertia compressors for heat pumps, hydraulic pumps and linear alternators.

To date, the full commercialization of FPSE's has been advancing slowly. One of the difficulties arises from the close interaction between thermodynamics of the working gas and dynamics of the moving parts. The close intereaction makes it difficult to analyze the performance of FPSE's under various load conditions. The resulting mismatch between a FPSE and the load can render the combined FPSE/Load System unsuitable for the original intended application.

The analytic difficulties and FPSE/Load mismatches can be avoided if one can test the FPSE with a dynamometer that can accurately simulate various load devices before a load device is designed and fabricated.

A truly versatile dynamometer for FPSE's will:

- help design better and suitable load devices for FPSE's,
- reduce the number of hardware modifications for the load device,
- reduce the need for elaborate Stirling engine analysis coupled with an elaborate load analysis,
- help understand FPSE's performance, and characteristics under many different loads and different ranges.

The objectives of the program are:

- preparation of a preliminary design of a dynamometer for FPSE's capable of detailed simulation of a double-acting inertia piston compressor and other loads;
- preparation of cost estimate for Phase II, Final Engineering Design and Fabrication of Prototype Linear Alternator Dynamometer.

The design requirements are the following:

- Compatibility with RE-1000 FPSE (manufactured by Sunpower, Inc., Ohio) - no changes in the engine working gas space should be required.
- Load simulation capacity - 0.5 ~ 3.0 kW
- Engine Frequency - up to 60 Hz
- Power piston stroke - up to 5 cm peak to peak.

2. PRELIMINARY DESIGN OF A LINEAR ALTERNATOR DYNAMOMETER

In this section, candidate dynamometer systems are investigated and selected. Necessary design effort and analyses are performed for the preliminary design.

2.1 Preliminary Design Process

There are two major components of a linear alternator dynamometer system: electromechanical transducer and control system. The elctro-mechanical transducer generally consists of an armature coil, a stator, and other structural elements. The control system generally consists of switching devices, microprocessors, power supplies, and instrumentation.

The approach taken for the Preliminary Design Process is illustrated in Figure 2.1. First, preliminary design concepts for the electromechanical transducer and the control system are generated. These design concepts are then investigated and compared with one another in order to select the best concepts for the particular application. Once the design concepts are selected, the effort is subdivided into three areas:

- Electromechanical Transducer Analysis and Design
- Dynamics and Thermodynamics Analyses of FPSE/LOAD, and
- Control System Design and Analysis.

Finally, the design integration of the elctromechanical transducer, control system, and RE-1000 FPSE is performed.

2.2 Electromechanical Transducer

In this section, seven preliminary design concepts for the Electromechanical Transducer for the dynamometer are compared with one another. A moving armature coil type with a permanent magnet field proves to be the most suitable for the dynamometer. A detailed magnetic field analysis is performed to arrive at a transducer preliminary design.

2.2.1 Preliminary Design Concepts

There are two general types of electromechanical transducers: linear motion and rotary motion. The linear motion type transducer is preferred because of the FPSE's reciprocating motion characteristic.

Candidate configurations of electromechanical transducers with linear motion include the following:

a. moving iron plunger (stationary armature and field coils)

b. stationary iron core (moving pole plunger, stationary armature and field coils)

c. moving permanent magnet (stationary armature and field coils)

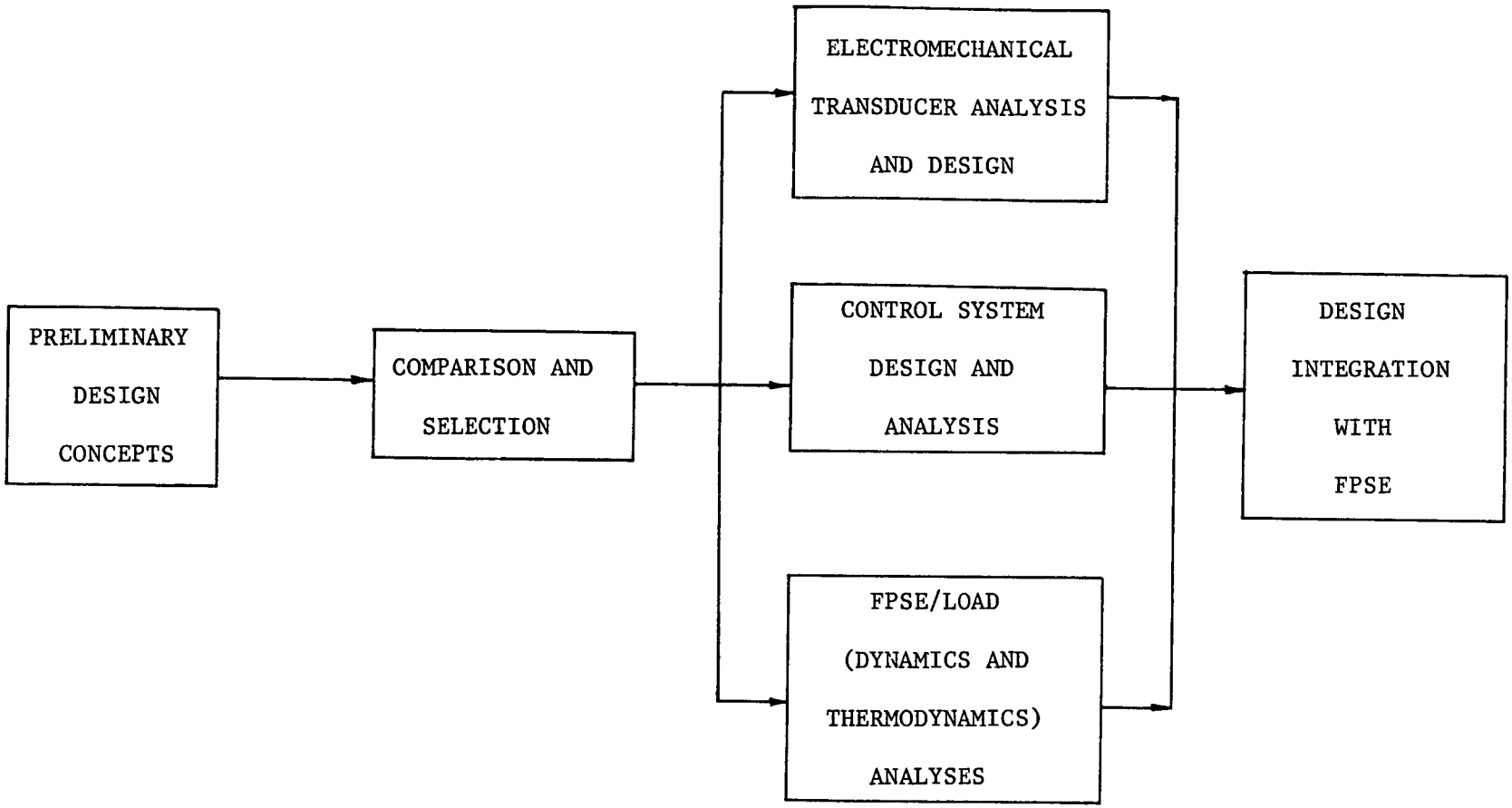

Figure 2.1: Preliminary Design Process

d. moving field coil plunger (stationary armature coil)

e. moving armature coil plunger (stationary electromagnet field)

f. moving armature coil plunger (stationary permanent magnet field)

g. moving conductor ring (stationary armature and field coil).

Each of these candidate configurations has advantages and disadvantages for the proposed dynamometer application. Brief discussions of each configuration are given below:

2.2.1.1 Moving Iron Plunger

The moving iron plunger type as shown in Figure 2.2 is the reciprocating equivalent of a flux-switching rotary machine sometimes referred to as an inductance alternator. All the electrically active coils, i.e., field and armature coils, are mounted on the stationary part of the machine. A magnetic iron plunger is the moving part, serving to switch the field across the armature coils. The advantages of this configurtion are simplicity, reliability, relatively high power density, and controllability of d-c field excitation. The disadvantages are heavy plunger mass and large side pull force. A heavy plunger will require a substantial effort to tune out its force by electrical means when other types of load are to be simulated.

2.2.1.2 Stationary Iron Core

Figure 2.3 shows how to make the mass of the oscillating plunger light by using a stationary shaft inside the thin plunger tube. For this configuration, the iron core, armature and field coils are stationary and only the salient poles of the plunger move.

2.2.1.3 Moving Permanent Magnet

In this configuration, a moving permanent magnet plunger replaces the moving iron plunger as shown in Figure 2.4. Conventionally, the armature coils are placed in slots in the surface of the stator magnetic circuit. However, if a rare-earth permanent magnet is used, it may be possible to use what might be called "air gap" armature winding, with a coil of turns located on the surface of the air-gap. The advantage of such an arrangement is its extremely low armature reactance and, as a result, a superior dynamic performance. This is because of the low permeance of rare-earth magnet materials and their consequent ability to operate with large air gaps. Another advantage is that the generated voltage can be made to be directly proportional to the piston velocity and independent of the piston positions by proper shaping of the magnet. Thererfore, it becomes possible to tailor the force-position-velocity profile of the alternator in a straightforward and accurate manner.

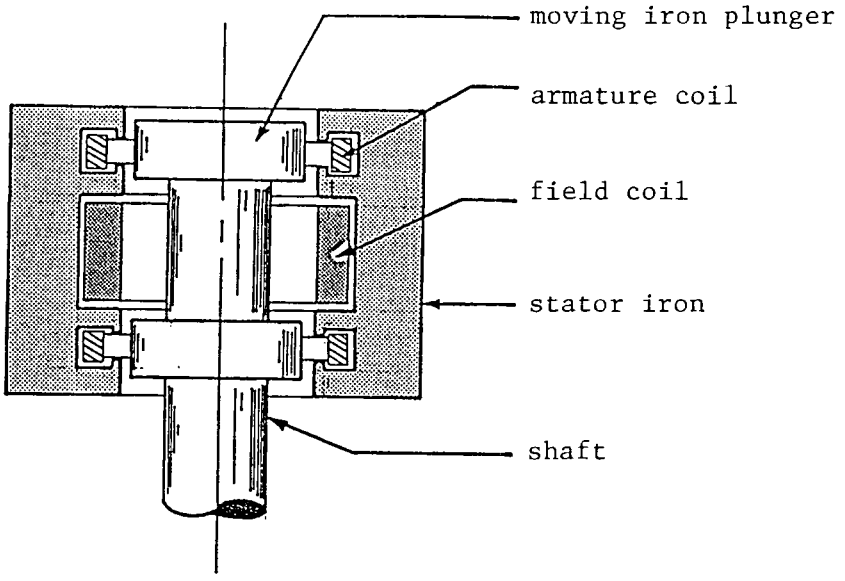

Figure 2.2: Moving Iron Plunger Reciprocating Transducer

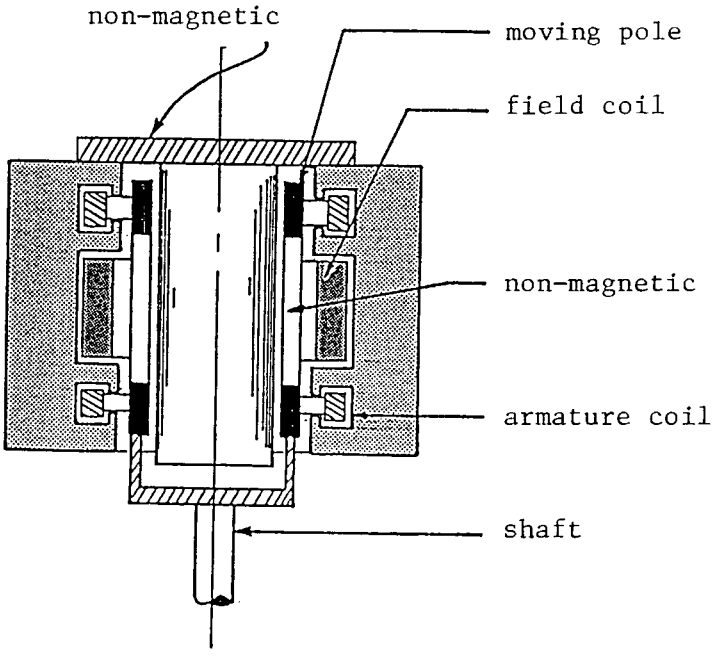

Figure 2.3: Moving Pole Reciprocating Transducer

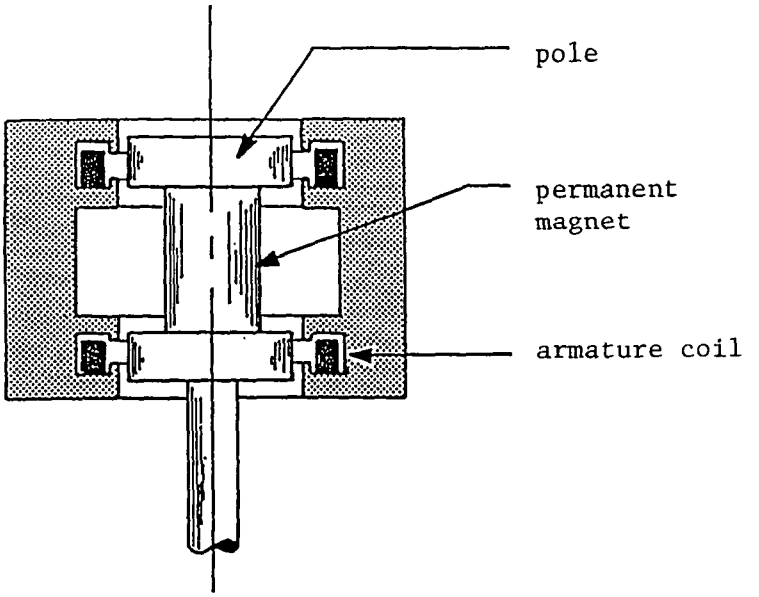

Figure 2.4: Moving Permanent Magnet Reciprocating Transducer

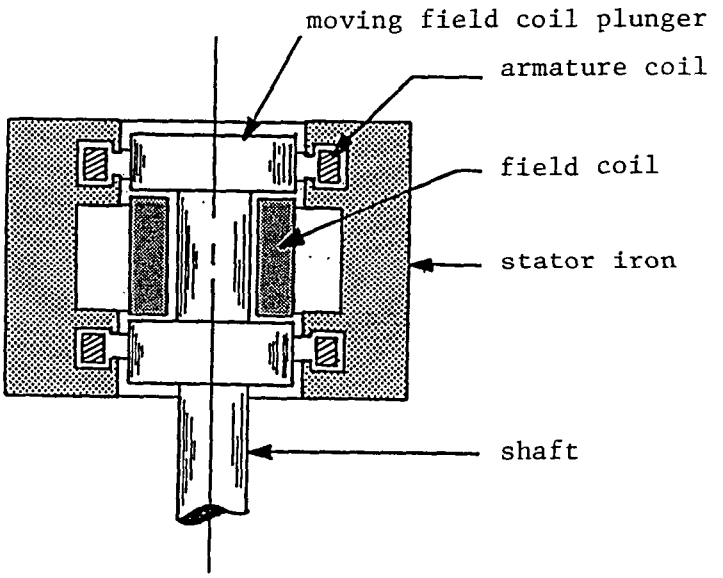

Figure 2.5: Moving Field Coil Reciprocating Transducer

2.2.1.4 Moving Field Coil Plunger

For the moving field coil configuration, the field winding is mounted on the shaft and moves past the armature winding as shown in Figure 2.5. It is the direct analog of a rotary synchronous machine. The advantages will include a high power density, flexibility of design, and high performance. Its disadvantages are that an electrical connection to the moving coil is required and that the plunger will be heavy.

2.2.1.5 Moving Armature Coil Plunger/Electromagnetic Field

This configuration as shown in Figure 2.6 is similar to a direct-radiator loud speaker. A voice coil, in this case an armature coil, moves to and fro in a radial magnetic field whose direction is perpendicular to the coil winding. Because there are no salient poles, it will be easier to analyze than the other configurations. The major advantages will include a very low moving mass and very low reactance, all of which are favorable for accurate load simulations. The disadvantage is that an electrical connection to the moving coil is required.

2.2.1.6 Moving Armature Coil Plunger/Permanent Magnet Field

Rare earth magnetic material such as Samarium cobalt can produce much higher magnetic flux than is practical for electromagnets with iron core with low saturation limits. When the overall size is a concern, this configuration with permanent magnet field and moving armature coil will be better suited than the one with the electromagnet field. A schematic of the moving armature coil plunger configuration is presented in Figure 2.7.

2.2.1.7 Moving Conductor Ring Transducer

It is possible to make linear transducers using a reciprocating, electrically shorted ring as shown in Figure 2.8. In this configuration, the moving ring is the "dual" of the moving iron plunger discussed earlier. The ring traps magnetic flux across the air gap and shuttles it back and forth across the armature winding. This configuration has some important advantages such as a relatively low reactance for good dynamic performance, light weight plunger, and stationary coils. One disadvantage is the complexity of the plunger shape required.

2.2.2 Comparison and Selection

The important selection criteria for a linear alternator dynamometer transducer include low mass, low reactance, and low internal losses, such as magnetic hysterises loss, eddy current loss, and flux leakage loss.

The reasons for using the above selection criteria are as follows:

In simulating load forces using a dynamometer, it will often be necessary to eliminate the force contribution due to the reciprocating mass, internal losses, and the reactance of the dynamometer. It is much easier to add, if necessary, the load forces representing mass, spring, and damping than to eliminate the existing excessive forces.

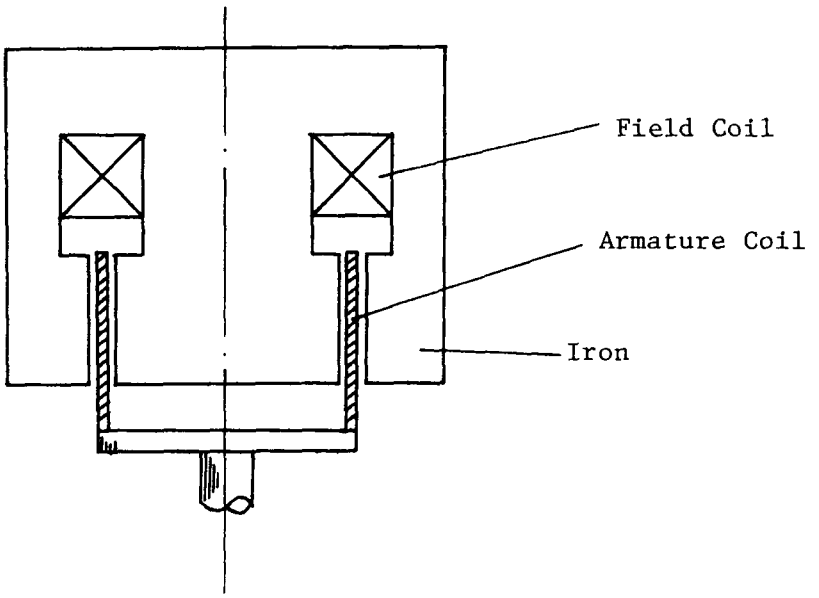

Figure 2.6: Moving Armature Coil/Electromagnetic Field Reciprocating Transducer

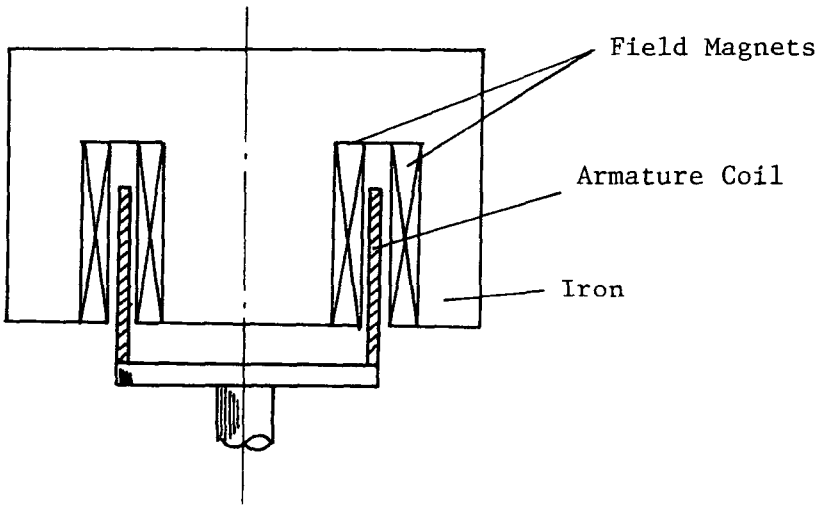

Figure 2.7: Moving Armature Coil/Permanent Magnet Field Reciprocating Transducer

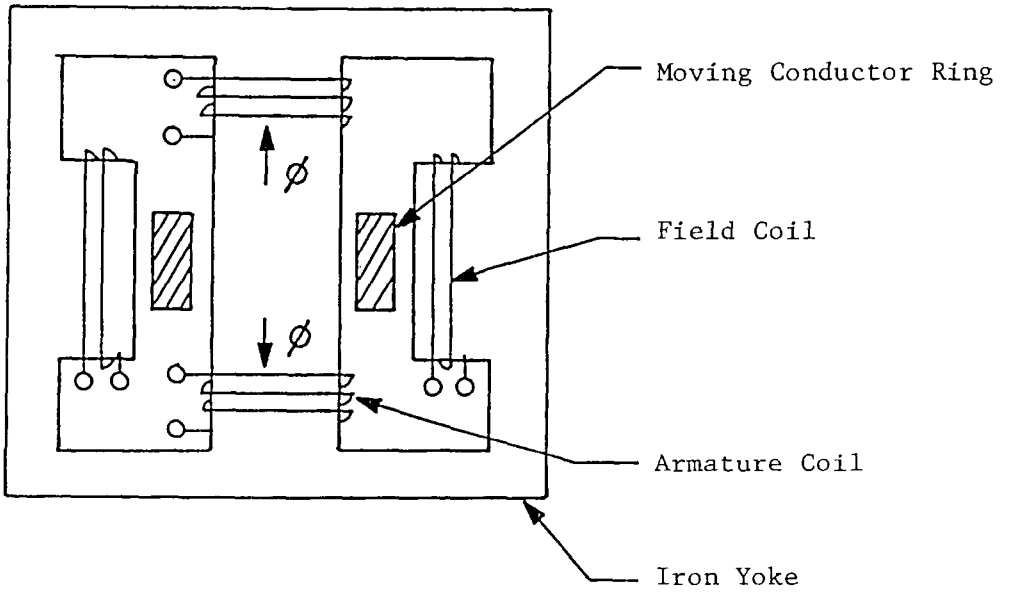

Figure 2.8: Moving Conductor Ring Reciprocating Transducer

Elimination of the dynamometer induced forces will be easier and more accurate if these forces are small.

High values of mass and reactance will tend to cause large undesirable errors. For example, any measurement error in phase angle between force and velocity will appear as power component. For dynamometer with small mass and reactance, the above error will be small.

Table 2.1 summarizes the relevant characteristics of the various types of the electromechanical transducers for the dynamometers that are described in Subsection 2.2.1.

The moving iron plunger and the moving field coil configurations are eliminated from further consideration due to the heavy plunger mass. The stationary iron core/moving pole configuration was eliminated due to its relatively high reactance and the difficulty of analyzing its internal losses. The moving permanent magnet required a relatively heavy plunger mass and was eliminated. The moving conductor ring configuration has a favorable combination of characteristics except that its internal losses and magnet field are relatively difficult to analyze.

Of the remaining two moving armature coil configurations, the one with the electromagnet field was discarded because the iron coremagnetic saturation will make the overall dynamometer size larger and the plunger mass heavier than the one with the permanent magnet field.

The moving armature coil with permanent magnet field was the best choice of the seven configurations. It has the following salient characteristics:

- the lowest reciprocating mass,
- the lowest dynamometer reactance,
- almost uniform magnetic field, which is easy to analyze,
- very low internal losses due to eddy current, flux leakage, and almost no magnetic hysteresis loss due to almost constant magnetic field,
- very close to a linear electromechanical transducer, which is easy to analyze and model,
- reasonably high power density,
- the flexible electrical connection, required in this configuration, can be easily designed, as will be shown in Subsection 2.2.4 and Appendix D, to meet the dynamometer operating requirements.

2.2.3 Magnetic Field Analysis

A three-dimensional magnetic field analysis was performed for the selected design concept shown in Figure 2.7. The magnetic analysis is presented in detail in Appendix A.

Table 2.1: Comparison of Linear Alternator Type Dynamometer Configurations

Linear Alternator Dynamometer Configuration	Plunger Mass	Internal Losses (very low and easy to analyze)	Alternator Reactance	Magnetic Field Strength Control	Flexible Connection Required	Recommendation
Moving Iron Plunger	Heavy	No	High	Yes	No	No
Stationary Iron Core/ Moving Pole	Light	No	High	Yes	No	No
Moving Permanent Magnet	Light	Yes	Very Low	NO	No	No
Moving Field Coil	Heavy	No	High	Yes	Yes	No
Moving Armature Coil/ Electromagnet Field	Very Light	Yes	Very Low	Yes	Yes	No
Moving Armature Coil/ Permanent Magnet Field	Extremely Light	Yes	Very Low	No	Yes	Yes
Moving Conductor Ring	Very Light	No	Moderate	Yes	No	No

The electromagnetic force exerted on a circumferentially wound coil of length l, carrying a current i, and moving axially in a concentric gap with radial magnetic flux of density B, is given by

$$F = B\,i\,l \tag{2-1}$$

In order to design a dynamometer with accurate force simulation capability, the above relationship has to be known accurately. In particular, the distribution of the magnetic flux density along the axial travel length of the coils is of primary interest.

Figure 2.9 illustrates the normalized average magnetic flux density, B_{av}, predicted by the magnetic analysis, as a function of the coil tube location. It shows that the coils, averaged over the axial length of the windings, experience nearly constant magnetic field along the travel distance. It is only at the maximum travel positions of coils (2.5 cm from the midstroke position) that there is an appreciable drop of approximately 5.8 percent in magnetic flux density. It is shown that as long as the coil tube travels within 75 percent of the maximum allowable stroke, the force exerted on the coil tube will be directly proportional to the current, i. The near linear force-current relationship is advantageous in achieving an accurate force simulation.

Based on the above magnetic analysis, a Magnetic Field Analysis Computer program was written to assist in the preliminary design of the dynamometer. The listing of this computer program is given in Appendix A. The input variables include: magnet characteristics, number of poles, overall dimensions of coil tube, air gap distance, coil dimensions, operating frequency, stroke, etc. The output of the program gives power, peak force, power dissipation, voltage, current required, etc. The program can be run interactively. A preliminary design obtained using the program for an electromechanical transducer is summarized in Table 2.2. The average power rating and operating points are 3kW, 30 Hz, and 5 cm, respectively.

The average power rating of 3kw is estimated based on the assumption of sinusoidal current and velocity. The peak force of 3440 N is based on the working flux density, the total coil length, and the peak coil current. Since the load force profile will not be sinusoidal in general, these values for average power and peak force should be regarded as only a general indicator of capability.

Mechanical power factor is the cosine of the phase angle between the piston velocity and the load force on the piston. Mechanical power factor of 0.37 was given as an input quantity. In actual dynamometer testing of a FPSE, the power factor will be a dependent variable.

The resistance of the coil, 0.0954 Ohms, is calculated from the resistivity of copper. The coil resistance could be further brought down to reduce the heat dissipation by shortening the length, and increasing the wire cross section. However, that approach would make the overall radial dimension of the transducer larger than desired. Also, a high energy conversion efficiency for the dynamometer is not our primary objective.

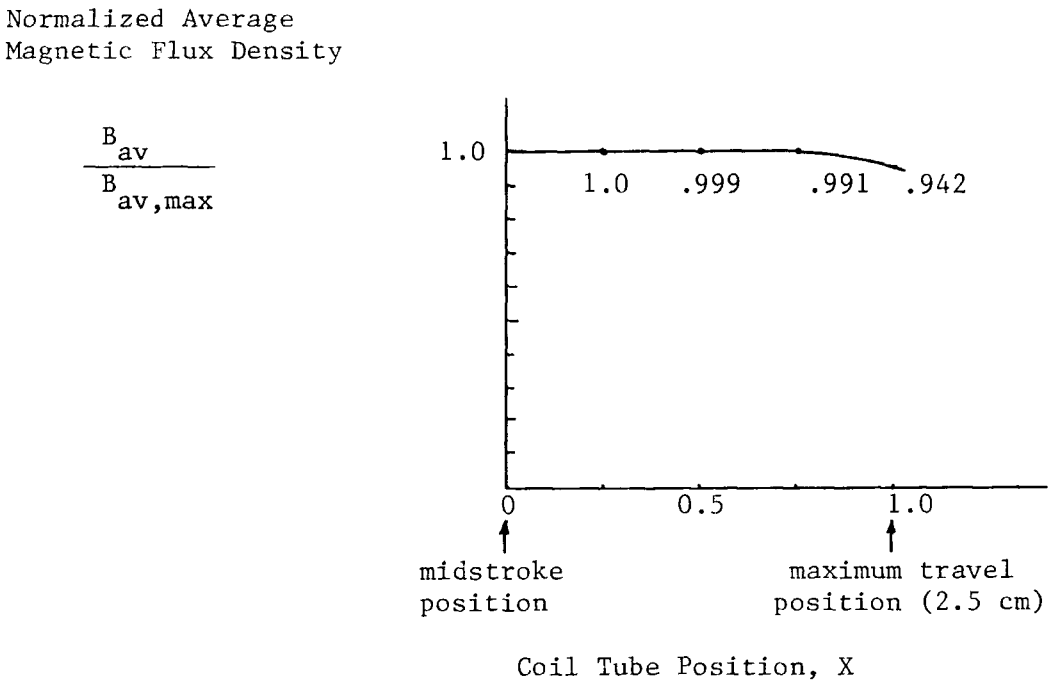

Figure 2.9: Average Magnetic Flux Density versus Coil Tube Location

The heat dissipation of 845 W is due to the i^2R loss in the coil. The heat will be dissipated into the ambient gas, which will then be cooled by water-cooled iron cylinders. Based on a simple heat transfer model described in Appendix A, the coil will be approximately 31 C above that of the ambient gas.

The reactive impedance of 0.000196 Ohms is small enough to satisfy the requirement for low dynamometer reactance.

Notice that the moving coil weighs only 1.8 kg, whereas the stationary permanent magnet weighs almost 21.4 kg. When the weights of the coil, coil tube and other structure of the plunger to be described in Subsection 2.24 are added up, the reciprocating mass of the plunger is approximately 3 kg, which is relatively small for the dynamometer power capacity.

The envelope for the dynamometer is a flanged cylinder with a spherical cap. It can be mounted on the existing RE-1000 FPSE's pressure vessel flanges. A more detailed description of the transducer preliminary design follows in the next subsection.

2.2.4 Transducer Preliminary Design

Figure 2.10 is the assembly drawing for the preliminary design of the linear alternator dynamometer transducer. In Table 2.2 is presented the list of component drawings. The numbering sequence corresponds to that of the assembly drawing. The drawings for the components are presented in Figures 2.11 through 2.21. These drawings are "preliminary." It means that detailing of the drawings such as dimensional and tolerance checks remains to be done in Phase II of the program. The design shown is the culmination of a design effort that included a detailed magnetic field analysis described in Section 2.2.3, and summarized in Table 2.3. Brief discussions on salient features of the preliminary design are given below.

As shown in Figure 2.10, the magnets, made of Samarium Cobalt, are arranged in a four-pole configuration with the magnetic flux alternating radially outward and inward. The inner magnets and outer magnets are shown in Figure 2.11 and 2.12, respectively. There are also two sets of half-length magnets at both ends. The magnets are arranged to reinforce each other, so at each pole location, a north magnet pole faces a south pole. The length of the magnets is designed to allow the maximum stroke requirement of 5 cm.

There are two iron cylinders that make up the magnetic return circuit: the inner iron cylinder (Figure 2.13) and the outer iron cylinder (Figure 2.14). These two iron cylinders are sized so that they are adequate to carry the flux produced by the magnets without being saturated. The iron cylinders also support the magnetic forces of the magnets. The iron cylinders would be twice as thick as required without the half-length end magnets. It is because that while the inner two magnet poles have two magnet return paths, the end magnets would have only one magnet return path without the half-length end magnets. Notice that the end magnets do not have coils. The end magnets merely provide one of the two magnetic return paths for the adjacent full-length magnets. The inner and outer iron cylinders also have water coolant passages to remove the heat from the coil, engine working gas, and magnets.

LEGEND:
1. Inner Magnets
2. Outer Magnets
3. Inner Iron Cylinder
4. Outer Iron Cylinder
5. Lower Mounting Cylinder
6. Non-Magnetic Support for Iron Cylinders
7. Coil Tube Assembly
8. Center Shaft Assembly
9. Lower Bearing Assembly
10. Upper Bearing Assembly
11. Flexible Connection Ribbon

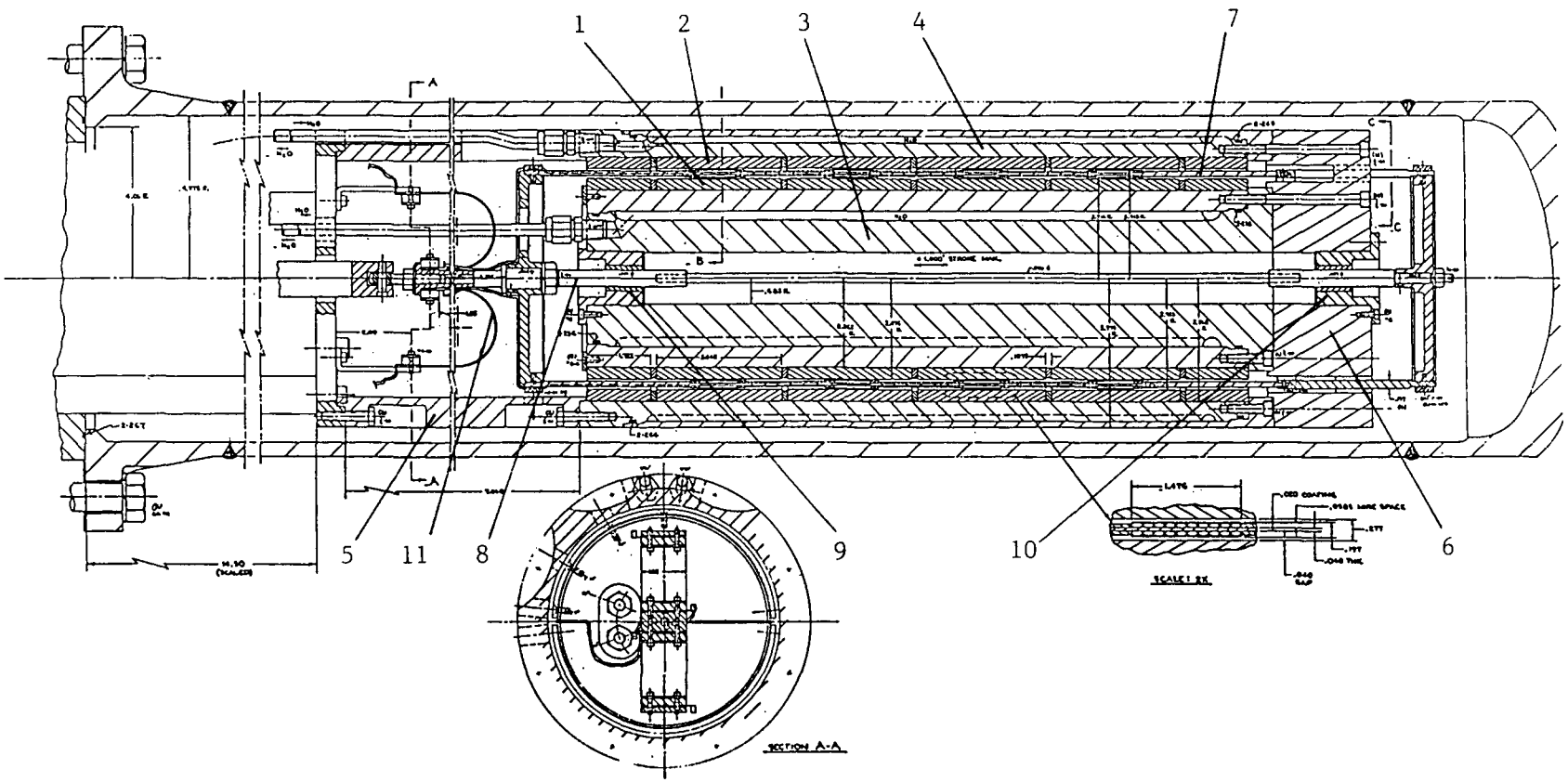

Figure 2.10: Preliminary Assembly Drawing for Linear Alternator Dynamometer for Free Piston Stirling Engines

Table 2.2: List of Component Drawings

Component No.	Description	Figure No.
1	Inner Magnet	2.11
2	Outer Magnet	2.12
3	Inner Iron Cylinder Assembly	2.13
4	Outer Iron Cylinder Assembly	2.14
5	Lower Mounting Cylinder	2.15
6	Non-Magnetic Support for Iron Cylinders	2.16
7	Coil Tube Assembly	2.17
8	Center Shaft Assembly	2.18
9	Lower Bearing Assembly	2.19
10	Upper Bearing Assembly	2.20
11	Flexible Connection Ribbon	2.21

Table 2.3: Electromechanical Transducer Preliminary Design Summary

	Value	Input/Output
Operating Point		
Frequency	30 Hz	I
Stroke	5 cm	I
Rating		
Average Power	2999 W	O
Peak Force	3440 N	O
Mechanical Power Factor	0.37	I
Dissipation	845 W	O
Voltage	127 V	O
Current	133 A	O
Coil (Copper)		
Resistance	0.0954 Ohms	O
Reactive Impedance	0.000196 Ohms	O
Number of Pole Pairs	2	I
Space Factor	0.6	I
Temperature Rise	31 C	O
Magnets (Samarium Cobalt)		
Residual Flux Density	1.05 T	I
Working Flux Density	0.72 T	O
Dimensions & Weights		
Inner Iron Cylinder	37.3 kg	O
Outer Iron Cylinder	37.3 kg	O
Coils	1.8 kg	O
Magnets	21.4 kg	O
Coil Tube	0.411 kg	O
Pressure Vessel	22 cm (i.d.)	
	125 cm (length)	I
Air Gap	0.1 cm	I

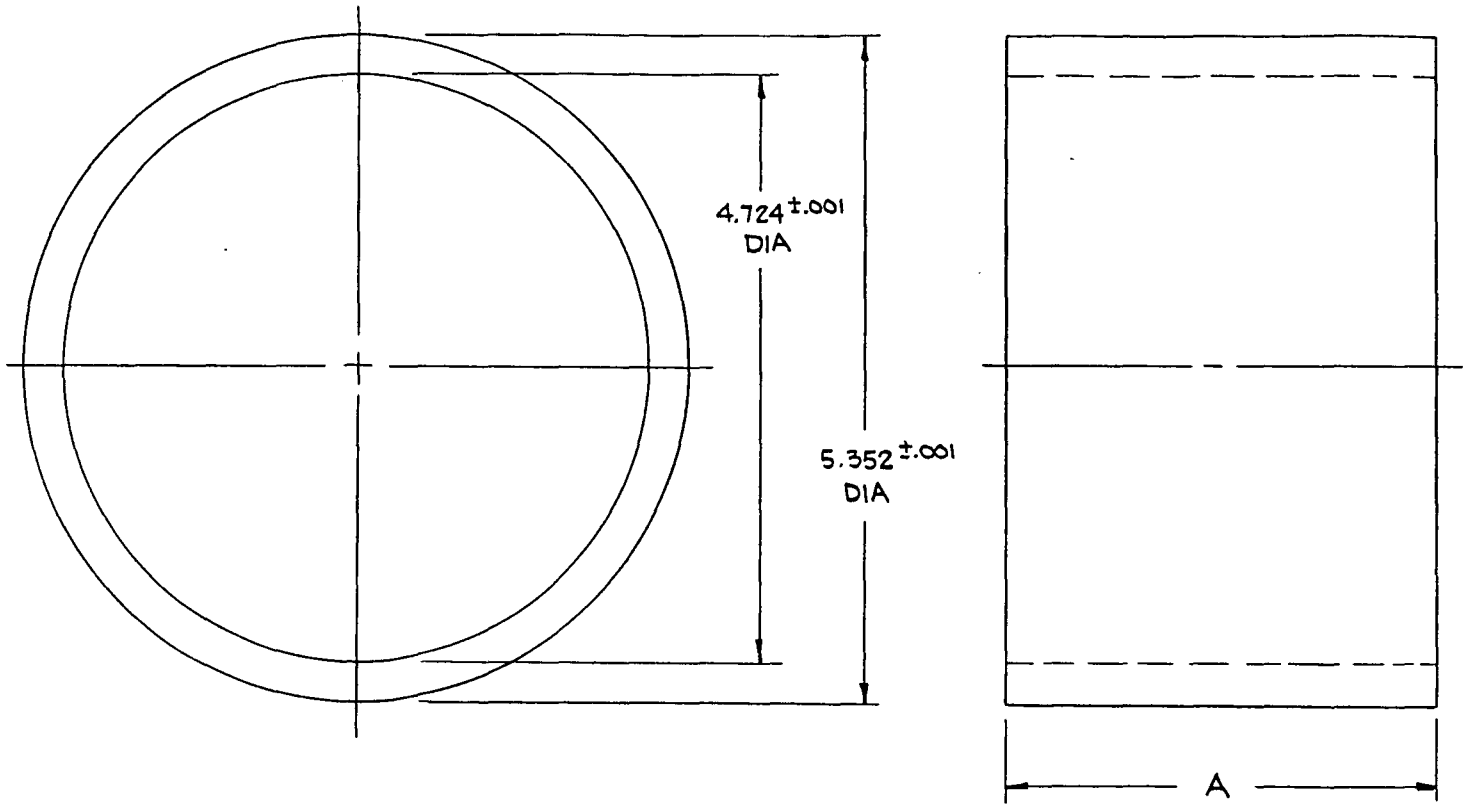

Figure 2.11: Inner Magnet

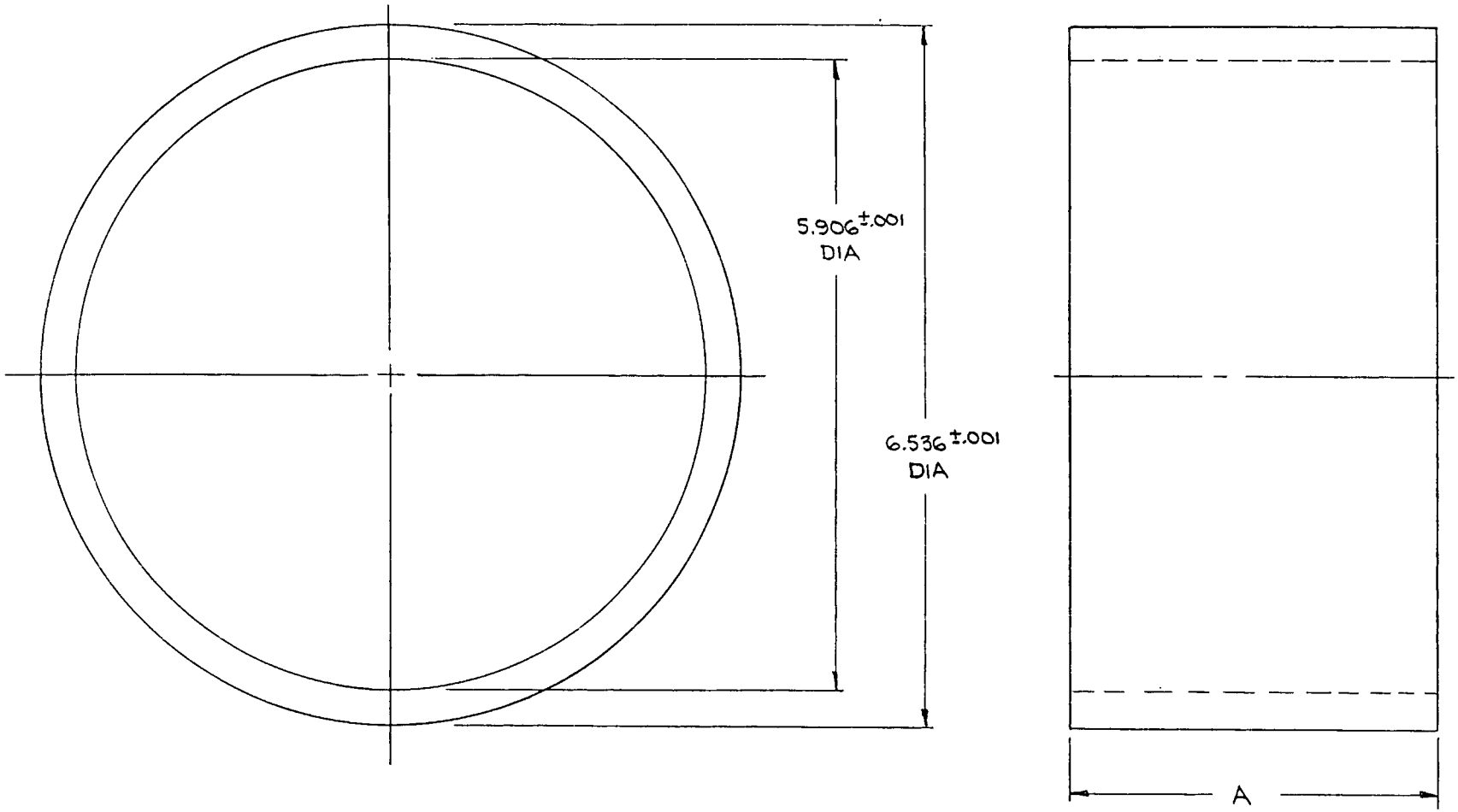

Figure 2.12: Outer Magnet

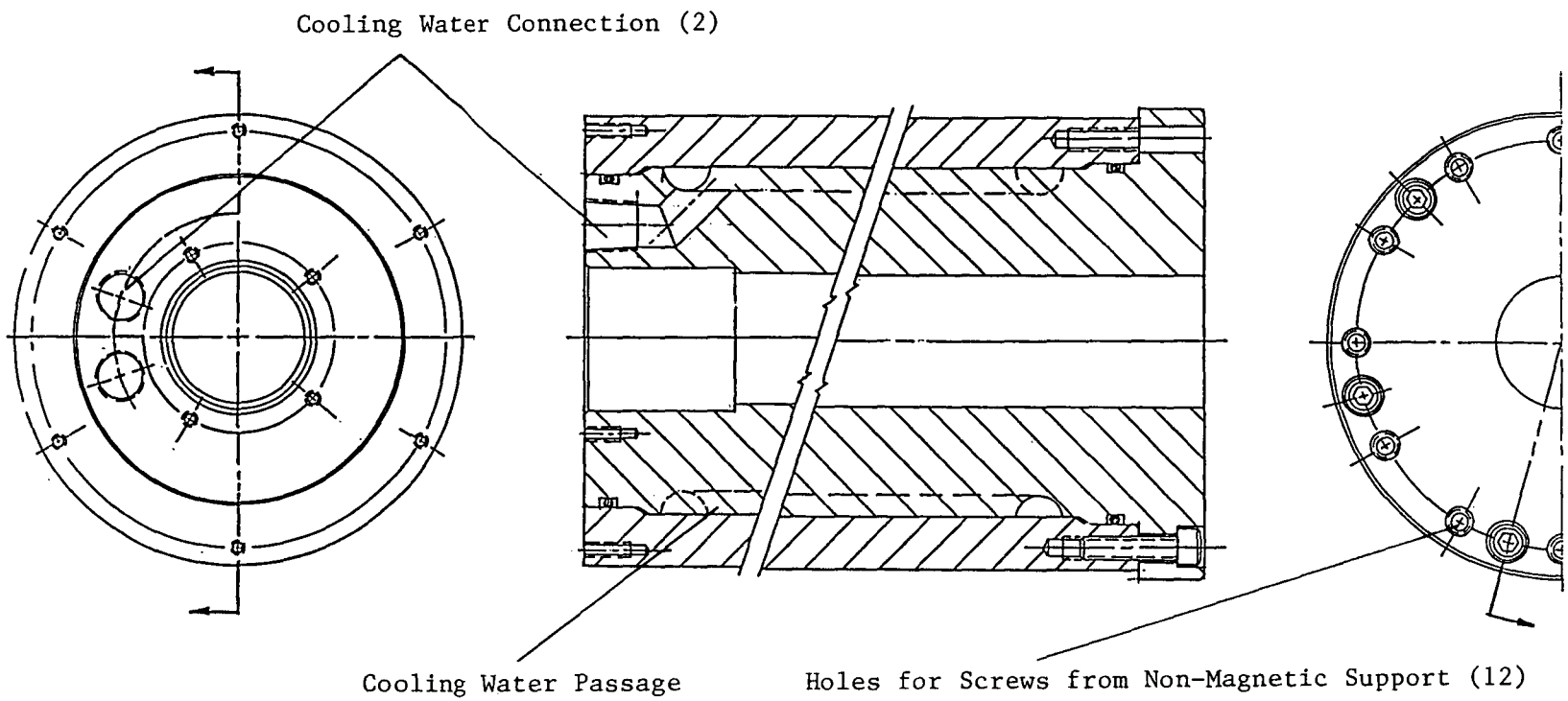

Figure 2.13: Inner Iron Cylinder Assembly

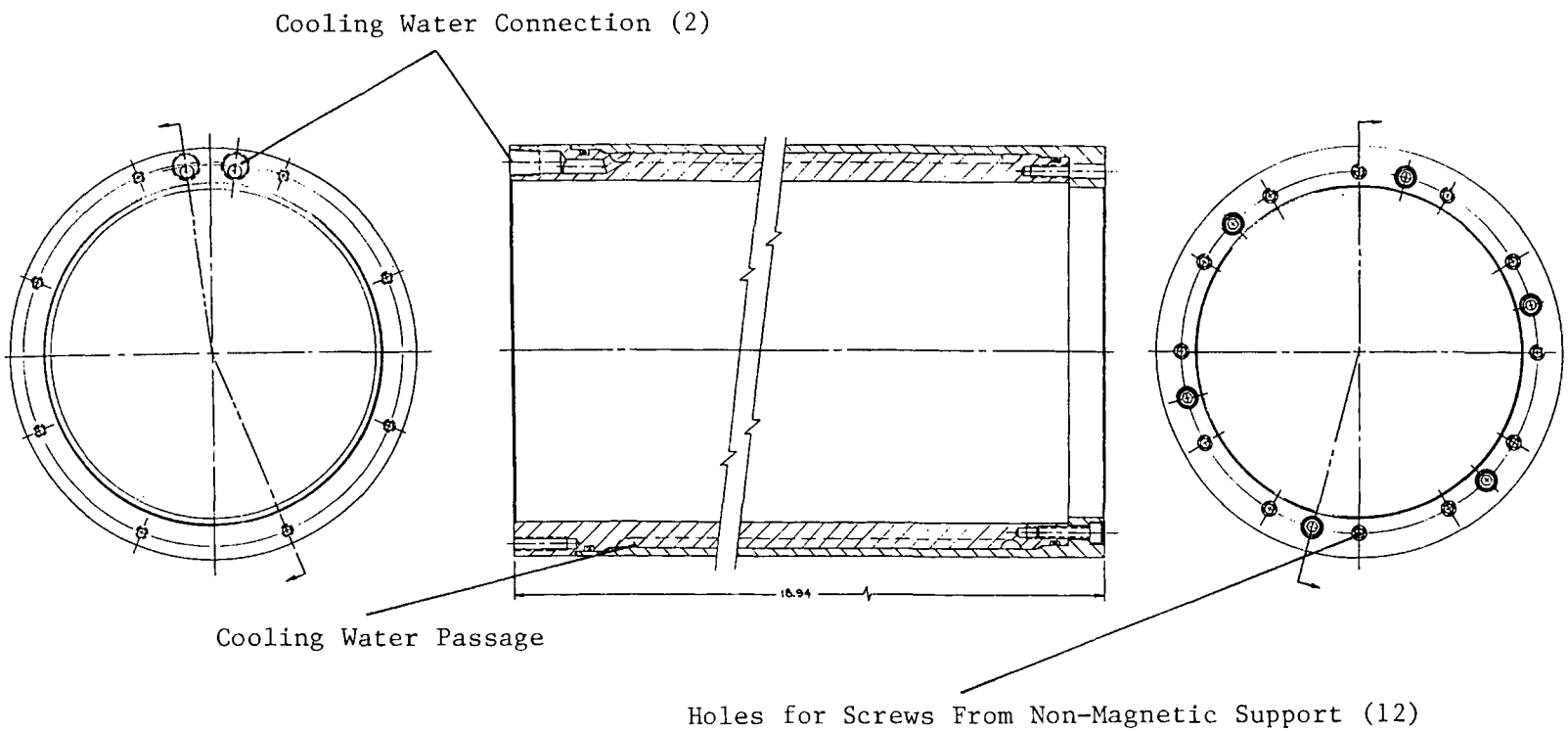

Figure 2.14: Outer Iron Cylinder Assembly

The lower mounting cylinder, as shown in Figure 2.10, will be attached to the disk that is currently used to support the damper load device for the RE-1000 FPSE. The details of the lower mounting cylinder are given in Figure 2.15. The lower mounting cylinder supports the outer iron cylinder. The outer and inner iron cylinders are held together by the non-magnetic cap shown in Figure 2.16.

The major structure of the moving coil assembly is the tube of fiber-reinforced epoxy, shown in Figure 2.17. The coil tube assembly reciprocates in the annular gap between the two rows of concentric permanent magnets. There are four sets of coils. Each set of coils has two layers of coils with ten windings located inside and outside the epoxy cylinders. The coils are to be bonded to the tube using an impregnation process to ensure a tight bond.

The coil winding direction at the four pole locations alternates from right helix to left helix starting from the lower end on the outside of the epoxy tube and going up to the upper end on the outside of the epoxy tube and coming down from the upper end on the inside of the epoxy tube and ending at the lower end on the inside of the epoxy tube. At the upper end coil location, the inside coil and the outside coil are connected through a hole in the tube. The alternately wound coils move between the alternately arranged magnets described previously. This makes forces acting on the individual coils point in the same direction at a given time; the total force is the algebraic sum of all the forces.

The lower rim of the epoxy tube is inserted into the groove of the lower disk and fastened by screws. The lower disk is connected to the engine piston via rod end bearings and force transducer. The upper rim of the epoxy tube is reinforced by a stainless steel ring with a circumferential groove for holding and fastening the tube. The ring has six legs that are attached to the upper disk. The six legs move back and forth inside six slots in the non-magnetic cap. These legs support the plastic tube in the radial direction.

The lower disk and the upper disk are connected by the center shaft assembly shown in Figure 2.18. At both ends of the center shaft, there are clearance bearings and positive stop dampers made of nylon blocks as shown in Figures 2.19 and 2.20.

There are two flexible connections to be made to the moving coil: one to the lead wire for the four coil windings glued to the inside of the epoxy tube, and the other to the lead wire for the four coil windings glued to the outside of the epoxy tube. These two moving wires are to be connected electrically to the two stationary posts. The electrical connections are accomplished using flexible leads specifically designed for this purpose.

As shown in Figure 2.10, these flexible leads are bent in a U shape, with a half circle in the middle, one flat section attached to the stationary post, the other flat section attached to the plunger rod. As one end of the flat section that is attached to the plunger rod reciprocates with the plunger, two flat sections roll up or roll down to maintain the half circle shape.

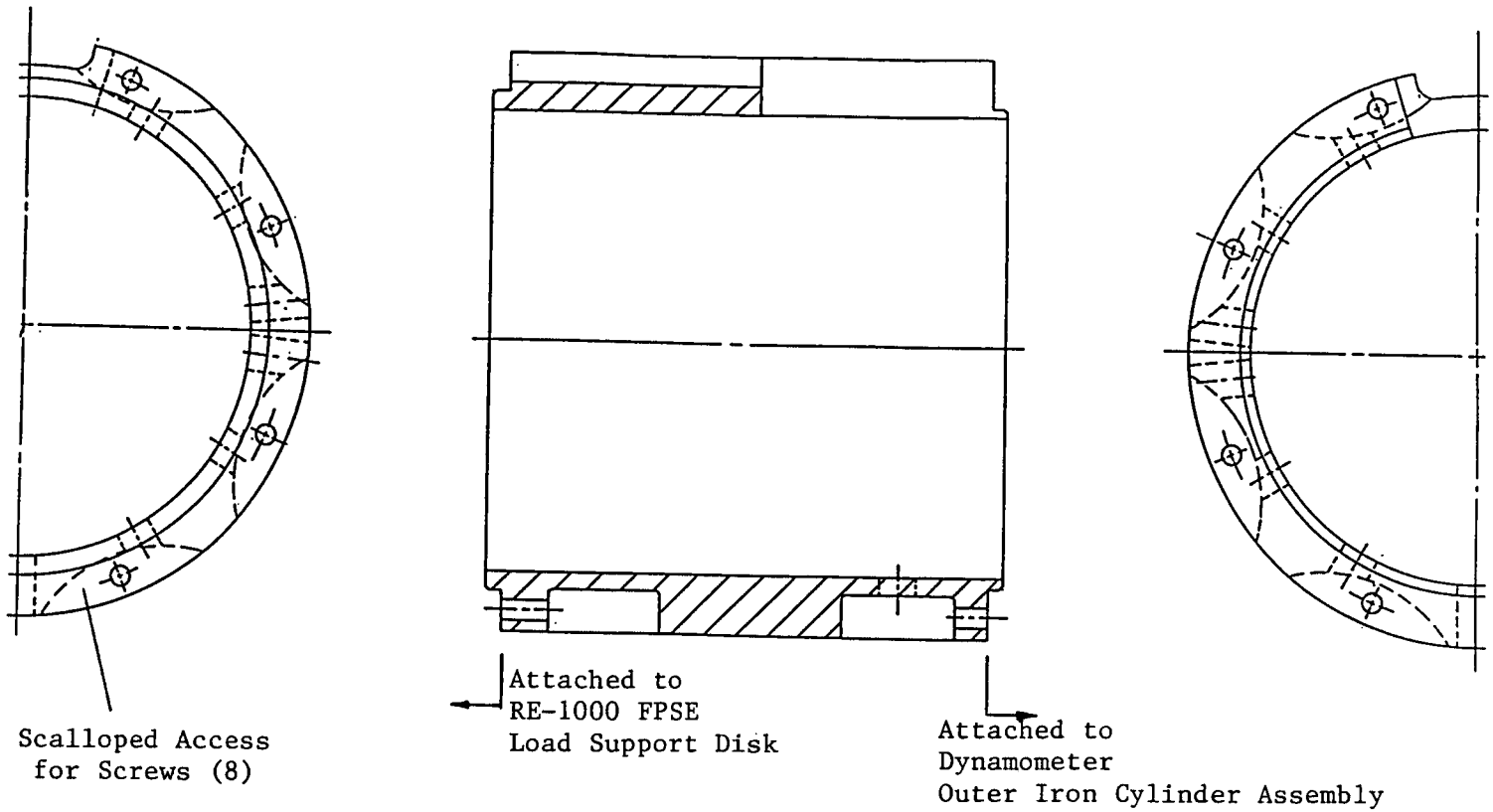

Figure 2.15: Lower Mounting Cylinder

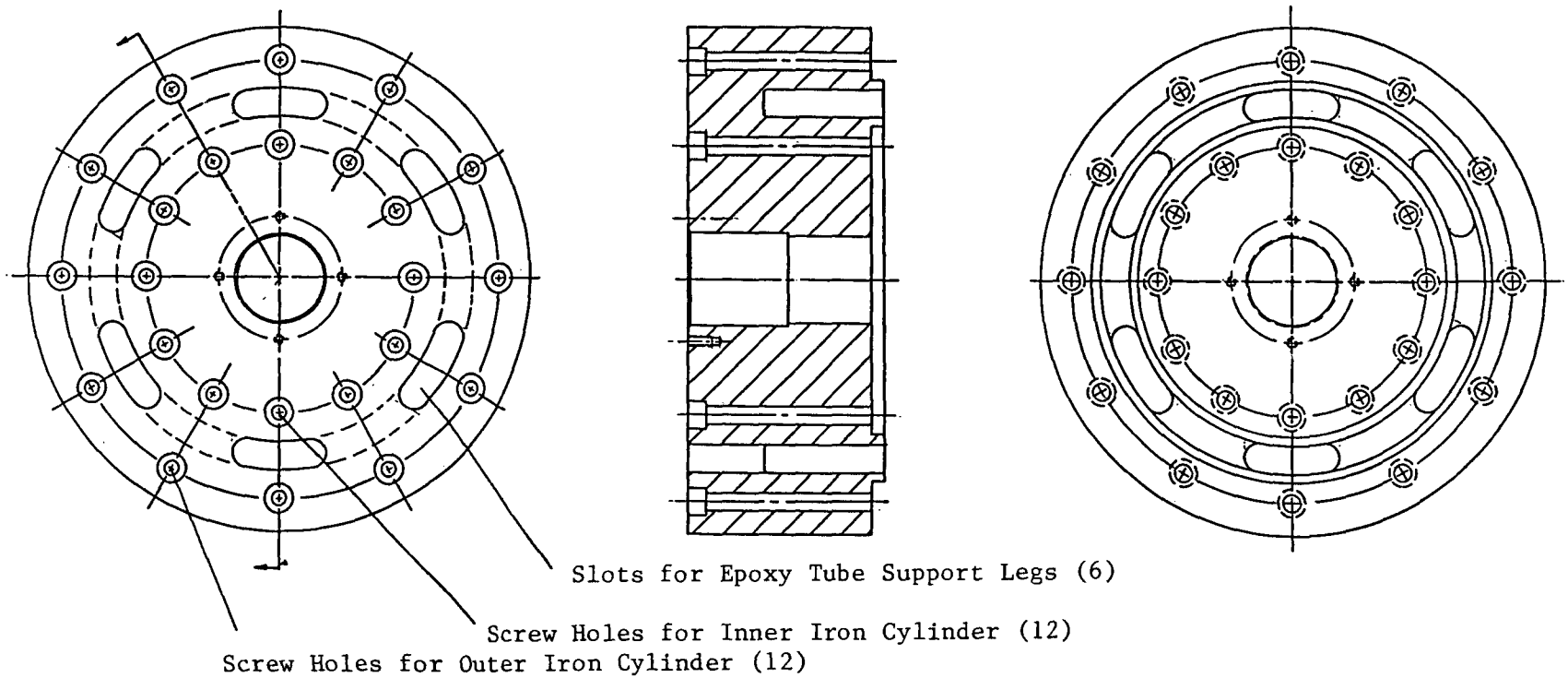

Figure 2.16: Non-Magnetic Cap for Iron Cylinders

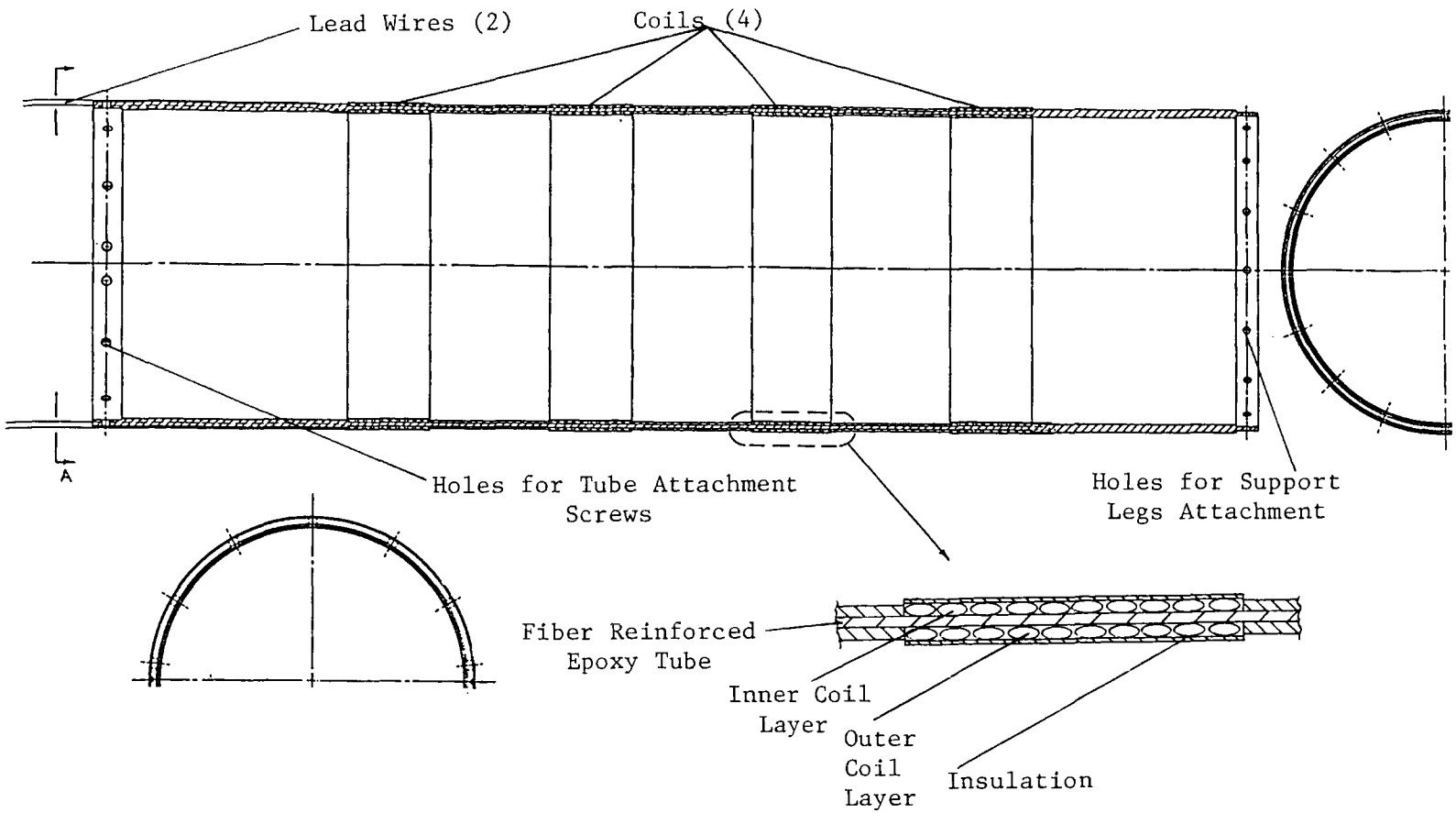

Figure 2.17: Coil Tube Assembly

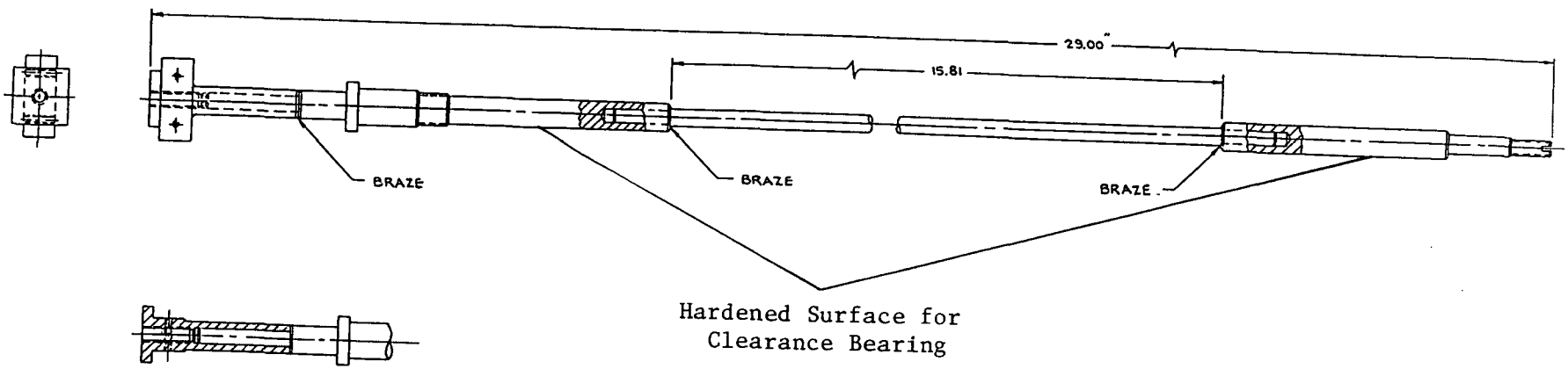

Figure 2.18: Center Shaft Assembly

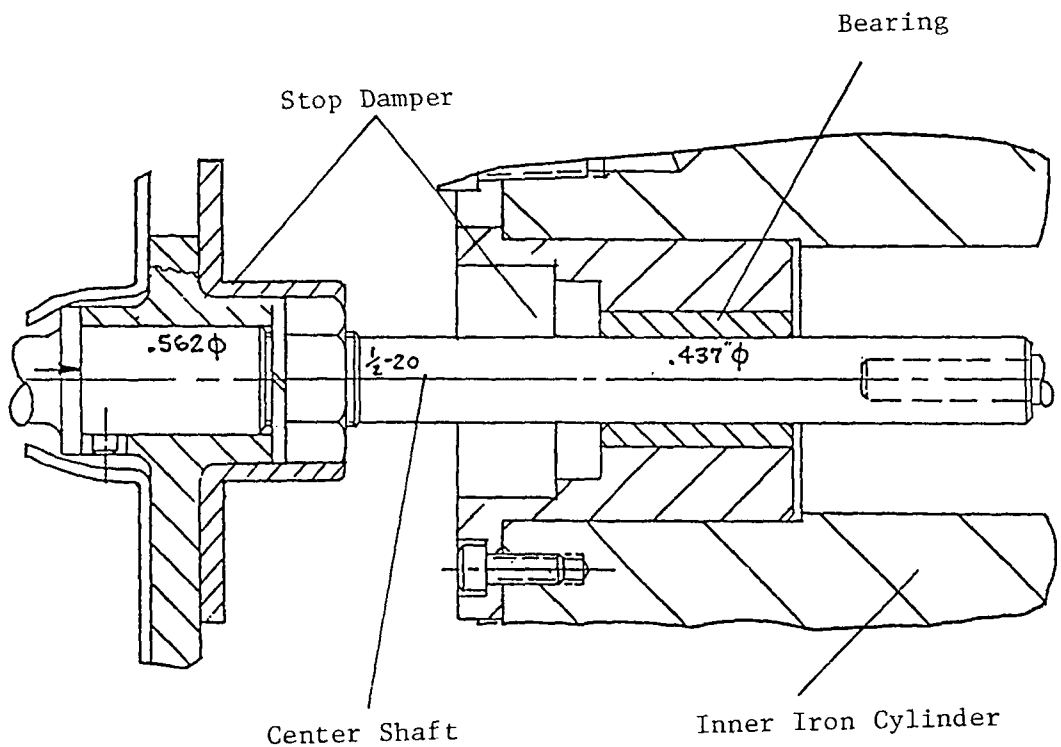

Figure 2.19: Lower Bearing Assembly

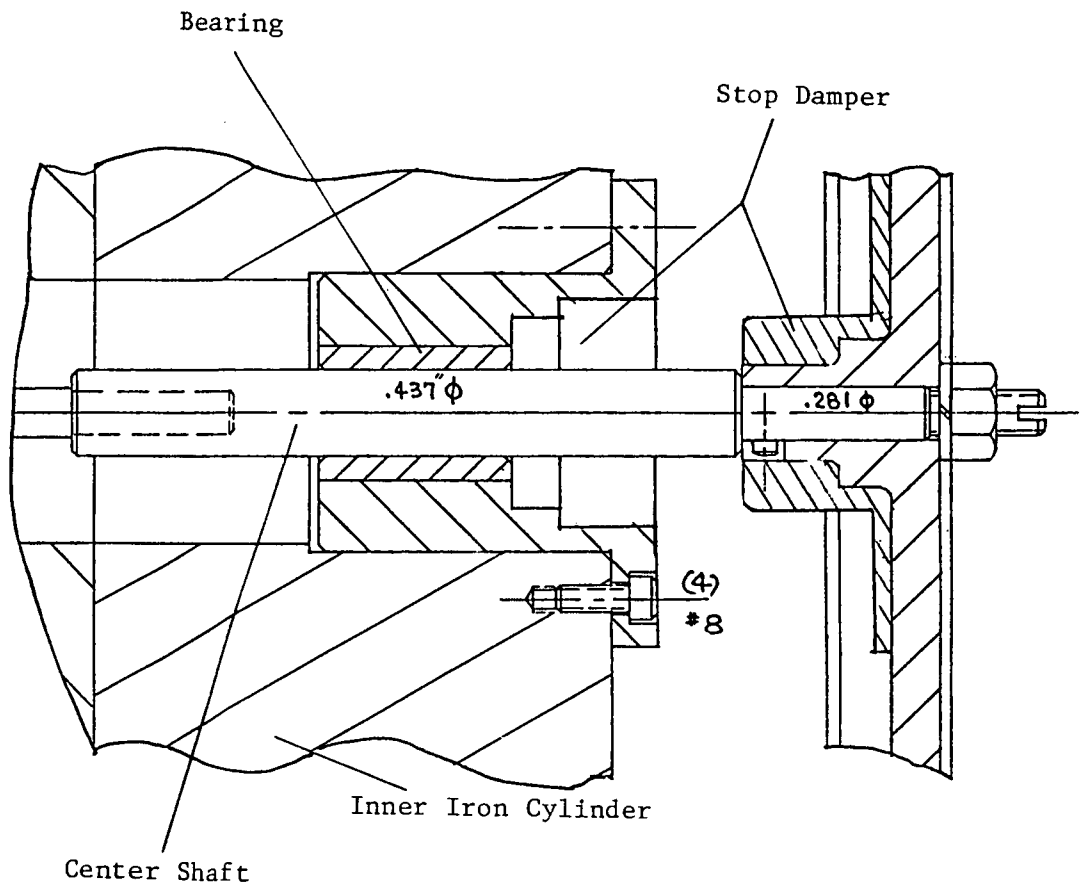

Figure 2.20: Upper Bearing Assembly

Table 2.4: Flexible Electrical Connection Design Summary

Shape	Thin Metal Strips Glued on Polyamid Ribbon Bent in U Shape
Number of Ribbons	2
Overall Size of Ribbons	0.075 mm Thick, 3.18 cm Wide, 18.14 cm Long
Mean Radius of Circular Section	2.54 cm
Electrical Conductors	
Material	Beryllium Copper
Dimension	0.1 mm Thick, 2.5 mm Wide, 15.6 cm Long
Number	20 (10 for each side)
Resistance	0.0411 Ohms
Buckling Stress	738 MPa
Yield Point	965 MPa
Endurance Stress	276 MPa
Maximum Bending Stress	258 MPa
Maximum Dynamic and Fluid Dynamic Stress	4 MPa
Maximum Operating Stress	262 MPa
Heat Dissipation	60 Watts at 133 A Peak Current
Temperature Rise	Less Than 68 Degrees C Above Helium Gas Temperature
Maximum Allowable Strip Temperature	200 Degrees C (Limited by the Glue Used to Attach Metal Strips to the Polyamid Ribbon)

The details of design calculation for the flexible leads are presented in Appendix D. Table 2.4 presents the design summary. As shown in Figure 2.21, the flexible leads are made of Beryllium Copper strips of 0.1 mm thickness, 2.5 mm width, and 18.14 cm length. Ten of these strips are glued on a high-temperature, high-strength polyamid ribbon for each flexible connection. Notice that only 15.6 cm long section is the active conductor. The remaining parts, at both ends, are covered with copper plates.

Beryllium Copper has a moderate electrical resistivity of 6.69 micro-ohm-cm, which is about four times that of pure copper. At 133 A peak current in the flexible connections, Joule heating loss is 60 Watts. The maximum allowable strip tempereature is about 200 C, which is the temperature limit imposed by the glue used to attach Beryllium Copper strips to the polyamid ribbon. The metal strips will experience heat transfer with the ambient gas. As calculated in Appendix D, the temperature of the metal strips will not be more than 68 C above the ambient helium gas temperature.

Beryllium Copper is a precipitation hardening alloy and is often used in bellows construction. It has excellent strength characteristics: yield point stress of 965 MPa, and endurance stress of 276 MPa.

Because the metal strips are very thin and narrow, the dynamic stress, of 3.7 MPa, due to the inertia of the metal strips, is quite negligible. The buckling stress for the flat section of the metal strips is about 738 MPa.

The maximum operating stress is designed below the endurance stress of 276 MPa. With the moderate temperature rise of 68 C, and the relatively low operating stress, the flexible leads are expected to last indefinitely.

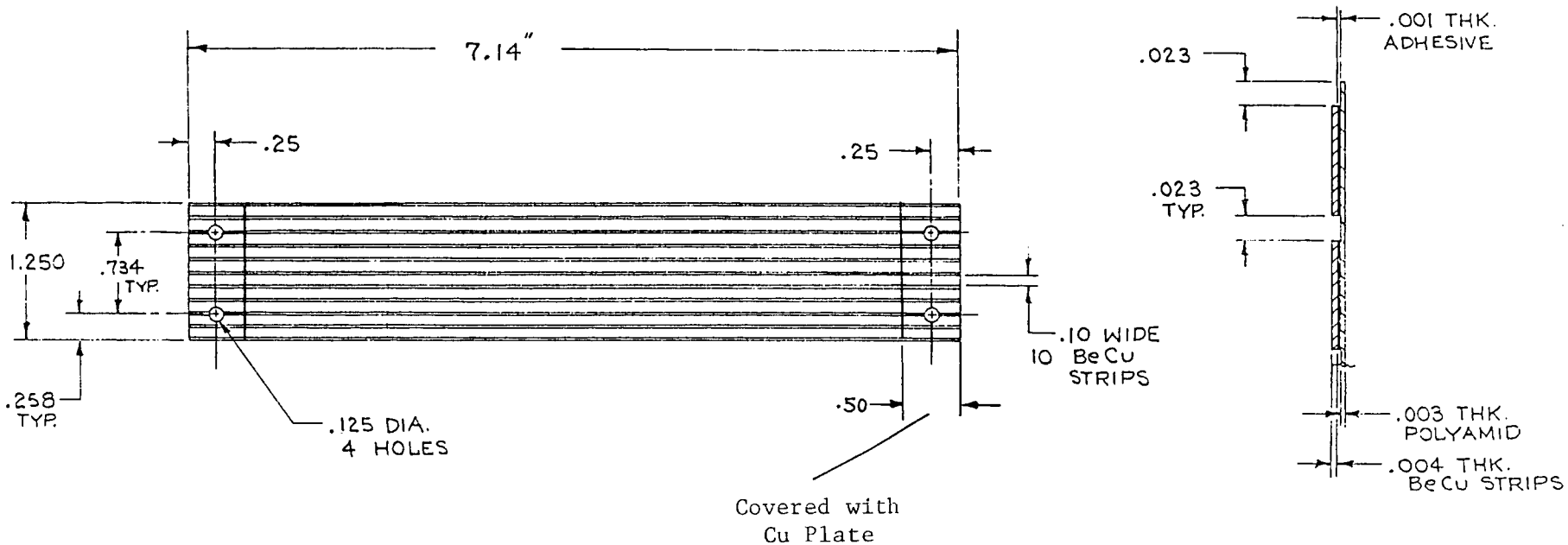

Figure 2.21: Flexible Connection Ribbon

2.3 Control System Design and Analysis *

In this subsection, preliminary design concepts of the control system for the linear alternator dynamometer are investigated. A Control System based on the Active Force Simulation is selected for its predicted simulation accuracy and flexibility in simulating various load forces. The algorithm for the dynamometer control system is described by block diagrams. The control system is digitally simulated to demonstrate its fast convergence and accurate load simulation capability.

2.3.1 Preliminary Design Concepts and Selection

Two methods of load force simulation were examined: Passive Force Simulation and Active Force Simulation

Passive Force Simulation

In Passive Force Simulation, load forces are simulated by connecting passive electrical elements, such as resistance, inductance, and capacitance, to the transducer output terminals. In order to simulate complicated load forces, this method will require a "library" of force elements to be switched on or off and probably to be modulated at the same time. Also, non-linearities of these force elements as well as those of the load to be simulated have to be understood and matched. This probably requires a microprocessor-based control system.

Active Force Simulation

In Active Force Simulation, load forces are simulated by modulating the transducer terminal current. The current will be supplied by a power supply that can supply power and absorb power. The control system will definitely be based on microprocessors. The control system algorithm will contain, as subroutines, the digital simulation of different load forces.

Of the two force simulation concepts, the Active Force Simulation method was selected for its perceived advantages in simulation accuracy and versatility.

2.3.2 Selected Control System for the Linear Alternator Dynamometer

In Figure 2.22 is presented the block diagram of the dynamometer control system based on the Active Force Simulation principle.

When the dynamometer/FPSE system is undergoing load testing, measurements are made of the FPSE piston displacement, velocity, and the load force.

The FPSE piston displacement is accurately detected by the Displacement Indexing Unit which transmits the information to the Pulse Generator and the Address Generator.

* This Subsection describes the work performed by Professor L. F. Goldberg of the University of Minnesota under ORNL Subcontract No. 11X-39005V.

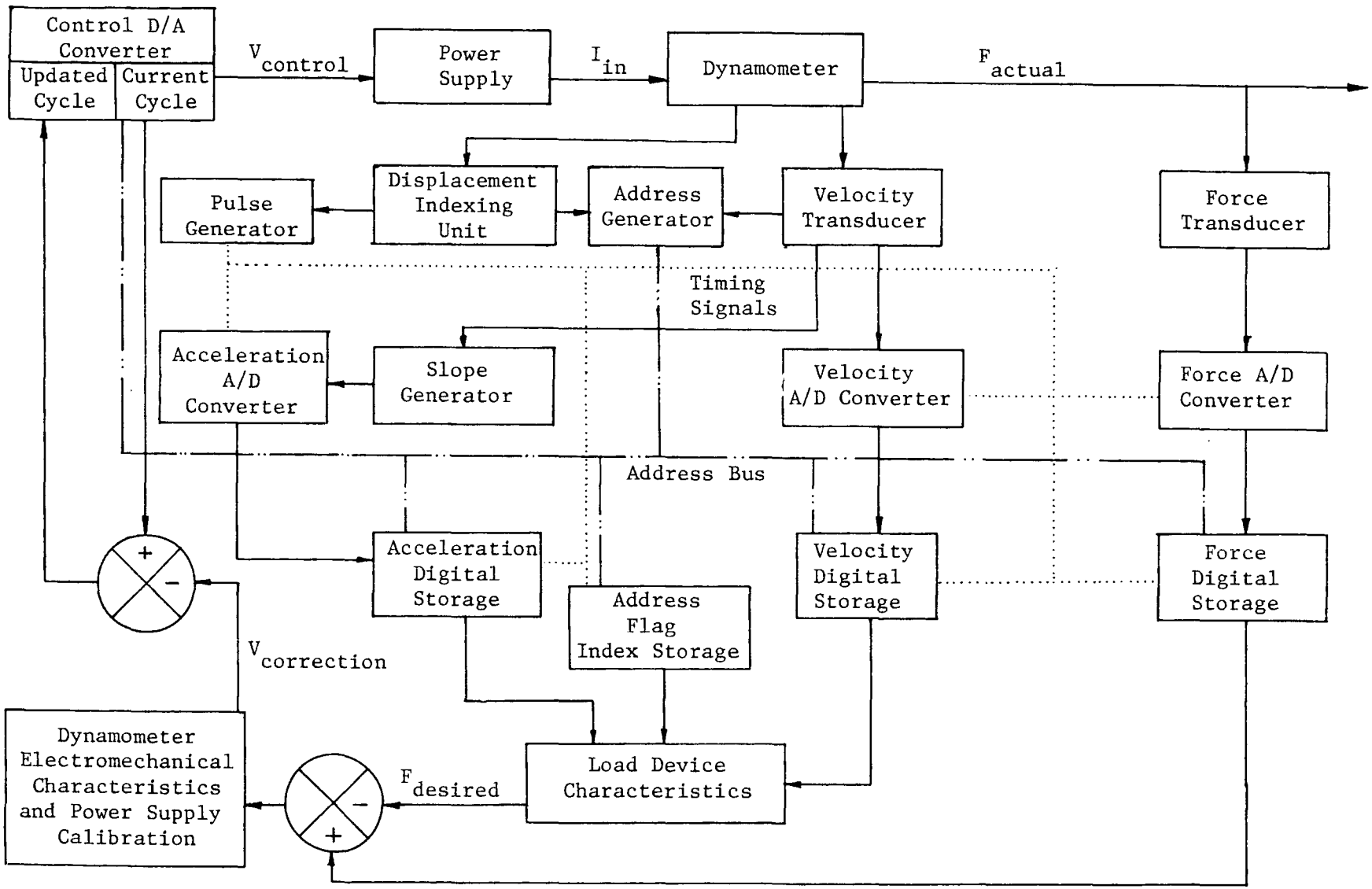

Figure 2.22: Block Diagram of the Dynamometer Control System

The piston velocity is measured by the Velocity Transducer and transmitted to the Address Generator. The analog velocity signal is converted to digital signal in the Velocity A/D Converter and stored in the Velocity Digital Storage. The slope of the velocity, acceleration is generated by the Slope Generator, converted into digital signal and stored in Acceleration Digital Storage.

The load force is measured by the force transducer located between the dynamometer plunger and the FPSE piston. The analog force signal is also converted into digital signal and stored in the Force Digital Storage.

The address generator transmits the current address instantaneously through the Address Bus to Control D/A Converter (current cycle), the four storages for acceleration, velocity, force, and the Address Flag Index. Also, the timing signal generated by the Pulse Generator is instantaneously transmitted to the three A/D converters, and to the four storages for acceleration, velocity, force, and address flag index.

The control system operates in two modes simultaneously: the foreground mode and the background mode. In the foreground mode, the current cycle table in the Control D/A Converter sends the control voltage to the power supply. The power supply, in turn, supplies the corresponding current to the dynamometer. There is no computation requirement in this mode, and the current cycle block simply sends out prescribed control voltage corresponding to the displacement communicated by the address bus. Therefore, there is practically no time delay in the dynamometer force simulation operating in the foreground mode.

While the dynamometer simulates FPSE load forces using the foreground mode, in the background mode, the load device characteristics block calculates the force desired corresponding to the updated stored acceleration, velocity and address flag index. The calculated desired force profile, $F_{desired}$, is compared with the stored force profile in the force digital storage. The resulting force correction signal is transmitted to the block called "dynamometer electromechanical characteristics and power supply calibration," which in turn generates voltage correction information $V_{correction}$. $V_{correction}$ is then applied to the control voltage profile in Current Cycle Table of the Control D/A Converter to generate the Updated Cycle Table.

When the updating is completed, the updated force values will be transferred to "current cycle" to be used in the foreground mode. A new updating process will begin in the background mode. This periodic updating constitutes a negative feedback loop intermittently closed. The updating process will continue until the FPSE/Dynamometer system reaches a converged state.

The convergence characteristics of the control system described above will be digitally simulated in Section 2.3.3.

2.3.3 A Simulation Assessment of the Stability, Accuracy, and Convergence of the Selected Linear Alternator Dynamometer Control System*

2.3.3.1 Objectives

The objectives of the assessment of the linear alternator dynamometer (LAD) and its control system are as follows:

a. To determine whether the control system described in Section 2.3.2 is convergent and, if not, what modifications are necessary to achieve convergence.

b. To investigate the effect (if any) of various strategies for dealing with under- and over-stroking occurring as a result of dynamic changes in the load/displacement profile.

c. To determine the minimum resolution of the displacement indexing unit necessary for convergence (that is, the number of pulses per unit length).

d. To check the control system convergence for a variety of arabitrary driving and loading devices in any combination.

The method specified for the fulfillment of these objectives is to devise a numerical algorithm for simulating the dynamometer and its control system when coupled to a nominal free-piston Stirling engine whose geometrical and topological characteristics correspond to those of the Sunpower RE-1000 FPSE. Furthermore, the operating point (in terms of charge pressure, heat exchanger gas temperatures, etc.) at which the simulation tests are to be performed should correspond to one of the data points established during the NASA-Lewis RE-1000 FPSE performance test series.

2.3.3.2 Research Approach

In order to fully meet the specified objectives, it is apparent that the dynamometer and its control system need to be tested in the context of a physically realistic engine operating environment. In particular, the primary requirement for determining the convergence as well as the stability and accuracy of the dynamometer imply that the engine dynamics be faithfully replicated such that the interactions between the dynamometer control system and the engine displacer and piston oscillations can be objectively determined. This implies that simplistic approaches to developing a simulation algorithm which appear at first to be attractive options are completely unsuitable. An example of such an approach would be the specification of given harmonic piston and displacer amplitudes which may then be used to generate a working space pressure in order to perform a force balance on the piston/dynamometer armature. Clearly, such a methodology neither tests the convergence of the dynamometer, nor does it give any indication of how the control system affects the engine dynamics as manifested by the operating frequency and the displacer and piston amplitudes.

* The work described herein has been undertaken by Louis F. Goldberg under the auspices of Martin Marietta Energy Systems, Inc., Subcontract No. 11X-39005V.

The only suitable method of providing a realistic simulation environment is to implement a coupled dynamic/gas dynamic simulation of the RE-1000 free piston Stirling engine in which all the dynamic characteristics (frequency, amplitude, and phase angle) are treated as dependent variables. The literature is sparse in the description of such simulation models, most of which treat the above-mentioned dynamic characteristics as independent variables either by specifying harmonic profiles or by using empirical data. The reasons for this devolve upon the intricacies of linking the engine dynamics and gas dynamics together in the context of a boundary value problem in which the dynamic boundary conditions are themselves dependent variables.

Based on the work as reported in References [3 and 4], as well as a considerable body of unpublished research performed by L. F. Goldberg [5] subsequently, a completely stable and convergent algorithm for simulating a free piston Stirling engine as a combined dynamic/gas dynamic system with arbitrarily complex mathematical descriptions of the dynamics and gas dynamics has been developed and validated. This algorithm provides the physically realistic representation of a free piston Stirling engine which enables the dynamometer and its control system to be tested in such a way that the stated objectives may be met.

2.3.3.3 Engine Stability Considerations

Within the context of the combined dynamic/gas dynamic simulation algorithm, there is complete freedom to choose any model to represent the gas dynamics of the engine. In the case of free piston Stirling engines, the choice of gas dynamic model has two gross implications:

a. The accuracy of the predicted cyclic work output and heat transfer with the environment is dependent on the nature of the assumptions made.

b. The stability characteristics of the engine are critically dependent on the assumptions made in modelling the gas dynamic processes in the working spaces.

The former implication has been well documented in the literature and needs no elaboration here. The latter implication is perhaps less well understood and, furthermore, is of critical importance in the context of the dynamometer simulation. When viewed as a system, the dynamometer and engine can only exhibit overall stability; in other words, if either component is unstable, the entire system exhibits instability. Hence, even though a particular dynamometer control system may be perfectly stable, if coupled to an unstable engine, the overall system would appear unstable despite the fact that the dynamometer is faithfully replicating the desired loading characteristics in the presence of the engine instability. Under these conditions, no conclusions on the dynamometer stability and convergence may be drawn. This predicates that the stability of the engine must be established before it is attached to the dynamometer so that the system stability and convergence may be correctly interpreted as demonstrating the performance of the dynamometer.

Therefore, it is apparent that a gas dynamic model which accurately replicates the characteristics of a real engine should be the model of choice. In particular, the model needs to be capable of modelling in one dimension at

least the momentum of the gas in the working spaces as this is perhaps one of the dominant factors from a stability perspective. In view of the complexity of such a model, its use is completely beyond the scope of the limited budgetary and temporal constraints of this project. Hence, of necessity, use must be made of a simpler thermodynamic model which can be implemented within the imposed constraints but still enable the project objectives to be met. The choice of models thus devolves to either an assumption of isothermal or adiabatic working spaces coupled to an isothermal heat exchanger assembly. Neither method has a clear advantage from a stability perspective and, hence, the isothermal model is chosen owing to its greater simplicity and ease of programming. Nevertheless, it may be mentioned at this stage that the computer program embodying the simulation algorithm is completely tractable and extendable such that the isothermal model used may be replaced with any model of arbitrary complexity at will.

The effect of using an isothermal model on the engine stability may be understood in terms of a state-space description of the free piston Stirling engine. It can be rigorously demonstrated that, irrespective of the gas dynamic model used, the piston and the displacer will oscillate stably with zero damping if and only if the engine parameters fall on the stability boundary hypersurface in the parameter space. Under these conditions, the exponents of the piston and displacer dynamic variable amplitude multipliers are zero. These exponents may be referred to as the engine damping factors and they may be negative, positive as well as zero. When the parameters fall within the stability boundary hypersurface, the amplitudes decay, while similarly when the hypersurface is exceeded, the amplitudes increrase. In the latter case, the amplitudes increase until the total dissipation and work done equals the indicated work, at which point the damping factors again become zero.

These stability phenomena are analytically tractable for an isothermal engine if the load can be described as a linear function of piston displacement and/or velocity with constant coefficients. In these circumstances, a parameter set may be derived for a given piston loading such that the piston and displacer oscillate with zero damping within the confines of their stroke limits. However, in the case of a load simulated by a dynamometer under the influence of a control system, the engine load is neither linear nor are the load coefficients constant both within a cycle and between cycles. Thus the stability boundary hypersurface continuously changes its locus as the load changes. These factors make an a priori analytic computation of a suitable parameter set infeasible. Hence, in order to quantify the effect of the gas dynamic model on the engine stability, it is necessary to introduce the concept of a stability band. This may be defined as that region of the parameter space confining the stability boundary hypersurface such that the displacer and piston oscillate within their stroke limits. The magnitude of this band or its bandwidth is a measure of the ability of a free piston Stirling engine to respond to non-uniform and continuously varying loads while maintaining stroke amplitudes within the confines of its casing. A broad bandwidth is thus practically important as it enables the large irreversibilities and consequent decrease in efficiency associated with end stop impacts to be avoided.

In the case of a real engine, the stability bandwidth is broad, which means that the piston and displacer will asymptotically converge to a condition at which the damping terms become zero for a wide range of intra- and extra-cyclically varying loads. Hence, as the load is increased, the displacement amplitudes decrease uniformly within the stability band limits and vice versa. Furthermore, the piston and displacer will only hit their respective end stops when the load becomes small.

In contrast, an engine which has theoretically isothermal working spaces has an extremely narrow stability bandwidth. In the context of a dynamometer applied load, this means that for stability boundary hypersurface loci within the stability band, as the dynamometer responds to changes in the piston dynamics, the damping factors continuously change sign which is manifested by seemingly unstable engine/dynamometer behavior. It may be noted that changes of less than 10 percent in piston loading when expressed in linear constant coefficient terms are sufficient to span the stability band while the dynamometer control system typically changes the imposed loading in a non-linear and non-uniform manner by as much as several thousand percent during the convergence process. Thus, the stability of the dynamometer itself cannot be investigated under these conditions. This dilemma may be overcome by choosing an initial parameter set such that under converged loading conditions, the engine operates just beyond the confines of the stability band. A pragmatic definition of the "just beyond the stability band" condi- tion has been found to be a parameter set which results in the piston alone hitting its bottom stop at a converged operating state.

In reality, this frame of reference for defining the converged free piston Stirling engine operating state under isothermal conditions poses a more severe test for the dynamometer control system than would occur under real conditions. The control system must be capable of compensating for the inertial and gravitational effects of the relatively large dynamometer armature mass (1/3 that of the piston itself) by adjusting the driving current continuously throughout the cycle in order that the simulated load faithfully tracks that desired. The discontinuity in the piston dynamic profiles caused by the end stop being hit results in a similar discontinuity in the load profile. This discontinuity serves to exascerbate the demands made upon the control system compensation process owing to the presence of the armature mass.

Hence, although the isothermal engine model used as the simulation test bench for evaluating the dynamometer does not possess the stability band of a real engine, the model provides a completely adequate test environment. Not only does the engine model fall within the definition of the "arbitrary" driving device specified, but also it results in a more severe operating environment for the dynamometer than can be reasonably expected in reality. Hence, the findings and conclusions with regard to the dynamometer convergence, stability, and accuracy apply without qualification to any likely free piston Stirling engine operating environment.

2.3.3.4 Overstroke Control

One of the objectives of the investigation is to determine the effect of various strategies for dealing with under- and over-stroking of the piston and displacer as a result of the changes caused in the load profile by the dynamometer control system during the convergence process. There appear to be two prime reasons to be concerned with over-stroking in particular. These are:

- to prevent physical damage to the engine and dynamometer, and
- to accelerate the convergence process.

It may be recognized that there are two distinct aspects to the over-stroke control problem; one pertaining to the displacer, and the other to the piston. In terms of the design of the RE-1000 FPSE in particular, which has a displacer that is sprung to ground, there is no dynamic coupling between the piston and displacer. This means that the control system has no knowledge of the displacer stroke and, hence, there is no means by which the control system may attempt to prevent displacer over-stroking by adjusting the effective load profile experienced by the piston. In this respect, the dynamometer and its control system mimic the characteristics of most real loads which likewise have no knowledge of the displacer dynamics.

It is, however, theoretically possible to measure the displacer acceleration, velocity, and displacement and build a model of the engine dynamics into the control system. This would enable negative feedback corrections to be superimposed upon the armature current corrections such that attempts at displacer over-stroke control may be made. However, such a dynamometer would no longer be truly representative of a real load and, in addition, would result in a significantly increased cost and complexity for the control system. Thus, it may be concluded that in terms of the project constraints and objectives, control of displacer over-stroking via the dynamometer control system is not possible. It may also be recognized that, depending on the displacer dynamics, in actual engines, the displacer and piston strokes tend to be approximately equal. Hence, maintaining the piston within its stroke limits would tend to keep the displacer within its stroke limits as well.

In terms of the narrow stability band of the isothermal engine model used in the simulation as well as the designated operating stability point of requiring the piston to hit its bottom stop, the investigation of various over-stroke control methodologies proved to be an extremely delicate and time-consuming process. This arises since any over-stroke control method attempted which is successful in preventing the piston from bottoming out immediately results in the stability band being traversed and the isothermal engine becoming unstable. This is physically consistent for an over-stroke control scheme implemented as part of the feedback process which results in the piston being subjected to a load profile which is different from that determined by the dynamics of the desired load alone. Nevertheless, a wide variety of over-stroke control schemes were attempted, some of which are:

a. Fixed loads of opposite sign to those of the velocity were applied to the armature at the top of the upward piston stroke and the bottom of its downward stroke. These loads were assigned a magnitude corresponding to the maximum available design current of 127 A (yielding approximately 3300 N) and were applied over various lengths. These load currents were held constant and were not subject to control system feedback correction.

b. The same scheme as above except that the end stroke loads were subject to control system feedback correction.

c. The displacement addresses not traversed by the piston during the previous stroke were loaded with currents determined from an extrapolation of the stored force, velocity, and acceleration profiles. Various extrapolation techniques were attempted, such as using the maximum recorded force values for each stroke direction as well as linear, quadratic, and sinusoidal profiles determined by using stroke magnitude scaled values.

d. Preloading the armature with a set of currents representing a linear base load designed such that the engine would operate within its stability band.

Each of these strategies was complimented with various changes to the feedback scheme in an attempt to prevent the engine from becoming unstable. The most success was achieved with option b. listed above, the least with option a. Both schemes, however, prevented convergence from being attained. Schemes c. and d. had no effect on the intermediate or ultimate converged over-stroking behavior of the engine/dynamometer system, the latter behavior being entirely a function of the engine/load parameter set. The only effect of these strategies was to cause a large decrease in the convergence rate, which resulted in convergence being achieved in five times (or greater) as many machine cycles as would occur without the over-stroke control strategy. This phenomenon is intuitively reasonable, since the control system needs to overcome the artificial effects caused by the over-stroke control strategy which are out of alignment with the dynamic characteristics of the desired loading in the contest of the negative feedback modus operandi.

At the termination of this experimentation, it was realized that the implementation of piston over-stroke control via the dynamometer control system is irreconcilable in rigorous terms with the goal of having the dynamometer duplicate the characteristics of any desired loading as accurately as possible. This arises since the introduction of over-stroke control strategies (such as those of schemes a. and b. above) into the feedback loop corrupts the feedback process such that the control system attempts to converge to two loading characteristics simultaneously. The corruption is exascerbated if the characteristics are mutually exclusive. This results in predictable hunting as the control system begins to converge to a set of currents corresponding to the over-stroke control load and then switches to converging towards the desired load currents.

Hence, it is concluded that over-stroke control should be completely excluded from the dynamometer control loop. This enables the control system to monolithically converge towards the faithful replication of the desired loading which philosophically seems to be the ideal. If a real loading device would cause the engine to over-stroke, then if the dynamometer were intended to exactly mimic the loading device, it should also cause the engine to over-stroke.

In the context of a real free piston Stirling engine with a broad stability band, the over-stroke control problem essentially vanishes if the control system is capable of duplicating the desired load in a transient manner. This arises since if an actual load coupled to an actual engine does not produce over- stroking, then the dynamometer should also not produce any over-stroking. This has been verified using the simulation program by tracing the oscillation of the system when started from rest, firstly with the load coupled directly to the piston without the presence of the dynamometer, and then with the load being applied via the dynamometer. In both cases, the over-stroking behavior of the displacer and piston was congruent.

This, from an overall perspective, to the extent that piston and/or displacer over-stroking is liable to be a problem, it should be dealt with mechanically by including dampers in the engine/dynamometer hardware. Such an arrangement would prevent over-stroking from causing any damage while simultaneously maintaining the integrity of the dynamometer control system feedback process.

Piston under-stroking control was demonstrated to be irrelevant in view of the control system convergence performance. The control system is inherently fail-safe in that the applied load can never exceed the desired load. This results from the characteristics of the negative feedback loop as well as a fixed upper limit on the power supply current.

2.3.3.5 Discussion of Results

The results are presented in two sections. The first discusses the engine parameter set, while the second describes a representative series of simulation runs which demonstrate the convergence, accuracy, and stability characteristics of the dynamometer control system.

System Parameter Set

The baseline parameter set is described in Table 2.5. The parameters chosen represent the Sunpower RE-1000 free piston Stirling engine as reported by Schreiber [6]. The displacer parameters represent those for displacer 1 which has a design phase angle of 45° with respect to the piston and a design stroke equal to that of the piston. The operating parameters (expansion and compression space temperatures, charge pressure, and working fluid) are taken from Tables I and V of Schreiber's report which correspond to an actual engine test performed at NASA-Lewis Research Center.

Table 2.5: Simulation Test Sequence Baseline Parameter Set

EXPANSION SPACE		
1	Midstroke volume (cm) =	64.005
2	Isothermal temperature (deg C) =	578.000
3	Cylinder nominal diameter (mm) =	56.700
HEATER		
1	Number of tubes =	34.000
2	Tube inside diameter (mm) =	2.362
3	Length (mm) =	183.400
REGENERATOR		
1	Annular gap outer diameter (mm) =	71.800
2	Annular gap inner diameter (mm) =	60.700
3	Length (mm) =	64.460
4	Matrix porosity (percent) =	75.900
COOLER		
1	Number of passages =	135.000
2	Passage width (mm) =	.508
3	Passage depth (mm) =	3.760
4	Length (mm) =	79.200
COMPRESSION SPACE		
1	Midstroke volume (cm) =	158.288
2	Isothermal temperature (deg C) =	40.000
WORKING FLUID		
1	Charge pressure (bar) =	70.000
2	Type (1 = Helium, 2 = Hydrogen, 3 = Air) =	1.000

Table 2.5: Simulation Test Sequence Baseline Parameter Set (continued)

DISPLACER

1	Guiding rod diameter (mm) =	16.630
2	Gas spring midstroke volume (cm) =	31.790
3	Linear damping coefficient (kg/s) =	40.000
4	Mass (kg) =	0.426
5	Maximum stroke between stops (mm) =	40.400

PISTON

1	Bounce space midstroke volume (cm) =	20500.000
2	Linear damping coefficient (kg/s) =	10.000
3	Mass (kg) =	6.200
4	Maximum stroke between stops (mm) =	42.000

DYNAMOMETER ARMATURE

1	Wire length (m) =	35.940
2	Linear damping coefficient (kg/s) =	0.500
3	Mass (kg) =	2.200

DYNAMOMETER STATOR

1	Magnetic flux density (T) =	0.719

DISPLACEMENT TRANSDUCER

1	Resolution (1000 maximum) =	500.000
2	Graticule aperture (mm) =	0.020

USER DEFINED LOAD

1	Mass (kg) =	0.000
2	Linear damping coefficient (kg/s) =	0.000
3	Quadratic damping coefficient (kg/m) =	60.000
4	Coulombic damping coefficient (N m/s) =	0.000
5	Thermodynamic constant coefficient (1/N) =	0.000
6	Thermodynamic displacement coefficient (1/N m) =	0.000

The dynamometer armature and stator characteristics are design values given in Table 2.5 with the exception of the linear damping coefficient. No design value is available for this parameter with the qualification that it is expected to be small. The value of 0.5 kg/s used is an arbitrary value whose magnitude is largely irrelevant since, as discussed previously, the control system completely compensates for its effect.

The linear damping characteristics assigned to the piston and displacer are again largely arbitrary, as no empirical data which would enable their more exact determination could be obtained. The values chosen are thus selected to enable the desired converged engine operating stability criterion to be achieved; namely, a state at which the piston alone impacts its bottom stop. The approximately correct 45° displacer/piston phasing is obtained by adjusting the displacer linear damping coefficient. The values in the range of 40-80 kg/s used during the simulation testing process are perhaps a little high; nevertheless, it should be noted that these damping coefficients are the only means of accounting for all the displacer dynamic as well as all the gas dynamic dissipation effects.

The only other parameter that is varied in order to achieve the defined stability point is the displacer guiding rod diameter. The 16.63 mm diameter of the actual displacer rod causes both the displacer and the piston to over-stroke under isothermal working space conditions as may be expected. A reduction of this diameter to 14 mm effectively compensates for the higher work output of the isothermal engine and enables the specified converged operating condition to be achieved.

The only other parameters warranting comment are those pertaining to the displacement transducer. The program is structured in terms of its data storage capability to permit the use of a displacement transducer with a resolution of 1000 points over the maximum piston stroke of 42 mm. In the case of the optical displacement transducer design envisioned as part of the displacement indexing unit (Figure 2.22), this would result in a graticule spacing of 0.042 mm. Although technically feasible, such a resolution is considered to be finer than necessary and, hence, the program only allows a maximum graticule spacing of 0.127 mm. This results in a resolution of 331 points over the 42 mm maximum piston stroke such that all user input resolutions greater than this value cause the 331 point resolution to be assigned by default. This choice has been completely justified during the testing process. However, the program may easily be changed to permit the 1000 point resolution to be used. Similarly, a minimum opaque space between graticule apertures of 0.0635 mm is permitted, although this again is believed to be conservative. Some existing optical displacement transducers, for example, have graticule spacings of as low as 0.0254 mm. In conjunction with the selected transducer resolution, the opaque space length determines the allowable graticule aperture which is thus assigned a default value if the input aperture value results in the minimum opaque space length being reduced. In reality, the graticule aperture required is dependent on the response time of the displacement indexing unit electronics as well as the sampling rate of the analog-to-digital conversion and digital storage processes. The detailed design of the displalcement indexing unit does not form part of the control system evaluation process and, hence, the 0.02 mm value chosen for the graticule aperture is believed to be conservative.

Numerical Results

During the course of the investigation into the performance of the dynamometer and its control system, several dozen simulation runs were performed. The results of nine of the most representative and significant of these runs have been selected for discussion, as they encapsulate the findings garnered from all the runs performed and, hence, enable the conclusions drawn to be justified. The results of the nine runs selected are summarized in Table 2.6. Sample printouts produced by the simulation program for run 9 are included in Appendix B.

The parameters listed in Table 2.6 fall into two groups. The first group describes the parameters varied during the simulation runs, while the second group gives an indication of the overall engine/dynamometer system performance. All the parameters listed are essentially self-explanatory. The closure indicator is a measure of the degree to which the p-V diagram closes upon itself when the cumulative enclosed angle reaches or just exceeds 360°. Generally, a closure indicator of less than 0.005 indicates full closure, the residual being caused by cyclic overshoot (that is, closure angles greater than 360°) resultant from the stepped integration process. It may also be observed that for all the runs reported, the sum of the net dissipation and shaft works is less than the indicated cyclic work. The balance is the kinetic energy loss resultant from the displacer and/or piston hitting their respective end stops. The number of machine cycles to convergence is taken to be that number of complete thermodynamic cycles executed in order to achieve a maximum force error ratio of 0.5 percent or less. The convergence process is always commenced from an initial state at which the engine is at rest (zero displacer and piston velocities and displacements). This provides the severest framework for assessing the control system convergence performance.

Runs 1 and 2 investigate the extent to which the dynamometer adulterates the desired load. The nominal RE-1000 FPSE displacer rod diameter of 16.63 mm was used which produced piston and displacer over-stroking. The designated quadratic load is applied directly to the piston in Run 1 as part of the differential equation describing the piston acceleration, while in Run 2, the same load is applied via the dynamometer. During the convergence process, the piston and displacer exhibited similar dynamic characteristics during both runs with the rate of increase of the stroke amplitudes being similar. In terms of the engine performance, at convergence, both runs produced identical indicated works, almost identical operating frequencies, and cyclic shaft work outputs which differ by 0.21 percent. The dissipation produced by Run 2 is greater than that of Run 1 owing to the work done against the linear damping force exerted on the armature itself. At convergence after 23 machine cycles, Run 2 produced a maximum force error of order 0.001 N which corresponds to an error of 0.0014 percent.

Using an identical load to Runs 1 and 2, Run 3 differs by the increase of the displacer linear damping factor to a value of 80 kg/s and the decrease of the displacer guiding rod diameter to 14.0 mm. This run culminated the end of a series of runs performed to fine tune these two parameters to yield the desired converged operating state defined by the piston alone hitting its bottom stop. The parameter set thus obtained results in the engine almost achieving operation within its stability band as evinced by the relatively large number of cycles to convergence. Under these conditions, the simulated

Table 2.6: Dynamometer Simulation Results

Parameter	Simulation Run Number								
	1	2	3	4	5	6	7	8	9
Displacer guiding rod diameter (mm)	16.63	16.63	14.00	14.00	14.00	14.00	14.00	14.00	14.00
Displacer linear damping coefficient	40.00	40.00	80.00	70.00	70.00	70.00	70.00	70.00	70.00
Displacement transducer resolution	331	331	331	331	200	250	250	250	250
Load Characteristics (1)		$-60v^2$			$-1.5a - 60v^2$				(2)
Load application	Direct	Dynam	Dynam	Dynam	Dynam	Dynam	Dynam	Dynam	Dynam
Overstroke control	None	None	None	None	None	None	Fixed	Feedback	None
Closure indicator	0	0	.00133	0	0	0	No closure	No closure	0-.001
Frequency (Hz)	41.318	41.315	32.407	30.986	30.961	30.977	31	31	30.887 30.934
Cyclic indicated work (J)	207.16	207.16	106.40	118.94	116.48	117.95	103-118	106.109	114.44 118.31
Net dissipation (J)	19.184	19.369	13.701	14.530	14.52	14.533	14-16	14	14.564 14.583
Shaft work (J)	96.258	96.060	59.076	63.673	63.555	63.683	70-76	73-76	63.809 63.947
Max. force error (N)	n/a	.00122	.00632	.00037	.00121	.00049	158-407	15-80	.00038 .00073
Max. force error ratio (%)	n/a	.0014	.0662	.0062	.0120	.0033	769-8585	58-999+	.0573 .4963
Max. current (A)	n/a	(3)	(3)	(3)	(3)	43.13	200	230	42.64
Machine cycles to convergence	8	23	49	33	27	27	n/a	n/a	33

Notes: (1) d=displacement in m; v=velocity in m/s; a=acceleration in m/s^2

(2) Load = $-1.5a \quad -15v \quad -55v^2 \quad -20/v\Big|_{|v|>.1} + 1/(.05 + .001d)$

(3) Not recorded, but all less than 50A

frequency of 32.4 Hz obtained is much closer to the measured test frequency of 30.2 Hz [6] compared with the 41.3 Hz of Runs 1 and 2. This indicates the extent to which the Run 3 parameter set compensates for the effect of the isothermal working spaces by reducing the displacer rod diameter. It may be noted that in Runs 2 and 3, the dynamometer control system is required to entirely offset the inertial and gravitational effects of the 2.2 kg armature mass. This perhaps represents the severest test which the control system passed as shown by the smallness of the force errors.

Runs 4 to 6 demonstrate the effect of changing the displacement transducer resolution. In Run 4 and its successors, the displacer linear damping coefficient is reduced to 70 kg/s which slightly increases the definiteness of the desired converged operating state and results in the simulated and measured engine frequencies differing by 0.8 Hz. In addition, for Runs 4 to 8, the load characteristics are updated to include the effect of a 1.5 kg inertial mass, although this load is hypothetical, since the load characteristics do not include the gravitational force component of the inertial mass. This has the effect of somewhat reducing the armature mass compensation requirement while also providing a more realistic load characteristic. The only ostensible effects caused by varying the displacement transducer resolution are small changes in the maximum force error at convergence. There is no definite relationship linking the maximum force error to the resolution, suffice it to say that the resolution of 200 points produces two to three times the error of the higher resolutions. However, both the 200 and 250 point resolution runs reached the 0.5 percent convergence error level after 27 machine cycles compared with the 33 cycles for the maximum default resolution of 331 points. As the resolution of 250 points produced the smallest error, this may be taken to represent a pragmatic optimum. Clearly, in view of the smallness of the force errors produced, transducer resolutions in the range of 200 to 331 points over a 42 mm stroke are more than adequate to produce dynamometer control system convergence, stability, and accuracy, at least in the presence of a continuous load characteristic. Higher resolutions are thus not necessary.

The effects of incorporating various over-stroke control strategies are depicted by Runs 6 to 8. Run 6 demonstrates that convergence is obtained without any over-stroke control. Using the identical set of parameters, Runs 7 and 8 portray the effect of introducing two of the over-stroke control strategies mentioned in Subsection 2.3.3.4. Run 7 incorporates a fixed control mechanism whereby the dynamometer current is fixed at -127 A for the displacement addresses contained within the upmost 2.5 mm of the piston positive stroke, and at +127 A for the addresses within the bottom 2.5 mm of the negative going stroke. These currents are not subject to control system negative feedback correction. Run 7 reveals the oscillatory pattern of the force errors as well as the lack of convergence. This is a manifestation of how the feedback process is thwarted by the fixed armature currents at the piston stroke extremities. It should be recognized that the feedback correction process needs to be operable over the entire stroke, as the armature currents at all displacement addresses are mutually dependent such that it is their combined effect that enables small force errors to be achieved over the entire cycle.

The same over-stroke control strategy used in Run 7 is transplanted into Run 8 with the exception that the desired forces at the stroke extremities are

set to be equivalent to +127 A. This is analagous to changing the characteristics of the desired load such that it represents the superposition of the ($-1.5a - 60v^2$) load and the over-stroke control load. These loads are not related and are discontinuous at their juncture. The resulting non-convergent behavior of the control system is shown by Run 8. The effect of the control system attempting to converge to two different load cycles simultaneously is apparent by the way in which the force errors decline for a few cycles and then suddently diverge beyond the formatted variable output length before beginning to decline again.

Table 2-6 shows the range over which the system performance variables of Runs 7 and 8 oscillate when the steady-state level of non-convergence is attained. In addition, in order to implement these over-stroke control strategies, the maximum dynamometer currents required far exceed the design capacity of the power supply. Hence, other factors being equal, this alone is sufficient to demonstrate the impracticality of including piston over-stroke control as part of the control system function.

Finally, Run 9 demonstrates the convergence of the control system when modelling the most complex load tested. The load consists of a combination of inertial and gravitational forces, linear, quadratic, and Coulombic damping as well as a typical oscillatory, thermodynamic type pressure load. As an extra complication, the load includes a discontinuity such that the Coulombic damping is applied only when the piston velocity has an absolute value which exceeds 0.1 m/s. This results in a desired stepwise application of a 200 N load at four points in the cycle. This is an extreme manifestation of real effects such as the closing of non-return valves in an inertia compressor load. With this load discontinuity, at convergence, the engine exhibits a varying maximum force error characteristic with a value in the range of 0.0004 N to 0.0007 N with a corresponding error ratio in the range of 0.06 percent to 0.5 percent. This is a consequence of the negative feedback error correction mechanism which results in the discontinuities never occurring at precisely the same address from cycle to cycle. As the displacer resolution is increased, the convergence variation may be expected to decrease accordingly. Therefore, even in the presence of sharp discontinuities, resolutions in the range of 250 to 331 points over a 42 mm piston stroke are still adequate to produce control system convergence.

When viewed as a whole, the simulation runs performed demonstrate the convergence, stability, and accuracy of the dynamometer control system without the incorporation of any over-stroke control mechanisms. The worst convergence error obtained of 0.5 percent in ratio terms and 0.006 N in absolute terms are felt to be entirely adequate for all practical purposes. The dynamometer armature currents required are well within the specified capability of the power supply, which leaves considerable scope for applying much greater loads to the engine. Hence, the dynamometer is also capable of being used with engines possessing a higher power rating than the Sunpower RE-1000 FPSE. In all cases, convergence at the 0.5 percent error level is achieved within 50 machine cycles at a nominal 30 Hz which corresponds to a real convergence time of two seconds. This is achieved for a control computer that can complete the armature current updating process within 30 ms which is theoretically within the capabilities of an IBM Personal Computer. However,

even if this processing speed is decreased by a factor of 100, convergence may still be obtained within four minutes. This should be adequate for the practical use of the dynamometer as an engine testing device.

The simulation run results indicate that the four objectives of the investigation have been met such that the performance of the dynamometer control system as well as its ramifications in terms of over-stroke control strategies have been determined. However, it is felt that before any hardware development is commenced, the dynamometer should be simulated in an environment with the engine described by a more physically representative gas dynamic model than the ideal isothermal analysis used in this investigation. The results thereby obtained can be fully expected to confirm the convergence, accuracy, and stability of the control system demonstrated thus far.

2.3.3.6 Findings and Conclusions

a. Conclusions about the dynamometer control system stability may only be inferred from the dynamometer/free piston Stirling engine system behavior if the engine itself is known to be stable when subjected to the desired loading.

b. A free piston Stirling engine modelled with isothermal working spaces has a narrow stability band in comparison with the broad stability band of an actual engine. Hence, the isothermal engine model does not have the same stability characteristics as a real engine when coupled to nonlinear loads which mandates a different definition of its stable operating state. The definition adopted which defines the stability point as occurring when the engine oscillates just beyond its stability band such that the piston alone impacts its bottom stop, results in a more severe dynamometer operating environment than would occur in reality. Hence, if the control system exhibits stability and convergence under such conditions, it will also exhibit similar properties in less severe conditions. Therefore, use of the isothermal engine model provides an adequate simulation environment to test the dynamometer control system stability and convergence.

c. The dynamometer control system is capable of tracking intra- and extra-cyclic transient load changes such that the convergence process may be executed continuously without the necessity of waiting for intermediate equilibrium to be reached. Hence, the rate of convergence only is dependent on the control processor speed, a maximum convergence rate being attained if the armature currents can be updated every cycle.

d. Precise knowledge of the dynamometer armature dynamic and electrical characteristics as well as the power supply calibration is not required, as the control system automatically compensates for all the effects resultant from these uncertainties.

e. Displacer over-stroke control cannot be implemented using the proposed dynamometer control system. Modifications to the control system which would make such control hypothetically possible may only be achieved at the expense of reducing the accuracy of the system in duplicating the desired loading characteristics.

f. In view of the narrow stability band of the isothermal engine model used in the simulation which requires partial piston over-stroking in order to be a useful driving device for convergence and stability testing purposes, the effects of the piston over-stroke control strategies investigated do not warrant unqualified extrapolation to situations in which the dynamometer is coupled to engines which possess a broad stability band. In such situations which typify real hardware, the convergence and accuracy of the control system would in all probability make the necessity of explicit piston over-stroke control practically and philosophically redundant.

g. In the operating environment of an isothermal engine, piston over-stroke control strategies which rely on extrapolations of existing stored piston dynamic data were demonstrated to be ineffective in controlling piston and/or displacer over-stroking. Such strategies caused the rate of convergence to be significantly reduced.

h. In the operating environment of an isothermal engine, piston over-stroke control strategies based upon the imposition of arbitrary end stroke load profiles which are unrelated to the characteristics of the desired load prevent convergence from being achieved. This results from the control system attempting to converge to two mutually exclusive load profiles simultaneously which causes inherent feedback instability.

i. Irrespective of the driving device, piston over-stroke control is apparently optimally implemented by incorporating dashpot dampers or similar mechanical devices into the dynamometer hardware. This permits the control system to monotonically converge while simultaneously guarding against hardware damage.

j. Explicit piston under-stroke control is unnecessary as it is implemented as an intrinsic part of the control system negative feedback process.

k. Using a nominal Sunpower RE-1000 free piston Stirling engine configuration parameter set with the displacer guiding rod diameter and the piston and displacer damping factors adjusted so as to compensate for the effects of the assumed isothermal working spaces, the dynamometer/engine system exhibited the following performance at the defined stability point:

- Over the range of arbitrary loads tested, the maximum force error (that is, the error between the desired load and the shaft load experienced by the piston over an entire cycle) at convergence is less than 0.5 percent. The maximum absolute error magnitude recorded is less than 0.0065 N.

- Convergence at the 0.5 percent maximum force error level is obtained within a maximum of 50 machine cycles from rest over the test sequence, with a mode convergence being attained in the range of 27 to 33 machine cycles.

- The maximum armature driving currents required during the test sequence never exceeded the maximum design capability of the dynamometer. Typical maximum values recorded are below 50 A.

1. During the test sequence, convergence was achieved for an overall control system resolution within the range of 200 to 331 points over a piston stroke of 42 mm. Higher resolutions are thus not necessary, even in the presence of sharp discontinuities in the load profile.

In summary, it may be concluded that all the stipulated objectives have been met and that the convergence, stability, and accuracy of the dynamometer control system have been demonstrated for a variety of arbitrary loading devices when coupled to a representative arbitrary free piston Stirling engine driving device.

2.3.3.7 Recommendations

The computer program embodying the simulation of the free piston Stirling engine and dynamometer together with the control system serves as a dynamic blueprint for any hardware design that may be contemplated. The program may, therefore, be used to parametrically evaluate various design options before they are transformed into actual hardware.

In order to definitely confirm the conclusions drawn with regard to the piston over-stroking behavior, it is suggested that the simulation program be modified to include an engine gas dynamic model incorporating momentum in the working spaces.

The high order of convergence, stability, and accuracy exhibited by the simulated control system serves as an adequate indication that the control system will work satisfactorily in practice. Hence, further development of the linear alternator dynamometer may be undertaken with confidence.

2.4 Free Piston Stirling Engine/Load Analysis and Simulation

This subsection describes supporting thermodynamic/dynamic analyses for the design of a linear alternator dynamometer. The analyses include:

a. A FPSE load model, specifically a double acting inertia compressor,

b. A simulation of double-acting inertia compressor with a prescribed housing motion, and

c. A combined simulation of the RE-1000 FPSE and the double-acting inertia compressor load.

2.4.1 Modeling and Simulation of the Double-Acting Inertia Compressor Load

The FPSE load device that the linear alternator dynamometer is primarily designed to simulate is a double-acting inertia compressor for heat pump applications [1]. The term "inertia compressor" indicates that the compressor has a reciprocating housing and an almost stationary heavy inertia piston inside.

Figure 2.23 represents a schematic of a double-acting inertia compressor. The housing and the power piston of a FPSE (not shown) attached together reciprocate as a unit. The inertia piston consists of two piston disks connected by a piston rod. The housing and the two piston disks of the inertia piston form the two compressor spaces. The space between the two piston disks are separated into two gas spring spaces by a dividing wall. The dividing wall has a hole at the center to accommodate the reciprocating rod of the inertia piston.

The compressor spaces have check valves for suction and discharge. In order to prevent the drifting of the mean position of the inertia piston relative to the housing, the centering port is provided as indicated in the dividing wall and the piston rod.

Based on the schematic for a Double Acting Inertia Compressor shown in Figure 2.23, a computer program was written to simulate the operation of the compressor given, as input, the housing motion specified as a truncated Fourier series. Terms up to the third harmonic are included in the specification of housing motion.

The simulation problem was set up as a system of differential equations evolving in time. Pressure (P) and Density (ρ) of the compressor and gas spring chambers along with inertia piston position and velocity were the solved variables in the system. Equations of continuity and energy were used to specify the time derivatives of P and ρ in the four freon spaces. By differentiating the equation for density, $\rho = M/V$, one obtains:

$$d\rho/dt = 1/V\ (dM/dt - \rho \times dV/dt) \qquad (2\text{-}2)$$

where: dM/dt = rate of mass flow across space boundaries
dV/dt = space volumetric rate of change.

The energy balance equation for each space can be written:

$$(c_v/R)(V \times dP/dt) = -H + Q - (c_p/R)(P \times dV/dt) \qquad (2\text{-}3)$$

where: H = rate of enthalpy transport across valves and seals
Q = heat input from walls.

Equations (2-2) and (2-3) applied to each of the four spaces, together with Newton's equations of motion for the inertia piston, comprise the differential equation system for the simulation.

Some of the key assumptions in the model shown in Figure 2-23 are of interest.

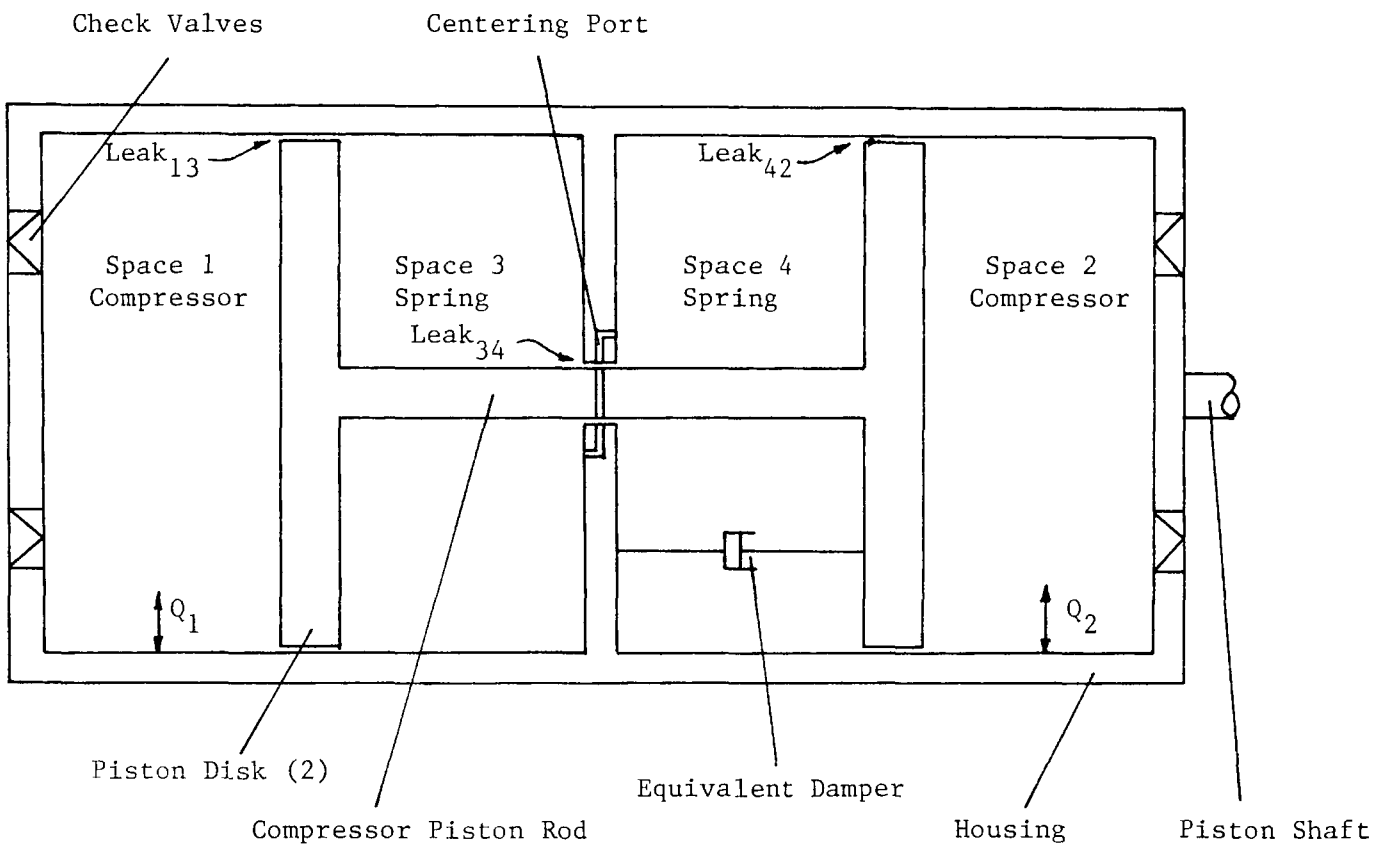

Figure 2.23: Schematic of Double-Acting Inertia Compressor

Cylinder Heat Transfer

Heat transfer between the gas and wall in the compressor spaces was modeled using constant overall heat transfer coefficients based on the following formula [7]:

$$Nu = 0.053 \times Nr^{0.8} \times Npr^{0.6} \qquad (2\text{-}4)$$

where:

- $Nu = h \times d/k$; Nusselt number
- $Nr = \rho \times d^2 \times \omega/(2 \times \mu)$; Reynolds number
- $Npr = \mu \times Cp/k$; Prandtl number
- h = film coefficient
- $d = 4.71 \times D^2 \times z/(3.14 \times D \times z+1.57 \times D^2)$; Adjusted diameter
- D = cylinder diameter
- z = mean clearance between cylinder and piston
- k = gas conductivity
- ρ = gas density
- ω = 1.5 x angular frequency
- μ = gas viscosity

The value of h obtained from the above formula is multiplied by the mean cylinder surface area to obtain an overall heat transfer coefficient which is used as a data input.

Gas Springs

The compressor model contains two gas spring chambers. The pressure versus time in each chamber is solved as a differential equation system instead of approximated by an adiabatic or polytropic equation.

The power loss in the two gas spring spaces due to cyclic heat transfer effects is approximated by the formula [8] below:

$$PL = -\omega P_1^2 V_o (\gamma-1) G(y)/4\gamma P_o \qquad (2\text{-}5)$$

where:

- γ = ratio of specific heats
- $\omega = 2\pi \times$ frequency
- P_1 = pressure amplitude
- P_o = mean spring pressure
- V_o = mean spring volume.
- $G(y)$ = a function of y, non-dimensional hydraulic radius defined in [8].

The power loss is simply modeled by an ideal linear damper introduced between the inertia piston and the housing. The damper is a data input whose value is chosen to absorb the same power as is given by the above formula at the expected operating point. No explicit heat exchange is assumed to take place between the gas and the walls.

Leakage

To evaluate loss mechanisms and in order that equilibrium conditions may be achieved in the gas spring chambers, gas leakage between each gas spring chamber and its adjoining compressor space is modeled. Clearance piston seals are assumed between compressor and spring spaces with clearance gap and seal length specified by data input. Leakage between the two gas spring chambers is also modeled according to geometry specifications for the leak along the piston connecting rod. All leaks are governed by the following equation:

$$\dot{m} = \rho \times w\,[v \times g/2 - g^3 \times (p_2 - p_1)/(12 \times \mu \times L)] \qquad (2\text{-}6)$$

where:

$\dot{m}$ = mass flow rate
ρ = mean density
w = passage width
v = relative velocity between piston and cylinder
g = seal gap
p = pressure
L = passage length.

The first term represents the gas carried by the seal motion, and the second term the gas flow due to pressure drop.

Valves

For normal conditions, the flow through the main compressor valves is governed by the following equation:

$$\dot{m} = P_u \times A \times \mathrm{SQRT}[z \times (r^a - r^b)/(R \times T)] \qquad (2\text{-}7)$$

where:

P_u = Upstream pressure
A = Effective valve area
γ = ratio of specific heats
$z = 2 \times \gamma/(\gamma-1)$
r = Upstream/Downstream pressure ratio
$a = 2/\gamma$
$b = (\gamma+1)/\gamma$.

The program checks for choked sonic flow by monitoring the pressure ratio. If the pressure ratio rises above the critical pressure ratio given by:

$$r_{crit} = [2/(\gamma+1)]^c \qquad (2\text{-}8)$$

where: $c = \gamma/(\gamma-1)$

then the value of r_{crit} replaces r in the valve flow equation.

Bumps

Even though the housing motion is specified, the inertia piston motion is still free to move as the forces dictate. To limit the relative amplitude of the inertial piston in its housing, collision forces are established when

the piston approaches its theoretical limit in either direction. Letting S denote the maximum theoretic piston relative amplitude, the collision force comes into play within 0.075 x S of the extreme positions. This is out of the range of normal operation, since a clearance of 0.15 x S at both ends of the cylinder is normally allowed.

The collision force amounts to an inelastic collision, equivalent to a nonlinear spring force with zero rebound. The collision force rises in inverse proportion to separation as the piston approaches its limit, and drops to zero when the piston withdraws. The force is sized to absorb the momentum of the pending collision before the piston overshoots its theoretical limit.

Dynamics

Newton's equations of motion for the inertia piston must be based on a steady or so-called Newtonian reference frame to be valid. Unfortunately, the coordinate chosen for the motion of the inertial piston is its relative motion with respect to the housing. The housing is not a Newtonian reference frame; its motion is specified relative to the engine cylinder as a truncated Fourier series. Even worse, the engine cylinder is vibrating slightly, more or less depending on its mass. The cylinder is assumed to be suspended by weak springs so that there is negligible reaction from the engine mounts.

It is seen from this digression that the motion of the inertia piston cannot be determined without knowledge of the remainder of the system. For this reason, the masses of the compressor housing, engine cylinder, and displacer are all required as data input to the simulation program. The motion of the displacer is also required input even though it can be argued that the effect of the displacer motion is negligible due to its small mass. It is possible to make the engine cylinder motion negligible by giving it a large mass compared to everything else.

Validations

A Fortran program was written based on the preceding model for the double-acting inertia compressor. The listing of the program is in Appendix C.

The first test of the simulation program was to set it up to duplicate an idealized freon compressor (based on adiabatic analysis) by setting the cylinder heat transfer zero, using large area valves, and setting leak gaps to zero. This effort was assisted by the availability of existing theoretical work on directly driven freon compressors. It was possible to make the inertia compressor into the equivalent of a directly driven compressor by (1) driving the housing sinusoidally, (2) setting the inertia mass very large, and (3) giving the inertia piston the correct initial position and velocity. In this way, the inertia piston remained fixed while the housing moved in relation to it. The simulation was tested in this way and the results compared to those expected from idealized adiabatic compressor analysis. The Fourier decomposition of the pressure waves in the compression spaces agreed with the adiabatic model quite closely. The resultant PV power absorbed was also in good agreement. The adiabatic temperature rise in the compressor

cylinders also matched the theoretical values. In the spring spaces, the pressure changes were nearly those for a simple adiabatic gas spring with no leakage.

Additional tests were done to check the accuracy of some of the non-ideal components of the simulation model. They are the following:

- The heat transfer coefficients in the compressor cylinders were increased to extremely large values. As was expected, the gas temperatures in those spaces became nearly isothermal.

- The subroutines which predict leak and valve flow rates were independently checked for accuracy using several combinations of pressure ratios and relative seal velocities. The goal was to evaluate all possible conditional branches in the subroutines.

- A large interspring leak was simulated as a model for centering port. The pressure amplitudes decreased and PV losses increased in the spring spaces as was expected.

Compressor Simulations

Once the simulation model had been debugged and validated, it was necessary to define and model a more realistic compressor, sized to the Sunpower RE-1000 free piston Stirling engine. Realistic leak geometries, valve areas, and heat transfer coefficients were determined. The relative amplitude of the inertia piston with respect to the housing was arbitrarily chosen to be the same as the absolute amplitude of the housing (2.0E-2 m). It was necessary to use Fourier analysis of the pressure wave of an idealized adiabatic compressor analysis in order to estimate the inertial mass and/or gas spring stiffness required so that the amplitude would indeed approach a real case. This sort of dynamic analysis is always required in any free piston machine. Initially, trouble was encountered with piston collisions, off-center operation, and piston amplitudes either too large or too small. After experimenting with the gas spring stiffnesses and inertia piston mass, it was possible to achieve an operating mode which matched the power output of the RE-1000 at the operating frequency and stroke. The input data and output results of this simulation are included in Appendix C.

2.4.2 Unconstrained Simulation of Compressor and Engine System

The compressor simulation that was described in the previous subsection integrated into the Sunpower nodal analysis [2] so that an unconstrained simulation could be made of the entire engine/compressor system.

Normally, in a simulation problem as complicated as this, it would be quite difficult to put together a smoothly running machine. Fortunately, the results of subsection 2.4.1 were available as were previous results from constrained simulations of the RE-1000 FPSE. Since the compressor had been sized for desired operating point for the engine, it was fairly straightforward to combine the two. Analysis of the net resultant pressure force on the compressor housing, F_r, showed that the engine would see a force given by:

$$F_r = 5860 \sin(\omega t) - 699 \cos(\omega t) \qquad (2\text{-}9)$$

The cos term represents the power absorbed by the compressor, while the sin term represents an equivalent spring force. The power term was matched to the engine by compressor design. It was expected that by adjusting the compressor housing mass, the SIN term could be matched to the engine. Unfortunately, the SIN term turned out to represent the equivalent of a negative spring. A negative spring can be canceled by lightening the housing mass or adding an additional spring between the housing and the engine cylinder. The negative spring was so large, however, that the compressor would have required a negative housing mass to match the engine. It was decided to include an extra spring. The required stiffness of this spring was on the order of 3.8E5 N/m, which is sufficient to swing 8 kg at the design frequency. By varying the inertial piston mass, stroke, or other pump characteristics, it may have been possible to achieve an engine/compressor match without recourse to an added spring. Since this would have required significant work outside the scope of the project, it was never performed.

A simulation was made of the system with the additional spring which ran stably in close proximity to the design point. Since care had been taken earlier to insure that the power growth versus stroke of the compressor was significantly steeper than for the engine, this was no surprise.

The load model developed in subsection 2.4.1 will have to be included in the control system algorithm in Phase II. The results of the unconstrained simulation described in subsection 2.4.2 can be useful to verify the actual dynamometer testing of the RE-1000 FPSE.

3. PHASE II COST ESTIMATE

In this section, the program plan and cost estimate for the Phase II--Detail Design, Fabrication, and Testing of a Linear Alternator Dynamometer--are presented.

3.1 Phase II Program Plan

Phase II is divided into four tasks:

Task 1 - Detailed Analysis and Design

Task 2 - Fabrication of Laboratory Prototype

Task 3 - Installation and Startup Testing

Task 4 - Reports

Brief descriptions for each task are presented in the following subsections.

Task 1 - Detailed Analysis and Design

The objective of Task 1 is to perform a detailed analysis and design in order to finalize the design of the linear alternator dynamometer. Task 1 is divided into four subtasks:

Subtask 1.1 Electromechanical Transducer Final Design

Subtask 1.2 Control System Software Development

Subtask 1.3 Control System Final Design

Subtask 1.4 Preparation of Manufacturing Drawings for Laboratory Prototype

In Subtask 1.1, Electromechanical Transducer Final Design, all aspects of the electromechanical transducer preliminary design performed in Phase I will be reviewed. Included in the review will be transducer electromagnetic design, the coil cooling scheme, flexible lead design, and other design calculations. After the review and necessary design modifications, the transducer design will be finalized.

In Subtask 1.2, Control System Software Development, the detailed control system algorithm will be developed, based on the control system structure recommended in Phase I, as illustrated in Figure 2-22. This will involve detailed investigation of the characteristics of the control system hardware components such as power supplies, various digital storage devices, etc. The electromechanical characteristics of the dynamometer and load characteristics will be also included in the algorithm.

In Subtask 1.3, Control System Final Design, the control system hardware components will be selected and necessary modifications will be specified. The control system software and hardware design will be finalized.

In Subtask 1.4, Preparation of Manufacturing Drawings for Laboratory Prototype, the manufacturing drawings for the dynamometer will be prepared, based on the results of deatailed analysis and design effort. Dimensional tolerances will be checked, and the modifications necessary for ease of manufacturing, servicing, or component replacing will be incorporated in the manufacturing drawings.

Task 2 - Fabrication of Laboratory Prototype

Task 2 includes the procurement, modification, and fabrication of the dynamometer components. Task 2 is divided into two subtasks:

Subtask 2.1 Electromechanical Transducer Fabrication

Subtask 2.2 Control System Fabrication

In Subtask 2.1, Electromechanical Transducer Fabrication, various components of the transducer such as coil tube structure, flexible leads, pressure vessel, and iron cylinders will be procured or fabricated according to the manufacturing drawings.

In Subtask 2.2, Control System Fabrication, all the control system hardware components and accompanying transducers and instrumentation will be purchased. Necessary hardware modifications for the control system components will be performed. The software developed during Subtask 1.2 will be integrated with the hardware components. The control system will be prepared for installation.

Task 3 - Installation and Startup Testing

Task 3 is divided into two subtasks:

Subtask 3.1 Installation

Subtask 3.2 Startup Testing

In Subtask 3.1, the fabricated components of the linear alternator dynamometer will be shipped and installed at a test facility specified by ORNL. It is anticipated that this prototype dynamometer will be integrated with the RE-1000 FPSE or other free piston Stirling engine.

In Subtask 3.2, technical assistance will be given in the preparation of the startup testing. Basic dynamometer performance capabilities will be demonstrated during the startup testing.

Task 4 - Reports

The following reports will be delivered during the Phase II program:

- Project Plan and Quality Assurance Report
- Monthly Reports
- Final Report

Design Review Meetings will be held at the conclusion of Task 1 and Task 3.

Project Schedule

The project schedule that depicts the timing of initiation and completion of tasks, subtasks, various reports and meetings is given in Figure 3-1. The estimated project duration is eighteen months.

3.2 Phase II Cost Estimate*

The cost estimate for Phase II, Detail Design, Fabrication and Testing of a Linear Alternator Dynamometer is presented in this subsection. The cost estimate is based on the program plan briefly described in Subsection 3.1, the preliminary design drawings of Subsection 2.2, and the control system structure described in Subsection 2.3.

Table 3.1 shows the breakdown of Phase II Cost Estimate. The total estimated Phase II Cost and Fee is $272,200.

Table 3.1: Phase II Cost Estimate

Direct Labor Plus Burden	$ 73,380
Travel	12,500
Other Direct Costs	15,000
Direct Material	
Dynamometer/Control System	146,580
Total Phase II Cost:	$247,460
Fee:	24,740
Total Phase II Cost and Fixed Fee:	$272,200

Table 3.2 shows the breakdown of direct material cost. The transducer and other support structures will cost $44,940, and the control system will cost $101,640.

The cost figures given in Tables 3.1 and 3.2 include overhead expenses and general and administrative expenses where applicable.

* Cost estimate is based on the U.S. dollar as of December 31, 1984.

Task No.	Task Description	Months from Start of Phase II Contract (1 2 3 4 5 6 7 8 9 10 11 12 13 14 15 16 17 18)
1.	Detailed Analysis & Design	
1.1	Electromechanical Transducer Final Design	
1.2	Control System Software Development	
1.3	Control System Final Design	
1.4	Preparation of Manufacturing Drawings for Laboratory Prototype	
2.	Fabrication of Laboratory Prototype	
	2.1 Electromechanical Transducer Fabrication	
	2.2 Control System Fabrication	
3.	Installation & Startup Testing	
	3.1 Installation	
	3.2 Startup Testing	
4.	Reports	
	o Project Plan & Quality Assurance Report	▲
	o Monthly Report	▲ ▲ ▲ ▲ ▲ ▲ ▲ ▲ ▲ ▲ ▲ ▲ ▲ ▲ ▲ ▲ ▲
	o Final Report	
	- Draft	
	- Final	▲
	o Review Meeting	▲ ▲

Figure 3.1: Phase II Project Schedule

Table 3.2: Direct Material Cost Breakdown

Transducer and Other Structures		
Tube and Coil	$10,000	
Magnets and Spacers	10,130	
Tube Support Structure	2,560	
Flexible Connection	5,000	
Iron Cylinders and Supports	11,000	
Pressure Vessel	5,000	
Miscellaneous	1,250	
Subtotal:		$ 44,940
Control System		
Power Supply	$20,130	
Main Control System Components	26,500	
Computer & Peripherals	6,130	
Transducers	7,630	
Miscellaneous	3,750	
Software Development	30,000	
Hardware Modification	7,500	
Subtotal:		$101,640
Total Direct Material:		$146,580

4. SUMMARY AND RECOMMENDATIONS

A Preliminary design of a linear alternator type dynamometer is completed. The dynamometer was designed to be used as a versatile load device for free piston Stirling engines with power capacities up to 3 kW, strokes up to 5 cm, and frequencies up to 60 Hz.

The dynamometer has two major components: the electromechanical transducer and the control system. The electromechanical transducer is of moving armature coil/permanent magnet field type. The microprocessor based control system modulates the current in the armature coil according to desired load characteristics.

A detailed digital simulation of the dynamometer load/FPSE system predicts that the dynamometer load simulation will be extremely accurate and fast convergent. These favorable dynamometer characteristics result from the following dynamometer design features:

- very low moving mass,
- extremely low inductance,
- almost constant, uniform magnetic field,
- almost linear current-force relationship, and
- fast convergent and very stable control system.

The proposed dynamometer will be a valuable tool for further understanding of FPSE characteristics under diverse operating conditions and loads. The dynamometer will also help the design of load devices for specific applications by reducing the number and degree of hardware modifications.

It is estimated that the next developmental step, Phase II--Detailed Analysis, Design, Prototype Fabrication and Start-up Test, will take approximately 18 months and cost approximately $272,000.

We strongly recommend that Phase II be initiated soon in order to demonstrate the predictetd capabilities of the dynamometer, and eventually to expedite the commercialization of FPSE devices.

REFERENCES

1. Chiu, W., Hogan, J., Antoniak, Z., "Parametric Testing and Evaluation of A Free Piston Stirling Engine/Linear Compressor System," Proceedings of 18th Intersociety Energy Conversion Engineering Conference, Paper No. 839143, 1983.

2. Gedeon, D., "The Optimization of Stirling Cycle Machines," Proceedings of 13th Intersociety Energy Conversion Engineering Conference, Paper No. 789193, 1978.3.

3. Goldberg, L. F., A Computer Simulation and Experimental Development of Liquid Piston Stirling Cycle Engines. M.Sc. Dissertation, University of the Witwatersrand, Johannesburg, South Africa, 1979.

4. Goldberg, L. F., and Rallis, C. J., "A Prototype Liquid-Piston Free-Displacer Stirling Engine," Proceedings, 14th Intersociety Energy Conversion Engineering Conference, Paper No. 799239, 1979.

5. Goldberg, L. F., Unpublished Research Data and Results.

6. Schreiber, J., Testing and Performance Characteristics of a 1-kw Free Piston Stirling Engine. NASA Technical Memorandum 82999, Lewis Research Center, Cleveland, 1983.

7. Adair, R. P., and Qvale, E. B., "Instantaneous Heat Transfer to the Cylinder Wall in Reciprocating Compressors," Proceedings of 1972 Perdue Compressor Technology Conference, Lafayette, Indiana, 1972.

8. Lee, K. P., "Simplistic Model of Cyclic Heat Transfer Phenomena in Closed Spaces," Proceedings of 18th Intersociety Energy Conversion Engineering Conference, Paper No. 839116, 1983.

9. Roark, R. J., and Young, W. C., Formulas for Stress and Strain, 5th edition, McGraw-Hill, New York, 1975.

10. Rohsenow, W. M., and Choi, H., Heat, Mass, and Momentum Transfer, Prentice-Hall, New Jersey, 1961.

APPENDIX A: MAGNETIC FIELD ANALYSIS FOR THE LINEAR ALTERNATOR DYNAMOMETER

The magnetic field inside the linear alternator dynamometer shown in Figure 2.10 is modelled analytically. The analysis involves solving Maxwell's Equation that governs the electromagnetic phenomena. A computer program based on the analysis is provided.

A.1 Magnetic Field Analysis

Figure A.1 represents the geometry used for the analysis. It shows one pair of concentric permanent magnets situated inside the annulus formed by the two iron cylinders that serve as magnetic flux return paths. The coil, which consists of twenty turns of circumferentially wound wire, is represented by a short cylinder between the magnet cylinders.

The problem is periodic in the axial direction with the fundamental wave number, k, defined by

$$k = 2\pi/\text{period} = \pi/l_s.$$

Magnetization M is assumed constant in the magnets and is given by

$$M(z) = \sum_{n}^{\text{odd}} M_n \sin nkz, \tag{A-1}$$

where: $M_n = (4M_o/n\pi) \sin (n\pi l_m/2l_s)$

M_o = magnetization constant.

The general magnetic field solution is being sought. The Maxwell's equation that governs the electromagnetic phenomena at any point in space is:

$$\nabla \cdot \overline{B} = 0 \tag{A-2}$$

where: $\overline{B}$ is the magnetic flux density vector.

In free space, the magnetic field intensity vector, $\overline{H}$, and $\overline{B}$ are related by the constant, μ_o, known as the permeability of free space:

$$\overline{B} = \mu_o \overline{H}. \tag{A-3}$$

In a current free region,

$$\overline{H} = -\nabla\phi \tag{A-4}$$

where ϕ is a scalar magnetic potential.

Equations (A-2), (A-3) and (A-4) lead to the following equation for the magnetic potential, ϕ:

$$\nabla^2\phi = 0. \tag{A-5}$$

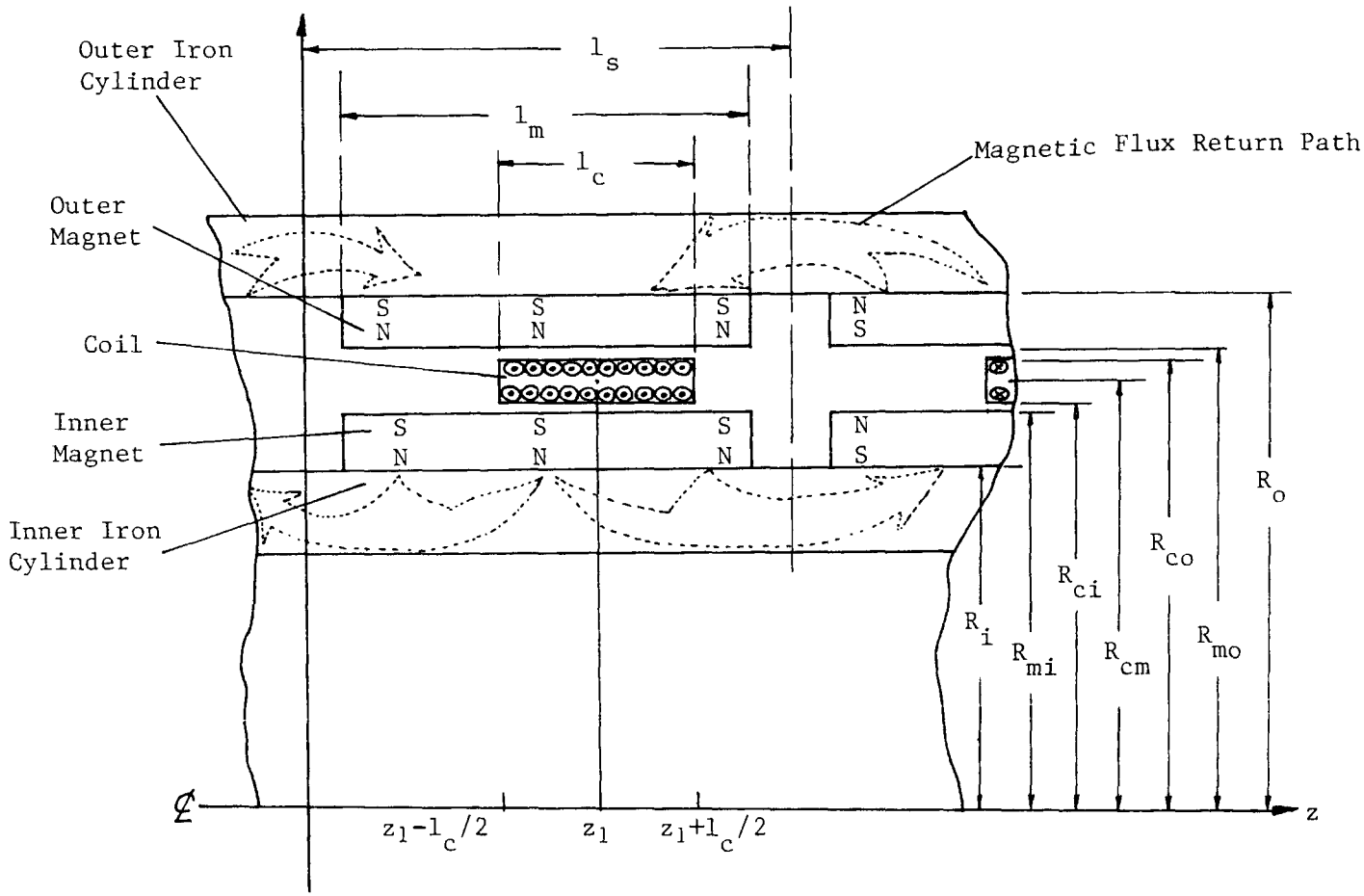

Figure A.1: Geometry and Parameter Definitions for The Magnetic Field Analysis

When ϕ is obtained by applying appropriate boundary conditions to equation (A-5), $\overline{H}$ and $\overline{B}$ can be calculated from equations (A-4) and (A-3), respectively.

The electromagnetic force on the circumferentially wound coil of length L carrying current i is given by the following scalar version of the Lorenz force equation:

$$F = L\ i\ B_r \tag{A-6}$$

where B_r is the radial component of the magnetic field intensity vector $\overline{B}$.

Solution of $\nabla^2\phi = 0$

Since the system is axisymmetric, the equation (A-5) reduces to the equation below:

$$\frac{1}{r}\frac{\partial}{\partial r} r \frac{\partial\phi}{\partial r} + \frac{\partial^2\phi}{\partial z^2} = 0. \tag{A-7}$$

The solution of equation (A-7) can be obtained using Separation of Variables method. The solution for magnetic potential, ϕ, is expressed by

$$\phi(r,z) = \sum_{n}^{odd} \left[A_n I_o(nkr) + B_n K_o(nkr)\right] \sin(nkz) \tag{A-7}$$

where I_o and K_o are modified hyperbolic Bessel Functions of Zeroth order, and n denotes n^{th} space harmonic.

From equations (A-4) and (A-7), the magnetic field intensity vector $\overline{H}$ can be obtained. The following two equations give the axial (z) and radial (r) component of $\overline{H}$:

$$\begin{aligned} H_z &= -\sum_{n}^{odd} nk \left[A_n I_o(nkr) + B_n K_o(nkr)\right] \cos(nkz) \\ H_r &= -\sum_{n}^{odd} nk \left[A_n I_o'(nkr) + B_n K_o'(nkr)\right] \sin(nkz). \end{aligned} \tag{A-8}$$

There are three regions to be considered for the magnetic field analysis:

- Region 1 - outer magnets,
- Region 2 - annular space between magnets, and
- Region 3 - inner magnets.

Each of these regions yields two sets of arbitrary constants A_n, and B_n, for n = odd. We need six boundary conditions to solve for the constants. They are:

$$\begin{aligned} H_{z1} &= 0 \quad \text{at} \quad r = R_o \quad \text{(magnetic boundary)} \\ H_{z1} &= H_{z2} \quad \text{at} \quad r = R_{mo} \quad \text{(Ampere's Law)} \end{aligned} \tag{A-9}$$

$$H_{r1} + M_r = H_{r2} \quad \text{at} \quad r = R_{mo} \quad \text{(Gauss' Law)}$$

$$H_{z2} = H_{z3} \quad \text{at} \quad r = R_{mi} \quad \text{(Ampere's Law)}$$

$$H_{r2} = H_{r3} + M_r \quad \text{at} \quad r = R_{mi} \quad \text{(Gauss' Law)} \tag{A-9}$$

$$H_{z3} = 0 \quad \text{at} \quad r = R_i \quad \text{(magnetic boundary)}$$

After considerable algebra which is omitted here, $H_r(Z)$, the radial magnetic field intensity experienced by the coil windings, is given by the following formula:

$$H_r(Z) = \sum_{j}^{i,o} \sum_{n}^{odd} H_n \sin(nkz)$$

where $H_n = M_n R_{mj} k F_{nj} \left[K(nkR_j) I_o'(nkR_c) - I_o(nkR_j) K_o'(nkR_c)\right]$,

$$M_n = (4M_o/n\pi) \sin(n\pi l_m/2l_s) \text{ and,} \tag{A-10}$$

$$F_{nj} = \left[I_o(nkR_{mj}) K_o(nkR_j) - I_o(nkR_j) K_o(nkR_{mj})\right] \Big/ \left[I_o(nkR_o) K_o(nkR_i) - I_o(nkR_i) K_o(nkR_o)\right] .$$

Force Calculation

In order to calculate the axial force acting on a coil using Equation (A-6), it is necessary to obtain the radial component of $\overline{B}$, $B_r(Z)$. From equations (A-3) and (A-10), $B_r(Z)$ is given as follows:

$$B_r(z) = \mu_o H_r(z),$$
$$= \mu_o \sum_{j}^{i,o} \sum_{n}^{odd} H_n \sin(nkz). \tag{A-11}$$

In the recommended design described in subsection 2.2, the coil wires are flattened to decrease the void volume between wires and thereby increase the space factor. It is reasonable to assume that the coil windings are continuous, not discrete, in the axial direction. Then the average magnetic flux density, B_{av}, for a coil of length l_c whose midpoint is located at $z = z_1$ is given by

$$B_{av} = (1/l_c) \int_{z_1-l_c/2}^{z_1+l_c/2} B_r(z)\, dz \tag{A-12}$$

$$= (2\mu_o/kl_c) \sum_{j}^{i,o} \sum_{n}^{odd} (H_n/n) \sin(nkz_1) \sin(nkl_c/2).$$

There is a total of N_t turns in the four coils shown in Figure 2.10. Since coil winding thickness is much smaller than the mean radius of the coil windings, R_{cm}, it will be assumed that all the coil windings have the radius of R_{cm}. As shown in Figure A.1, poles of the magnets and direction of the current flowing in the coils are arranged so that the forces on the coils are always in phase with one another. Therefore, the total Lorenz force acting on the coils is obtained from

$$F = L_c \; i \; B_{av}, \tag{A-13}$$

where L_c = total length of the coil wire

$= 2\pi R_{cm} N_t$

B_{av} = average flux density given by equation (A-12).

A.2 Other Design Calculations

To find the required thickness of iron in the return magnetic circuit paths, the flux carried by the circuit must be estimated. This is simply half of the flux crossing the gap over the length of a magnet. (Half of the flux of each magnet goes each way.) If the flux density in the return paths between magnets is taken to be the saturation flux density of iron, B_s, (assumed to be 1.5 T), then the iron cylinder thicknesses, t's, are calculated from the following equations:

$$\begin{aligned} &\text{Outer Iron:} \quad t = (\mathrm{SQRT}(R_{osi}\, R_{osi} + f_e\, B_d\, l_m\, R_{cm}/B_s) - R_i)/2 \\ &\text{Inner Iron:} \quad t = (R_i - \mathrm{SQRT}(R_i R_i - f_e \cdot B_d\, l_m\, R_{cm}/B_s) \;\; /2, \end{aligned} \tag{A-14}$$

where f_e is an empirical factor to account for the flux leakages, and B_d is the working flux density obtained by averaging the values of B_{av} over the coil travel distance.

A simple model for temperature rise is used in this calculation. First, dissipation is calculated based on the resistivity of copper (the coil material) and the existing current density. Then a two-layer model for temperature rise is used. One layer is the thermal resistance for an assumed layer of insulating material. The second layer is the film resistance to the cooling medium. Assumed were thermal conductivity of ordinary plastic materials, for the insulation, and for helium moving at mean piston speeds for the film coefficient.

Stress in the epoxy tube carrying coils is calculated to see if the design of that element is adequate. Again, to be conservative, the two components of stress, inertial forces on the coils and the force produced by the dynamometer, are added together as if they were in phase (they will not be in general). The area of the support cylinder is computed using the approximation that it is "thin."

Coil inductance is found by seeing that the permeance faced by a single coil is:

$$P = \mu_o\{\frac{l_c}{6} + \frac{l_s}{2}\}R_i \; ln \; (\frac{R_{osi}}{r}) \tag{A-15}$$

where

l_c is the axial length of the coil and
l_s is the length of the space between coils.

Total flux linked is then the sum of flux linked by all of the coils. Since each coil half faces a separate inductance, it is necessary to separate the winding into 4p sections, then add up 4p inductances. The total inductance is:

$$L = \frac{N_t^2}{4p} \mu_o R_i \; ln(\frac{R_{osi}}{R_i})\{\frac{l_c}{6} + \frac{l_s}{2}\}. \tag{A-16}$$

Speed voltage is computed from the peak velocity of the coils through the magnetic field:

$$v_s = \omega s \; B_d \; \pi \; R_{cm} \; N_t. \tag{A-17}$$

To find terminal voltage, refer to the phasor diagram shown as Figure A.2. Here, the angle is the mechanical power factor angle, ϕ_m. Here, current, representing force, is taken to be the reference. Speed voltage is proportional to, of course, speed and is thus in phase with speed. For the purpose of this calculation, it is assumed that inertia dominates the mechanical system, so that the relationship between inertial voltage and current is apparently capacitive. The resulting expression for terminal voltage (under sinusoidal conditions) is presented in the program.

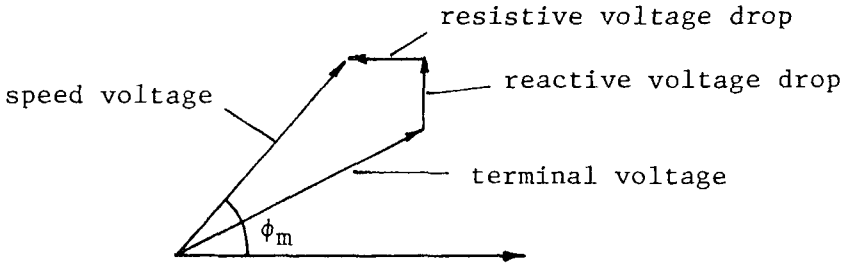

Figure A.2: Voltage Phasor Diagram

A.3 Listing of Dynamometer Design Program

A computer program was written in C language based on the analyses described above. The program listing given includes the main program called "Dyna7.C" which performs the design calculation, and the program

called "bessels.c" that generates the modified hyperbolic functions I_o and K_o. A sample output is given at the end of the listing.

```
#include "stdio.h"
#define pi 3.1415927
main ()
        {
                /* linear tubular dynamometer design program */
                /* Copyright 1983: James L. Kirtley Jr. */
                /* All Rights Reserved */
                /* This program designs multipole, linear, */
                /* tubular short-stroke actuators with */
                /* moving coil between permanent magnets */
                /* this version includes interactive input */
                /* design assumed: half length magnet ends */
                /* Version dyna7 and above use three- dimensional */
                /* field expressions */

                /* declaration of constants */

        double mu=1.25664e-6;    /* permeability of free space */
        double fl=1.1;           /* empirical leakage coefficient */
        double fr=1.2;           /* empirical reluctance coefficient */
        double sig=6.7e7;        /* conductivity of copper */
        double bsat=1.5;         /* saturation flux density of iron */
        double rhofe=7860.0;     /* mass density of steel */
        double rhocu=8910.0;     /* mass density of copper */
        double resin=5.0;        /* insulation thermal resistivity */
        double resfe=0.0125;     /* iron thermal resistivity */

                /* declaration of input parameters */

        double ri,g,tm,tc,lc,s,jc,br,p,nt;
        double om,lam,lmsr,tins,rhom,pf,ffilm;
        double tpl,rhopl;
        double npf,nhf;

                /* declaration of intermediate and output variables */

        double bd,lm,ac,rcm,bw,fp,pa;
        double ltot,rosi,roso,mos,mis,risi;
        double mm,mc,tbi,tbo,fins,fst,qdot,deltat;
        double pdiss,rw,xw,vs,ip,rf,vt,rco,rci;
        double mpl,spl,facc,pav,risq;
        double rmi,rmo,ls,*bav;
        int i,j,np,nh;

                /* declaration of used procedures */

        double sqrt(),log();
        int ninput();
        char *alloc();
        int rbav();

                /* declaration of interactive input variables */

        int cc=1;
        static char *vname[]=
                {"ri","g","tm","tc","lc","s","jc","br",
                 "p","nt","om","lam","lmsr","tins","rhom",
                 "pf","ffilm","tpl","rhopl","np","nh"};
        static double *vptr[21];
```

```
        /* setup pointers for interactive input */

vptr[0]=&ri; vptr[1]=&g; vptr[2]=&tm; vptr[3]=&tc;
vptr[4]=&lc; vptr[5]=&s; vptr[6]=&jc; vptr[7]=&br;
vptr[8]=&p; vptr[9]=&nt; vptr[10]=&om; vptr[11]=&lam;
vptr[12]=&lmsr; vptr[13]=&tins; vptr[14]=&rhom;
vptr[15]=&pf; vptr[16]=&ffilm; vptr[17]=&tpl; vptr[18]=&rhopl;
vptr[19]=&npf; vptr[20]=&nhf;

        /* get input parameters */

printf (" Tubular Linear Dynamometer Design Program: ");
printf ("November 22, 1983\n");
printf ("\n Please type in the following data in SI units:");
printf ("\n Number of magnet pairs ");
scanf ("%lf",&p);
printf (" Magnet inner radius ");
scanf ("%lf",&ri);
printf (" Magnet thickness ");
scanf ("%lf",&tm);
printf (" Relative motion gap ");
scanf ("%lf",&g);
printf (" Coil thickness ");
scanf ("%lf",&tc);
printf (" Coil axial length ");
scanf ("%lf",&lc);
printf (" Stroke ");
scanf ("%lf",&s);
printf (" Coil current density ");
scanf ("%lf",&jc);
printf (" Magnet residual flux density ");
scanf ("%lf",&br);
printf (" Operating radian frequency ");
scanf ("%lf",&om);
printf (" Coil space factor ");
scanf ("%lf",&lam);
printf (" Magnet spacing length ratio ");
scanf ("%lf",&lmsr);
printf (" Magnet mass density ");
scanf ("%lf",&rhom);
printf (" Insulation thickness ");
scanf ("%lf",&tins);
printf (" Number of turns ");
scanf ("%lf",&nt);
printf (" Mechanical power factor ");
scanf ("%lf",&pf);
printf (" Cooling film resistance ");
scanf ("%lf",&ffilm);
printf (" Thickness of plastic structural tube ");
scanf ("%lf",&tpl);
printf (" Density of plastic structural tube ");
scanf ("%lf",&rhopl);
printf (" Number of coil position points ");
scanf ("%lf",&npf);
printf (" Number of space harmonics to consider ");
scanf ("%lf",&nhf);

        /* beginning of the interactive input loop */
```

```
while (cc!=0)
{
if((cc=ninput (21,vname,vptr))==0) break;
        /* translation of integers */

np=npf;
nh=nhf;

        /* calculation of working flux density */
        /* coil mean radii */

rcm=ri+tm+g+0.5*tc;

        /* inner magnet outer radius */

rmi=ri+tm;

        /* outer magnet inner radius */

rmo=ri+tm+tc+2*g;

        /* outer shell inner radius */

rosi=rmo+tm;

        /* magnet length */

lm=lc+s;

        /* interactive section length */

ls=lm+tm*lmsr;

        /* calculation of average working flux */
        /* first, make up storage space */

bav=alloc(8*np);

        /* this next routine does all of the work */

rbav(ls,lm,lc,s,np,nh,ri,rosi,rmi,rmo,rcm,bav);

        /* now average the results over the stroke */

bd=0;
for (i=0;i<np;i++) bd=bd+br*(*(bav+i))/np;

        /* calculation of force capability */
        /* coil effective area */

ac=4.0*p*pi*rcm*lc;

        /* peak force */

fp=ac*jc*tc*bd;

        /* apparent power rating based on sinusoidal motion */
```

```
pa=0.25*fp*s*om;

        /* average power assuming sinusoidal motion */

pav=pa*pf;

        /* total assembly length */

ltot=(2.0*p+1)*(lm+tm*lmsr);

        /* calculation of weights */
        /* outer shell thickness and mass */

roso=sqrt(rosi*rosi+fl*bd*lm*rcm/bsat);
tbo=roso-rosi;
mos=pi*ltot*(roso*roso-rosi*rosi)*rhofe;

        /* inner shell */

if((risq=ri*ri-fl*bd*lm*rcm/bsat)<0)
        {
        risi=0;
        printf ("\n  Insufficient space for inner flux return");
        }
else risi=sqrt(risq);
tbi=ri-risi;
mis=pi*ltot*(ri*ri-risi*risi)*rhofe;

        /* magnets */

mm=2.0*pi*p*lm*((ri+tm)*(ri+tm)-ri*ri)*rhom
        +2.0*pi*p*lm*(rosi*rosi-(rosi-tm)*(rosi-tm))*rhom;

        /* coils */

rci=ri+tm+g;
rco=rci+tc;
mc=2.0*p*pi*lc*lam*(rco*rco-rci*rci)*rhocu;

        /* plastic structure */
        /* assume it is thin and in middle of coil */

mpl=pi*(rci+rco)*tpl*rhopl*ltot;

        /* acceleration force */

facc=0.5*s*om*om*(mc+mpl);

        /* max stress on plastic shell */

spl=(facc+fp)/(pi*(rci+rco)*tpl);

        /* temperature rise calculation: simpleminded */
        /* coil to gas rise, based on insulation */
        /* and gas film rise components */

fins=tins*resin;

        /* heat generated per unit area */
```

```
qdot=0.5*jc*jc*tc/(sig*lam);

        /* now temperature rise */

deltat=0.5*qdot*(fins+ffilm);

        /* total dissipation */

pdiss=qdot*ac;

        /* circuit parameters */
        /* resistance */

rw=2*pi*rcm*nt*nt/(2*p*sig*tc*lc*lam);

        /* inductive reactance */

xw=0.25*om*nt*nt*mu*ri*log(rosi/ri)*(lc/6.0+(lm*(1.0+lmsr)-lc)
        /2.0)/p;

        /* peak speed voltage */

vs=pi*om*s*bd*rcm*nt;

        /* peak current */

ip=2*p*jc*tc*lc/nt;

        /* estimate of terminal voltage */
        /* mechanical reactive power coefficient */

rf=sqrt(1.0-pf*pf);
vt=sqrt((xw*ip-vs*rf)*(xw*ip-vs*rf)+(rw*ip+vs*pf)*(rw*ip+vs*pf));

        /* now output important quantities */

printf ("\n\n\n      Dynamometer Design Summary ");
printf ("\n Design Type: Half length magnet ends, short coil");
printf ("\n\n      Dimensions (m) ");
printf ("\n Total length %g",ltot);
printf ("\n Inner radius %g",risi);
printf ("\n Inner iron thickness %g   Radius %g",tbi,ri);
printf ("\n Magnet thickness %g   Magnet length %g",tm,lm);
printf ("\n Gap dimension %g",g);
printf ("\n Coil thickness %g   Length %g",tc,lc);
printf ("\n Outer iron thickness %g  Outer radius %g",tbo,roso);
printf ("\n Support tube thickness %g",tpl);
printf ("\n Insulation thickness %g",tins);
printf ("\n Stroke %g",s);
printf ("\n Frequency %g rad/sec",om);
printf ("\n Heat transfer film resistance %g C/w m**2",ffilm);
printf ("\n Number of pole pairs %g",p);
printf ("\n      Magnets");
printf ("\n Residual flux density %g T",br);
printf ("\n Working flux density %g T",bd);
printf ("\n Mass density %g kg/m**3",rhom);
printf ("\n Axial spacing ratio %g",lmsr);
printf ("\n      Coils (copper)");
```

```
        printf ("\n Number of turns %g",nt);
        printf ("\n Space factor %g",lam);
        printf ("\n Superficial current density %g",jc);
        printf ("\n      Weights (kg) ");
        printf ("\n Outer Shell %g",mos);
        printf ("\n Coils %g",mc);
        printf ("\n Magnets %g",mm);
        printf ("\n Inner Shell %g",mis);
        printf ("\n Support cylinder %g",mpl);
        printf ("\n      Rating ");
        printf ("\n Peak force %g N",fp);
        printf ("\n Apparent power %g W",pa);
        printf ("\n Average power %g W",pav);
        printf ("\n Mechanical power factor %g",pf);
        printf ("\n Dissipation %g W",pdiss);
        printf ("\n Temperature rise %g C",deltat);
        printf ("\n Voltage %g V",vt);
        printf ("\n Current %g A",ip);
        printf ("\n Resistance %g ohms",rw);
        printf ("\n Reactive impedance %g ohms",xw);
        printf ("\n Support tube stress %g Pa",spl);
        printf ("\n Average relative flux density\n");
        j=0;
        for (i=0;i<np;i++)
                {
                if (j++==5){j=0;printf("\n");}
                printf ("%7.3f ",*(bav+i));
                }
        printf ("\n");
        }                       /* end of interactive input loop */
        }                       /* end of program */
ninput (n,vname,vptr)           /* interactive I/O routine */
int n;                          /* number of variables, array of variable */
char *vname[];                  /* names, and array of variable pointers */
double *vptr[];
        {
        int free (),strcmp();
        char *alloc();
        char *tstr;
        int i;
        int cc=1;               /* valid character read code */
        tstr=alloc(8);
        printf ("\n Mods");
        for (;;)                /* loop until something causes a return */
                {
                printf ("\n?");
                scanf ("%s",tstr);
                if (strcmp (tstr,";")==0)       /* done with input */
                        {
                        free (tstr);            /* free storage */
                        return (1);             /* successful */
                        }
                else if (strcmp (tstr,"/h")==0) /* ask for variables */
                        for (i=0;i<n;i++)
                                printf ("%s ",vname[i]);
                else if (strcmp (tstr,"/q")==0) /* return quit code */
                        {
                        free (tstr);
                        return (0);
```

```
                }
        else    {
                cc=0;                   /* looking for variable */
                for (i=0;i<n;i++)
                        if (strcmp(tstr,vname[i])==0)
                        {
                        cc=1;           /* we have a match */
                        scanf ("%lf",vptr[i]); /* read number */
                        break;
                        }
                if (cc==0) printf ("\n What?");
                }
        }
}

rbav(ls,lm,lc,s,np,nh,ri,ro,rmi,rmo,rc,optr)
double ls,lm,lc,s,ri,ro,rmi,rmo,rc,*optr;
int np,nh;
        {
                /* relative average magnetic flux density for a */
                /* tubular dynamometer, over coil position */
                /* ls,lm,lc are section, magnet, coil lengths */
                /* s is stroke length */
                /* np is number of points to be calculated */
                /* nh is number of space harmonics to consider */
                /* ri,ro,rc are iron inner, outer and coil radii */
                /* rmi and rmo are magnet air gap radii */
                /* optr is expected to be a pointer to enough */
                /* space to hold a vector of dimension np of */
                /* real numbers */
                /* what is calculated is the flux density relative */
                /* to the remnant flux density of the magnet */
                /* three- dimensional field theory is used */
                /* principal assumptions: magnetization is radial */
                /* and constant, permeability is muzero everywhere */

        int i,j,k;
        double xi,xo,xc,xmi,xmo,nthm;
        double sin(),bca(),bcb(),cos();
        double besi(),besk();
        double ao,bo,ai,bi,c,thd,bav,thc,nthc2;
        double *b,*aptr;
        char *alloc();
        int ip();
        double hno,hni;

        b=alloc(8*nh);

                /* first loop over space harmonic number */

        for (i=0;i<nh;i++)
                {
                j=1+2*i;        /* space harmonic index */

                xi=j*pi*ri/ls;  /* arguments to bessel functions */
                xo=j*pi*ro/ls;
                xc=j*pi*rc/ls;
                xmo=j*pi*rmo/ls;
                xmi=j*pi*rmi/ls;
```

```
                nthm=0.5*j*pi*lm/ls;     /* magnet angle */
                thc=pi*lc/ls;            /* coil angle */
                nthc2=0.5*j*thc;         /* electrical angle of coil */

                ao=bca(xi,xc);  /* intermediate combinations */
                ai=-bca(xo,xc);
                bo=bcb(xo,xmo);
                bi=bcb(xi,xmi);
                c=bcb(xi,xo);

                /* relative amplitude of harmonic component */

                hno=4.0*rmo*sin(nthm)*ao*bo/(c*ls);
                hni=4.0*rmi*sin(nthm)*ai*bi/(c*ls);

                *(b+i)=2.0*(hno+hni)*sin(nthc2)/(j*thc);

                }
        for (k=0;k<np;k++)       /* loop over coil positions */
                {
                thd=0.5*pi*k*s/((np-1)*ls);     /* coil electrical position */
                bav=0;
                for (i=0;i<nh;i++)       /* loop over space harmonics */
                        {
                        j=1+2*i;
                        bav=bav+(*(b+i))*cos(j*thd)*ip(j);
                        }

                aptr=optr+k;             /* output pointer location */
                *aptr=bav;               /* write down the answer */
                }                        /* end of position loop */
        }                                /* end of routine */

double bca(x,y)
double x,y;             /* combination function */
        {
        double besi(),besk();
        return (-besi(0,x)*besk(1,y)-besk(0,x)*besi(1,y));
        }

double bcb(x,y)
double x,y;
        {
        double besi(),besk();
        return (besi(0,x)*besk(0,y)-besk(0,x)*besi(0,y));
        }
int ip(n)
int n;
        {
        int j;
        j=n-1;
        if(j%2==0) return (1);
        else return (-1);
        }
```

```
#include "stdio.h"

#define pi 3.1415927
#define tol 1.0e-6
double besi (p,x)
double x;
int p;
        {
        double bi;
        int bia();
        double exp(),sqrt(),bis();
        if (p<0) abort (" besi: negative index");
        if (x<0) abort (" besi: negative argument");
        if (x>60) bi=exp(x)/sqrt(2*pi*x);
        if((x<12)||bia(p,x,&bi)) bi=bis(p,x);
        return (bi);
        }

double bis(p,x)
double x;
int p;
        {
        double fabs();
        double xx;
        int i,fk,k;
        double bi=0;
        double t=1;
        xx=x/2.;
        for (i=1;i<p+1;i++) t=t*xx/i;
        if (t<1.0e-36) bi=0;
        else
                {
                bi=t;
                xx=xx*xx;
                for (k=1;(k<1001)&&((fabs(t)-fabs(bi*tol))>0);k++)
                        {
                        fk=k*(p+k);
                        t=t*xx/fk;
                        bi=bi+t;
                        }
                }
        return (bi);
        }

int bia(p,x,pbi)
double x,*pbi;
int p;
        {
        int ist,fn,k,fk;
        double xx,bi,t;
        double fabs(),sqrt(),exp();
        fn=4*p*p;
        t=1.0;
        bi=1.0;
        xx=0.125/x;
        for (k=1;(k<30)&&((fabs(t)-fabs(bi*tol))>0);k++)
                {
                fk=(2*k-1)*(2*k-1);
                t=t*xx*(fk-fn)/k;
```

```
                bi=bi+t;
                }
        if (k==31) ist=1;
        else
                {
                ist=0;
                bi=bi*exp(x)/sqrt(2.0*pi*x);
                }
        *pbi=bi;
        return (ist);
        }

double besk(p,x)                /* modified bessel function Kp(x) */
double x;
int p;
        {
        double bk;
        double exp(),sqrt(),k0(),k1();
        if (p<0) abort (" besk: negative index ");
        if (x<0) abort (" besk: negative argument ");
        if (x>60) bk=exp(-x)/sqrt(2.0*x/pi);
        else if (p==0) bk=k0(x);
        else if (p==1) bk=k1(x);
        else    {
                double g0,g1,gj;
                int j;
                g0=k0(x);
                g1=k1(x);
                for (j=2;j<p+1;j++)
                        {
                        gj=2*(j-1)*g1/x+g0;
                        g0=g1;
                        g1=gj;
                        }
                bk=gj;
                }
        return (bk);
        }

double k0(x)
double x;
        {
        double bk;
        double log(),sqrt(),exp();
        if (x<1)
                {
                double a,b,z,c,g0,x2j,f,hj,rj;
                int j;
                b=0.5*x;
                a=.57721566+log(b);
                c=b*b;
                g0=-a;
                x2j=1;
                f=1;
                hj=0;
                for (j=1;j<7;j++)
                        {
                        rj=1.0/j;
                        x2j=x2j*c;
```

```
                        f=f*rj*rj;
                        hj=hj+rj;
                        g0=g0+x2j*f*(hj-a);
                        }
                bk=g0;
                }
        else
                {
                double t[12],a,b,c,pa;
                int l;
                a=exp(-x);
                b=1.0/x;
                c=sqrt(b);
                t[0]=b;
                for (l=1;l<12;l++) t[l]=t[l-1]*b;

                pa  = 1.2533141-.1566642*t[0];
                pa += .08811128*t[1]-.09139095*t[2];
                pa += .1344596*t[3]-.2299850*t[4];
                pa += .379241*t[5]-.5247277*t[6];
                pa += .5575368*t[7]-.4262633*t[8];
                pa += .2184518*t[9]-.06680977*t[10]+.009189383*t[11];

                bk=a*c*pa;
                }
        return (bk);
        }

double k1(x)
double x;
        {
        double bk;
        double log(),exp(),sqrt();
        if (x<1)
                {
                double a,b,c,g1,x2j,f,hj,rj;
                int j;
                b=x/2;
                a=.57721566+log(b);
                c=b*b;
                x2j=b;
                f=1;
                hj=1;
                g1=1.0/x+x2j*(.5+a-hj);
                for (j=2;j<9;j++)
                        {
                        x2j=x2j*c;
                        rj=1.0/j;
                        f=f*rj*rj;
                        hj=hj+rj;
                        g1=g1+x2j*f*(.5+(a-hj)*j);
                        }
                bk=g1;
                }
        else
                {
                double a,b,c,t[12],pa;
                int l;
                a=exp(-x);
```

```
                c=sqrt(b);
                t[0]=b;
                for (l=1;l<12;l++) t[l]=t[l-1]*b;

                pa  = 1.2533141+.469997*t[0]-.1468583*t[1];
                pa += .1280427*t[2]-.1736432*t[3]+.2847618*t[4];
                pa += -.4594342*t[5]+.6283381*t[6]-.6632295*t[7];
                pa += .5050239*t[8]-.2581304*t[9];
                pa += .07880001*t[10] -.01082418*t[11];

                bk=a*c*pa;
                }
        return (bk);
        }

double besip (p,arg)
int p;
double arg;
{
double x,y,z;
x = besi (p-1,arg);
y = p * besi (p,arg)/arg;
z = x - y;
return (z);
}

double beskp (p,arg)
int p;
double arg;
{
double x,y,z;
x = -besk (p-1,arg);
y = - p * besk (p,arg)/arg;
z = x + y;
return (z);
}
```

Dynamometer Design Summary
Design Type: Half length magnet ends, short coil

Dimensions (m)
Total length 0.4575
Inner radius 0.017353
Inner iron thickness 0.042647 Radius 0.06
Magnet thickness 0.008 Magnet length 0.0875
Gap dimension 0.001
Coil thickness 0.005 Length 0.0375
Outer iron thickness 0.017935 Outer radius 0.100935
Support tube thickness 0.001
Insulation thickness 0.0005
Stroke 0.05
Frequency 188.5 rad/sec
Heat transfer film resistance 0.0025 C/w m**2
Number of pole pairs 2
Magnets
Residual flux density 1.05 T
Working flux density 0.719033 T
Mass density 8500 kg/m**3
Axial spacing ratio 0.5
Coils (copper)
Number of turns 80
Space factor 0.6
Superficial current density 1.420000E+007
Weights (kg)
Outer Shell 37.267289
Coils 1.801259
Magnets 21.384193
Inner Shell 37.267289
Support cylinder 0.411062
Rating
Peak force 3440.204691 N
Apparent power 8105.982304 W
Average power 2999.213452 W
Mechanical power factor 0.37
Dissipation 845.021619 W
Temperature rise 31.349502 C
Voltage 127.002709 V
Current 133.125 A
Resistance 0.095363 ohms
Reactive impedance 0.000196 ohms
Support tube stress 1.203216E+007 Pa
Average relative flux density
0.694 0.694 0.693 0.688 0.654

APPENDIX B: DIGITAL SIMULATION OF THE CONTROL SYSTEM*

The control system described in subsection 2.3 is simulated by a computer program written in FORTRAN. The simulation algorithm is described in detail using flow charts. The listing and a sample output of the control system simulation program are provided in the following paragraphs.

B.1 Simulation Algorithm Description

The simulation algorithm is depicted in Figures B.1, B.2, and B.3. The overall algorithm is shown in Figure B.1. The algorithm has four principle components. The first component, represented by block 1, performs the simulation initialization process. During this phase, all the engine and dynamometer parameter numerical values are read into the program and transformed into simulation constants in consistent SI units. The displacement transducer input parameters are checked against physical limits, and if these limits are exceeded, default parameter values are computed and assigned. Finally, the various data storage arrays are zeroed and the dynamic variables are assigned initial values. The initialization process also takes care of various machine related functions, such as the assignment of storage, display and printer files.

* APPENDIX B describes the work performed by Professor L. F. Goldberg of the University of Minnesota under ORNL Subcontract No. 11X-39005V.

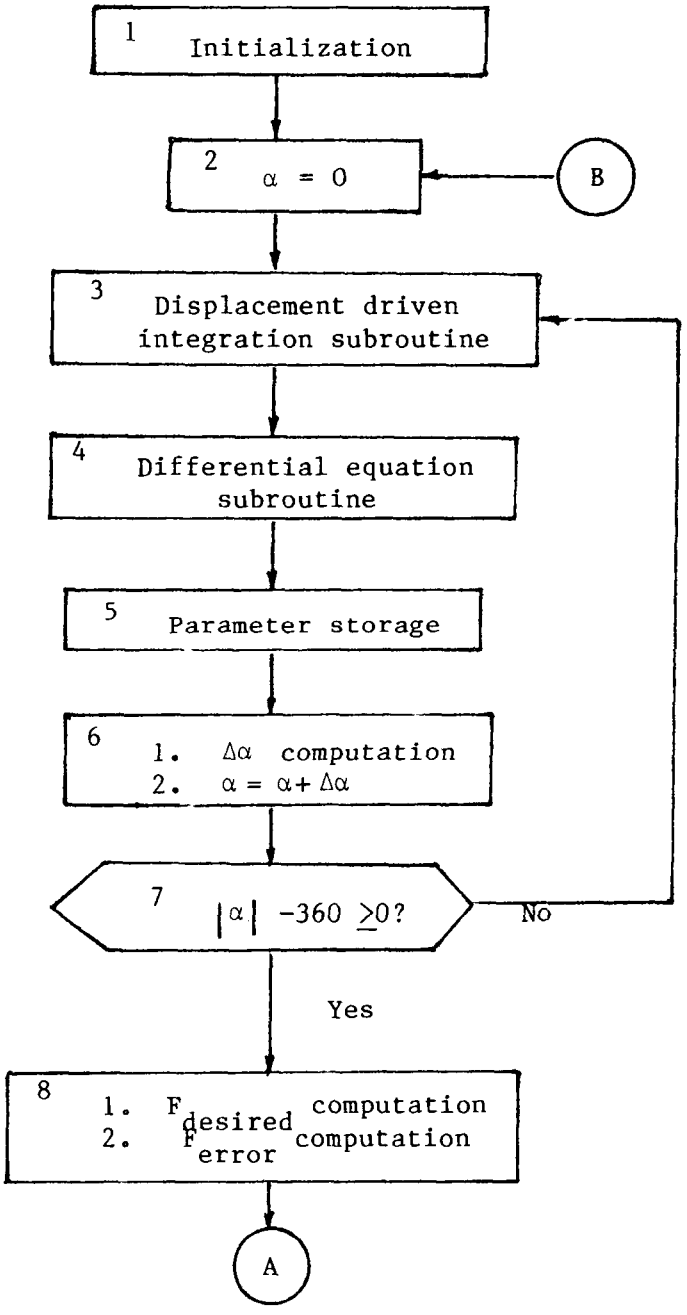

Figure B-1: Simulation Algorithm Main Routine Flowchart

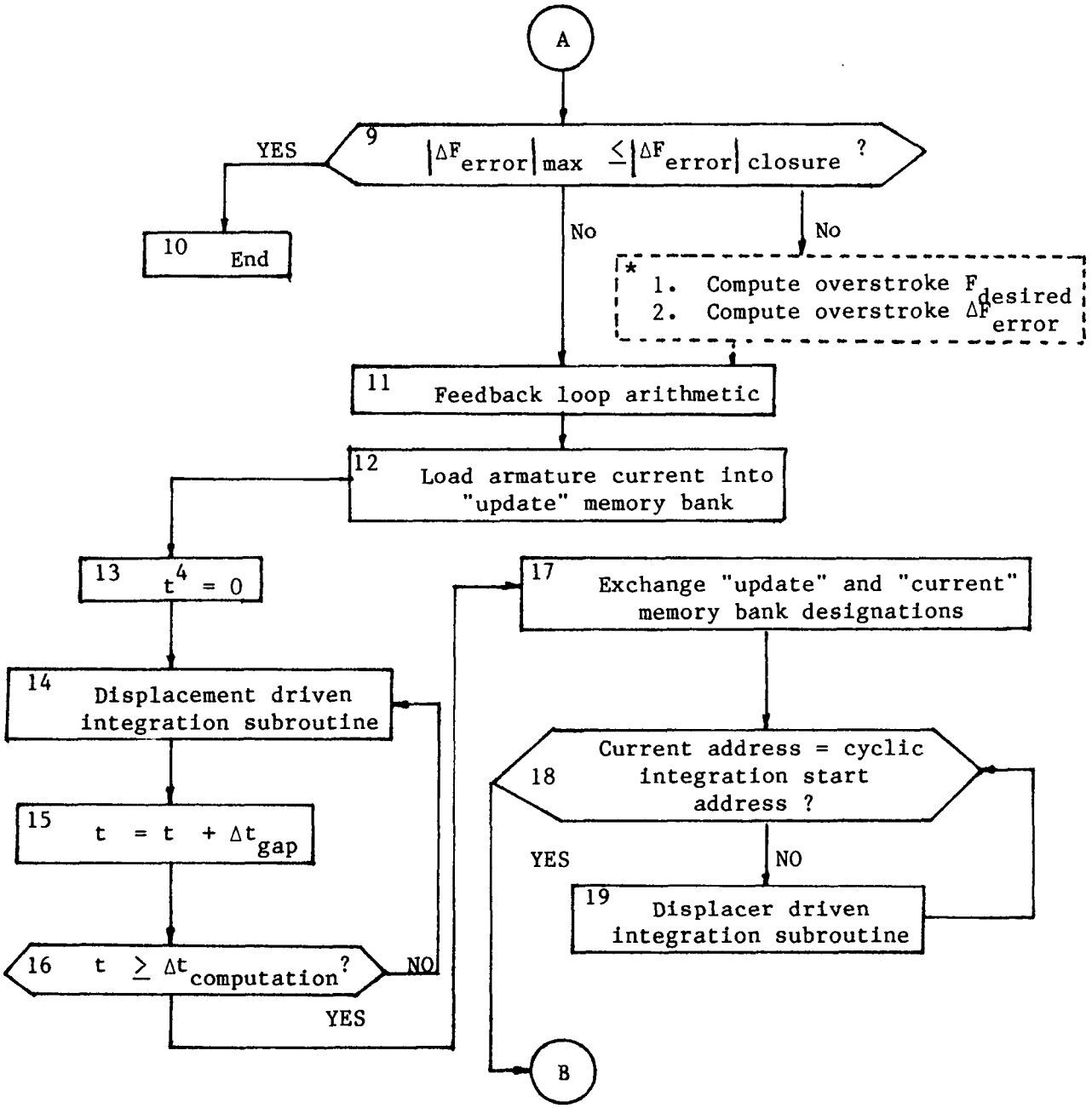

Figure B-1 (continued) - Main Routine Flowchart

The second principal component is represented by blocks 3 to 7. In this section, the set of differential equations describing the engine/dynamometer system is integrated through a complete cycle whose closure is rigorously tested by the thermodynamic condition expressed in block 7. This integration process simulates the digital behavior of the displacement indexing unit and address generator (see Figure 2.22) such that parameter storage occurs only when the transducer generates a new address. As the displacement driven integration subroutine (Figure B.2) simulates the pulsed output of the displacement indexing unit, all the engine variables are likewise recorded and manipulated in a pulsed manner (which duplicates the actual dynamometer mode of operation). This means that the cumulative cycle angle only fortuitously equals 360° at closure but more usually is slightly greater than 360°. This is reflected by all the integrated cyclic work values computed being slightly larger than their values at a closure point of exactly 360°. These work parameters are evaluated purely for the purpose of assessing the stability and convergence of the dynamometer and engine system. They are irrelevant to the function of the control system.

Blocks 8 to 12 define the third principal component of the simulation algorithm. These blocks implement the desired load computation and negative feedback loop portions of the control algorithm shown in Figure 2.22. Block 8 determines the desired force from the stored acceleration, velocity, and displacement (the latter determined by performing a digital-to-analogue conversion on the storage address) and computes the error between the desired and transducer monitored forces. Block 9 checks whether the maximum force error is below that desired and, if so, block 10 terminates the simulation. Block 11 performs the feedback loop arithmetic by converting the force error into an armature current correction and then subtracting the correction from the last used current value. These updated currents are then stored for use by the dynamometer at the appropriate instant (block 12). It may be noted that the simulation is cast in terms of the actual currents used to drive the armature while Figure 2.22 shows that there is an intermediate stage of converting these currents which are output by the power supply into power supply control voltages. As mentioned above, this step is completely immaterial to the dynamometer control system convergence, accuracy and stability characteristics, since it is solely dependent on the design of the particular power supply hardware chosen. Thus, this step is omitted from the simulation algorithm since the extra complication is unwarranted and does not introduce any additional computation but merely results in different numerical values for some constants. The over-stroke control block (as represented by dashed lines and an asterisk, *) is shown in dashed lines since it was found to be redundant (see subsection 2.3.3.4). The block is included in the control algorithm for completeness, since it depicts the methodology used to experiment with various over-stroke control methods during the simulation algorithm development phase.

The final principal compoment of the algorithm is described by blocks 13 to 19. Blocks 13 to 16 sequentially compensate for the real computation time increment during which the computer performs the calculations between blocks 8 and 12 inclusively. This corresponds to the computation time increment in a hardware implementation of the control system and is entirely dependent on the computer used. This real time increment is different from the machine time increment taken to perform the balance of the simulation algorithm which has no influence on the simulated dynamometer performance. Block 17 performs a

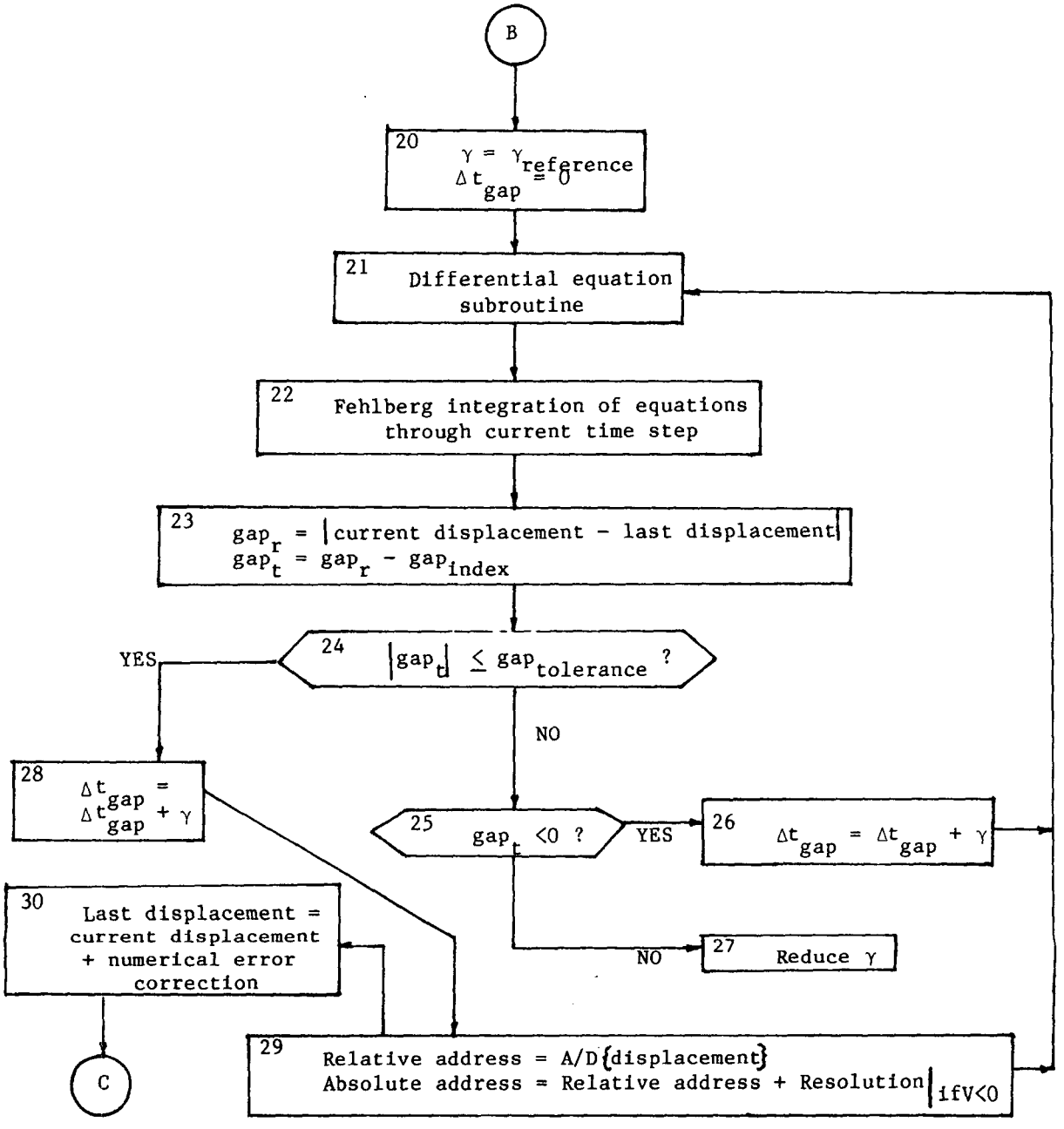

Figure B-2: Displacement Driven Integration Subroutine Flowchart

switching function which enables the dynamometer to commence operating off the most recently computed currents. Lastly, blocks 18 and 19 are included purely for numerical convenience in performing the cyclic integration to determine the various system work outputs. These two blocks once again are redundant to the control system function and have no effect on its simulated performance.

An examination of the control system algorithm as a whole reveals that one of the major concerns voiced about the effectiveness of the control system is resolved. This concern related to the ability of the dynamometer to simulate transient load changes both within and between cycles. The consensus was that prior to the armature currents being updated, the system would have to come to equilibrium. However, the control system simulation has demonstrated that this is not necessary and that the dynamometer currents can be updated continuously if this is physically possible. Indeed, if it were possible to update the armature currents for every address prior to the commencement of each new machine cycle, the fastest possible rate of convergence would be achieved. The convergence rate decreases as the number of machine cycles between updates increases, although convergence is always ultimately achieved.

Figure B.2 shows the details of the displacement driven integration subroutine. As discussed above, the integration process simulates the digital or pulsed output of the displacement indexing unit. Hence, the control variable determining the duration of the integration period is the length of the physical gap between the graticule apertures on the digital displacement transducer. Block 20 initializes the integration time increment to a reference value and zeros the cumulative gap traverse time. Block 22 integrates the equations of block 21 through the increment . Block 23 computes the residual gap length (gap_t) to be traversed after the increment . Blocks 24 to 27 determine the action to be taken as a function of gap_t. If gap_t is small enough, the integration loop is terminated; if the gap_t is negative (i.e., the physical gap is not yet traversed) block 26 is performed and the loop is reentered; and, if $gap_t>0$ indicating that the physical gap has been exceeded, block 27 is executed which reduces so that on the following iteration, gap_t is reduced. The iteration process is repeated until the condition of block 24 is fulfilled. Blocks 28 to 30 complete the displacement driven integration process. Block 28 updates the cumulative gap traverse time while block 29 converts the current analogue displacement to a digital address. Block 30 establishes the current displacement as the last displacement for the next integration process while including a correction for any numerical errors that have arisen in order to prevent the simulation from being polluted with systematic noise.

Finally, Figure B.3 (which is largely self-explanatory) depicts the structure of the differential equation subroutine. Essentially, this consists of a list of equations which enable the various dynamic and thermodynamic variables shown to be computed.

The discussion given in subsection 2.3 and the simulation algorithm flowcharts present an overview of the implementation of the computer program which performs the simulation. The program itself, which comprises over 500 lines of active code, of necessity is rather more intricate in its details than the overview might suggest. However, these details are not intrinsic to the substance of the control system simulation algorithm itself and tend to be

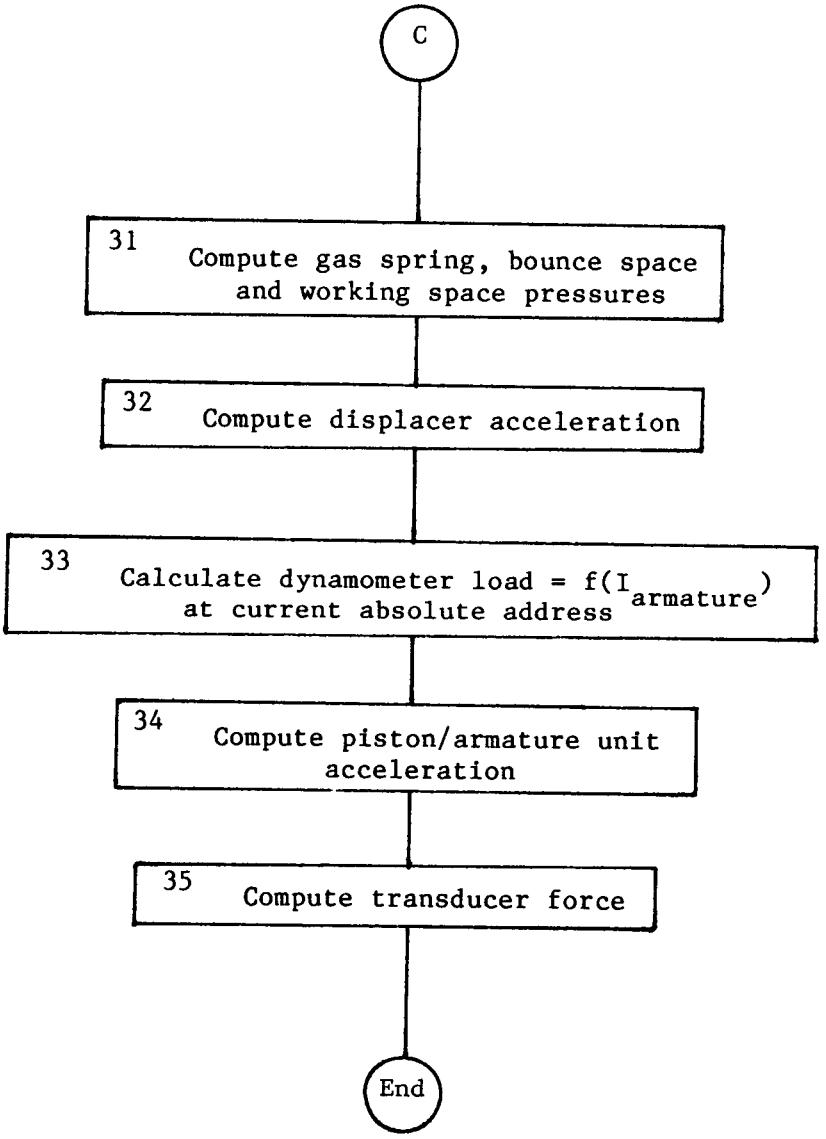

Figure B-3: Differential Equation Subroutine Flowchart

somewhat dependent on the style of the programmer. Hence, in the interest of brevity and clarity, the coding details will not be discussed here, but may be interpreted from the source code listing. The program has been developed and implemented on an IBM Personal Computer incorporating a mathematics co-processor and 576 kBytes of dynamic memory. The FORTRAN 77 standard source code has been compiled with a Microsoft Corporation Version 3.2 Fortran compiler and linked with a Version 2.40 8086 object code linker produced by the same company. The source code is completely transportable and may be implemented with minor modifications to the input/output statements and compiler directives on any computer supporting a standard FORTRAN 77 compiler.

B.2: SIMULATION PROGRAM LISTING AND A SAMPLE RUN PRINTOUT

AAFT	Transducer measured armature force
ADA	Displacer acceleration
ADZMAX	Maximum displacer displacement
ADZMIN	Minimum displacer displacement
ALOAD(*)	User-defined load coefficients
AMALC	Current p-V vector angle
AMALL	Previous p-V vector angle
AMALT	Cumulative p-V vector rotation angle
AMFLAG	Cold start indicator flag
APA	Piston acceleration
APZMAX	Maximum piston displacement
APZMIN	Minimum piston displacement
APZMNT	Minimum piston test displacement
APZMXT	Maximum piston test displacement
AW(1)	Displacer displacement
AW(2)	Piston displacement
AW(3)	Displacer velocity
AW(4)	Piston velocity
AW(5)	Cyclic work done
AW(6)	Cyclic dissipation
AW(7)	Shaft work
AWP	Current normalised working space pressure
AWPCS	Normalised pressure at start of cycle
AWPL	Previous normalised working space pressure
AWPNRM	Normalising working space pressure
AWZVC	Working space normalised cycle closure indicator
BELL	"Bell" control character
CPZ	Current piston displacement
CW(*)	Values of AW(*) at beginning of current time step
DGCV	Rate of change of compression space volume
DGEV	Rate of change of expansion space volume
DW(*)	Temporal derivatives of AW(*): DW(1)=AW(3) DW(2)=AW(4) DW(3)=ADA DW(4)=APA
ESC	"Escape" character
FCR	Force correction
FCRMAX	Maximum force correction
FD	Desired force
FERR	Fractional force error
FERRMX	Maximum fractional force error

GPLG	Current gap length
GPLGI	Displacement transducer slot gap
GPLGT	Test gap length
GPLGNC	Gap tolerance
GPLMAX	Piston stroke between stops
GWV	Current working space volume
GWVCS	Normalised volume at start of cycle
GWVL	Previous normalised working space volume
GWVNRM	Normalising working space volume
IDUM	Dummy integer variable
IMARK	Cycle integration initiation mark index
LIMFLG	Piston displacement limit check control indicator
NADA	Current absolute address
NARES	Displacement transducer resolution (1 in NARES)
NCOMHI	Input parameter index high limit
NCOMLO	Inout parameter index low limit
NCOMRG(*,*)	Component input parameter index range
NCOMP	Machine component selection number
NOFFS	Display list sequencing offset
NOUT	Output device number
NVLB	Input parameter index number
QNUM	p-V vector angle tangent numerator
QDEN	p-V vector angle tangent denominator
QDUM	Dummy real variable
QPI	Pi (3.14159...)
SACC(*)	Acceleration storage array
SIND(*)	Access/update indicator array
STFOR(*)	Transducer force storage array
SVEL(*)	Piston velocity storage array
TAU	Integration time increment
TAUR	Reference integration time increment
TCALC	Real computation time interval
TGAP	Gap traverse time
TGAPSM	Cumulative gap traverse time

YAC	Armature linear damping coefficient
YAI1(*)	Primary armature current table
YAI2(*)	Secondary armature current table
YAICR	Armature current correction
YAICU	Armature current at present address
YAIMAX	Maximum armature current
YAK	Dynamometer force constant
YAM	Armature mass
YBK	Bounce space adiabatic constant
YDC	Displacer linear damping coefficient
YDM	Displacer mass
YAFLAG	Armature current table indicator
YINPUT(*)	Input parameter values
YPC	Piston linear damping coefficient
YPM	Piston mass
YSK	Gas spring adiabatic constant

```
 1: $NOFLOATCALLS
 2: $STORAGE:2
 3:        PROGRAM WESTLAD
 4: C      VERSION A.7.4
 5:        IMPLICIT REAL (A-H),INTEGER (I-P),REAL (Q-Z)
 6:        LOGICAL YAFLAG,AMFLAG,SIND,LIMFLG
 7:        CHARACTER ESC,BELL
 8:        COMMON/CGEOM/GSA,GDA,GRV,GSVD,GBVD,GCVD,GEVD
 9:        COMMON/CGAS/AWM,AET,ART,ACT,YBK,YSK,SR,SGAM
10:        COMMON/CMECH/YDC,YDM,YPC,YPM
11:        COMMON/CARM/YAK,YAC,YAM,ALOAD(6)
12:        COMMON/CLIM/ADZMIN,ADZMAX,APZMIN,APZMAX,APZMNT,APZMXT,LIMFLG
13:        COMMON/VPAR/AW(7),AAFT,GWV,AWP,DW(7),YAICU
14:        COMMON/CURR/YAI1(2000),YAI2(2000),YAFLAG
15:        COMMON/VCONT/NADA,CPZ,GPLGI,GPLMAX,GPLGNC
16:        COMMON/ADDR/NARES
17:        COMMON/TIME/TAUR,TGAP,TCALC,TGAPSM
18:        COMMON/STOR/SIND(2000),SVEL(2000),STFOR(2000),SACC(2000)
19:        DIMENSION YINPUT(39)
20:        DATA QPI/3.141592654/
21:        ESC=CHAR(27)
22:        BELL=CHAR(7)
23:        WRITE(0,'(1X,A1,''[2J'')')ESC
24:        WRITE(0,'('' TYPE 1 FOR NEW DATA, 2 FOR OLD: '',\)')
25:        READ(*,'(I2)')IDUM
26: C
27: C      LOGICAL UNIT ASSIGNMENT
28: C
29:        OPEN(6,FILE='PRN')
30:        IF(IDUM.EQ.1)THEN
31:         OPEN(50,FILE='PARAM.DAT',STATUS='NEW',ACCESS='SEQUENTIAL',
32:       }FORM='UNFORMATTED')
33:        ELSE
34:         OPEN(50,FILE='PARAM.DAT',STATUS='OLD',ACCESS='SEQUENTIAL',
35:       }FORM='UNFORMATTED')
36:        ENDIF
37: C
38: C      PARAMETER INPUT
39: C
40:        IF(IDUM.EQ.1)THEN
41:         DO 10 I=1,12
42:         WRITE(0,'(1X,A1,''[2J'')')ESC
43:         CALL SELECT(I,0,NCOMLO,NCOMHI)
44:         DO 10 J=NCOMLO,NCOMHI
45:         CALL DATRIT(J,0)
46: 10      READ(*,*)YINPUT(J)
47:        ELSE
48:         READ(50)(YINPUT(I),I=1,39)
49:        ENDIF
50: C
51: C      UPDATE/DISPLAY INPUT PARAMETERS
52: C
53:        DO 190 I=1,12
54: 220    WRITE(0,'(1X,A1,''[2J'')')ESC
55:        CALL SELECT(I,0,NCOMLO,NCOMHI)
56:        NOFFS=NCOMLO-1
57:        DO 200 J=NCOMLO,NCOMHI
58:        WRITE(0,'(1X,I2,2X,\)')J-NOFFS
59:        CALL DATRIT(J,0)
```

```
 60: 200   WRITE(0,'(F10.3)')YINPUT(J)
 61:       WRITE(0,'(''0ENTER # OF PARAMETER TO BE UPDATED OR "RETURN"'',
 62:      }'' TO CONTINUE: '',\)')
 63:       READ(*,'(I2)')IDUM
 64:       IF(IDUM.LT.1)GOTO 190
 65: 210   IDUM=IDUM+NOFFS
 66:       IF(IDUM.LT.NCOMLO.OR.IDUM.GT.NCOMHI)THEN
 67:        WRITE(0,'(1X,A1)')BELL
 68:       ELSE
 69:        WRITE(0,'(1X,A1,''[1A'',A1,''[K'',\)')ESC,ESC
 70:        CALL DATRIT(IDUM,0)
 71:        READ(*,*)YINPUT(IDUM)
 72:       ENDIF
 73:       GOTO 220
 74: 190   CONTINUE
 75: C
 76: C     PRINT/DUMP INPUT PARAMETERS
 77: C
 78:       WRITE(0,'(1X,A1,''[2J'')')ESC
 79:       WRITE(0,'('' TYPE 1 TO LIST PARAMETERS, 2 TO CONTINUE: '',\)')
 80:       READ(*,'(I1)')IDUM
 81:       IF(IDUM.EQ.1)THEN
 82:        DO 55 I=1,12
 83:        CALL SELECT(I,6,NCOMLO,NCOMHI)
 84:        DO 50 J=NCOMLO,NCOMHI
 85:        CALL DATRIT(J,6)
 86: 50     WRITE(6,'(F10.3)')YINPUT(J)
 87: 55     WRITE(6,'(1X)')
 88:       ENDIF
 89:       REWIND(50)
 90:       WRITE(50)(YINPUT(I),I=1,39)
 91:       CLOSE(50)
 92: C
 93: C     INPUT PARAMETER CONDITIONING
 94: C
 95:       GEVD=YINPUT(1)*1.E-6+(YINPUT(4)*YINPUT(6)*QPI*
 96:      }YINPUT(5)**2/4.)*1.E-9
 97:       GDA=QPI*YINPUT(3)**2*1.E-6/4.
 98:       AET=YINPUT(2)+273.15
 99:       GCVD=YINPUT(15)*1.E-6+(YINPUT(11)*YINPUT(12)*YINPUT(13)*
100:      }YINPUT(14))*1.E-9
101:       ACT=YINPUT(16)+273.15
102:       GRV=(YINPUT(9)*.01*YINPUT(10)*QPI*(YINPUT(7)**2-
103:      }YINPUT(8)**2)/4.)*1.E-9
104:       GWVNRM=GEVD+GRV+GCVD
105:       ART=(AET-ACT)/LOG(AET/ACT)
106:       IDUM=INT(YINPUT(18))
107:       GOTO(22,24,26)IDUM
108: 22    SR=2079.
109:       SGAM=1.67
110:       GOTO 20
111: 24    SR=4116.
112:       SGAM=1.4
113:       GOTO 20
114: 26    SR=287.
115:       SGAM=1.4
116: 20    AWPNRM=YINPUT(17)*1.01325E5
117:       AWM=AWPNRM*(GEVD+GRV+GCVD)/SR/ACT
118:       AWPNRM=AWM*SR/(GEVD/AET+GRV/ART+GCVD/ACT)
119:       GSA=QPI*YINPUT(19)**2*1.E-6/4.
```

```
120:        GSVD=YINPUT(20)*1.E-6
121:        YDC=YINPUT(21)
122:        YDM=YINPUT(22)
123:        ADZMAX=.5*YINPUT(23)*1.E-3
124:        ADZMIN=-ADZMAX
125:        YSK=(AWPNRM+YDM*9.81/GSA)*GSVD**SGAM
126:        GBVD=YINPUT(24)*1.E-6
127:        YPC=YINPUT(25)
128:        YPM=YINPUT(26)
129:        GPLMAX=YINPUT(27)*1.E-3
130:        APZMAX=.5*GPLMAX
131:        APZMIN=-APZMAX
132:        YAC=YINPUT(29)
133:        YAM=YINPUT(30)
134:        YBK=(AWPNRM+YPM*9.81/GDA)*GBVD**SGAM
135:        YAK=YINPUT(31)*YINPUT(28)
136:        ALOAD(1)=YINPUT(34)
137:        ALOAD(2)=YINPUT(35)
138:        ALOAD(3)=YINPUT(36)
139:        ALOAD(4)=YINPUT(37)
140:        ALOAD(5)=YINPUT(38)
141:        ALOAD(6)=YINPUT(39)
142:        NARES=INT(YINPUT(32))
143:        GPLGI=GPLMAX/(NARES-1)
144:        IF(GPLGI-1.27E-4)30,35,35
145: 30     NARES=INT(GPLMAX/1.27E-4)+1
146:        GPLGI=GPLMAX/(NARES-1)
147:        WRITE(0,'(''0RESOLUTION PHYSICALLY UNATTAINABLE - DEFAULT ''
148:       }''RESOLUTION = '',I4,/)')NARES
149: 35     QDUM=GPLGI-YINPUT(33)*1.E-3
150:        IF(QDUM)42,42,44
151: 44     IF(QDUM-6.35E-5)42,46,46
152: 42     GPLGNC=.5*(GPLGI-6.35E-5)
153:        WRITE(0,'(''0GRATICULE APERTURE PHYSICALLY UNATTAINABLE - ''
154:       }''DEFAULT APERTURE(mm) = '',F5.3,/)')1.E3*GPLGNC
155:        GOTO 40
156: 46     GPLGNC=.5*YINPUT(33)*1.E-3
157: 40     APZMNT=APZMIN+GPLGNC
158:        APZMXT=APZMAX-GPLGNC
159: C
160: C      INITIALISATION
161: C
162:        DO 140 I=1,4
163: 140    AW(I)=0.
164:        WRITE(0,'(''0PISTON STARTING VELOCITY(m/s)='',\)')
165:        READ(0,'(F10.4)')QDUM
166:        AW(4)=QDUM
167:        NADA=NINT(1.+.5*GPLMAX/GPLGI)
168:        AW(2)=(NADA-1)*GPLGI-.5*GPLMAX
169:        CPZ=AW(2)
170:        IMARK=NINT(.5*NARES)
171:        TAUR=.001
172:        DO 120 I=1,2*NARES
173:        SIND(I)=.FALSE.
174:        YAI2(I)=0.
175: 120    YAI1(I)=0.
176:        YAFLAG=.TRUE.
177:        LIMFLG=.FALSE.
178: C
179: C      SIMULATION SEQUENCE START
```

```
C
170   WRITE(0,'(1X,A1,''[2J'',''CYCLIC INTEGRATION'',//)')ESC
      CALL DERIV
      AMFLAG=.TRUE.
      AMALT=0.
      TGAPSM=0.
      YAIMAX=0.
      DO 150 I=5,7
150   AW(I)=0.
      AWPCS=AWP/AWPNRM
      GWVCS=GWV/GWVNRM
C
C     CYCLIC INTEGRATION
C
100   AWPL=AWP/AWPNRM
      GWVL=GWV/GWVNRM
      CALL RUNKG
      CALL DERIV
C
C     DATA STORAGE MODULE
C
      SIND(NADA)=.TRUE.
      SVEL(NADA)=AW(4)
      STFOR(NADA)=AAFT
      SACC(NADA)=DW(4)
C
C     CLOSURE CHECK
C
      QNUM=AWP/AWPNRM-AWPL
      QDEN=GWV/GWVNRM-GWVL
      IF(QNUM)60,62,64
60    IF(QDEN)66,68,70
62    IF(QDEN)72,100,76
64    IF(QDEN)78,80,70
66    AMALC=-QPI+ATAN(QNUM/QDEN)
      GOTO 90
68    AMALC=-.5*QPI
      GOTO 90
70    AMALC=ATAN(QNUM/QDEN)
      GOTO 90
72    AMALC=QPI
      GOTO 90
76    AMALC=0.
      GOTO 90
78    AMALC=QPI+ATAN(QNUM/QDEN)
      GOTO 90
80    AMALC=.5*QPI
90    IF(AMFLAG)THEN
       AMFLAG=.FALSE.
       AMALL=AMALC
      ENDIF
      QDUM=AMALL-AMALC
      IF(ABS(QDUM)-QPI)92,92,94
94    IF(QDUM)96,92,98
96    QDUM=QDUM+2.*QPI
      GOTO 92
98    QDUM=QDUM-2.*QPI
92    AMALT=AMALT+QDUM
      AMALL=AMALC
      QDUM=ABS(YAICU)
```

```
      IF(QDUM.GT.YAIMAX)YAIMAX=QDUM
      WRITE(0,'(''+ADDRESS = '',I4,4X,''ANGLE = '',F8.3,4X,
     }''CURRENT = '',F8.2)')NADA,AMALT*180./QPI,YAICU
      IF(ABS(AMALT)-2.*QPI)100,110,110
110   QNUM=AWPL-AWPCS
      QDEN=GWVL-GWVCS
      AWZVC=SQRT(QNUM**2+QDEN**2)
      WRITE(6,'(''0CLOSURE INDICATOR='',F11.7,2X,''FREQUENCY(Hz)='',
     }F7.3,2X,''MAX CURRENT(A)='',F7.2)')AWZVC,1./TGAPSM,YAIMAX
      WRITE(6,'('' CYCLIC WORK='',E14.7,1X,''DISSIPATION='',E14.7,
     }1X,''SHAFT WORK='',E14.7)')AW(5),AW(6),AW(7)
      CALL DYNAM
C
C     REAL TIME COMPUTATION COMPENSATION
C
      WRITE(0,'(1X,A1,''[2J'',''REAL COMPUTATION TIME = '',F9.3,//)')
     }ESC,1000.*TCALC
      TCHEK=0.
180   CALL RUNKG
      TCHEK=TCHEK+TGAP
      WRITE(0,'(''+ADDRESS = '',I4,3X,''TIME = '',F9.3)')
     }NADA,TCHEK*1000.
      IF(TCHEK.LT.TCALC)GOTO 180
      YAFLAG=.NOT.YAFLAG
C
C     REFERENCE MARK LOCATION
C
      WRITE(0,'(1X,A1,''[2J'',''REFERENCE MARK ADDRESS = '',I4,//)')
     }ESC,IMARK
230   IF(NADA.EQ.IMARK)GOTO 170
      CALL RUNKG
      WRITE(0,'(''+ADDRESS = '',I4)')NADA
      GOTO 230
      STOP
      END
C
C     DISPLACEMENT DRIVEN INTEGRATION SUBROUTINE
C
      SUBROUTINE RUNKG
      IMPLICIT REAL (A-H),INTEGER (I-P),REAL (Q-Z)
      LOGICAL YAFLAG,LIMFLG
      COMMON/CLIM/ADZMIN,ADZMAX,APZMIN,APZMAX,APZMNT,APZMXT,LIMFLG
      COMMON/VPAR/AW(7),AAFT,GWV,AWP,DW(7),YAICU
      COMMON/VCONT/NADA,CPZ,GPLGI,GPLMAX,GPLGNC
      COMMON/ADDR/NARES
      COMMON/TIME/TAUR,TGAP,TCALC,TGAPSM
      DIMENSION AW1(7),AW2(7),AW3(7),CW(7)
      TAU=TAUR
      TGAP=0.
80    DO 10 I=1,7
10    CW(I)=AW(I)
C     *********3RD ORDER FEHLBERG PROCEDURE*********
C     *********FIRST CALL*********
90    CALL DERIV
      DW(1)=AW(3)
      DW(2)=AW(4)
      DO 20 I=1,7
      AW1(I)=TAU*DW(I)
C     *********SECOND CALL*********
20    AW(I)=CW(I)+.25*AW1(I)
```

```
300:        CALL DERIV
301:        DW(1)=AW(3)
302:        DW(2)=AW(4)
303:        DO 30 I=1,7
304:        AW2(I)=TAU*DW(I)
305: C      *********THIRD CALL*********
306: 30     AW(I)=CW(I)+(729.*AW2(I)-189.*AW1(I))/800.
307:        CALL DERIV
308:        DW(1)=AW(3)
309:        DW(2)=AW(4)
310:        DO 50 I=1,7
311: 50     AW(I)=CW(I)+AW2(I)/33.+(214.*AW1(I)+650.*TAU*DW(I))/891.
312: C
313: C      DISPLACER MOTION LIMIT CHECK
314: C
315:        IF(AW(1).GE.ADZMAX)THEN
316:        WRITE(0,'(''0LIMIT CHECK CALLED-DISPLACER MAXIMUM'',/)')
317:         AW(1)=ADZMAX
318:         AW(3)=0.
319:        ENDIF
320:        IF(AW(1).LE.ADZMIN)THEN
321:        WRITE(0,'(''0LIMIT CHECK CALLED-DISPLACER MINIMUM'',/)')
322:         AW(1)=ADZMIN
323:         AW(3)=0.
324:        ENDIF
325: C
326: C      PISTON MOTION LIMIT CHECK
327: C
328:        IF(LIMFLG)THEN
329:         IF(AW(2).GE.APZMAX)THEN
330:         WRITE(0,'(''0LIMIT CHECK CALLED-PISTON MAXIMUM'',/)')
331:          AW(2)=APZMAX
332:          AW(4)=0.
333:         ENDIF
334:         IF(AW(2).LE.APZMIN)THEN
335:         WRITE(0,'(''0LIMIT CHECK CALLED-PISTON MINIMUM'',/)')
336:          AW(2)=APZMIN
337:          AW(4)=0.
338:         ENDIF
339:        ENDIF
340: C
341: C      GAP CONVERGENCE PROCEDURE
342: C
343:        GPLG=ABS(AW(2)-CPZ)
344:        GPLGT=GPLG-GPLGI
345:        IF(ABS(GPLGT)-GPLGNC)60,60,65
346: 65     IF(GPLGT)70,70,75
347: 70     TGAP=TGAP+TAU
348:        GOTO 80
349: 75     TAU=TAU*GPLGI/GPLG
350:        DO 120 I=1,7
351: 120    AW(I)=CW(I)
352:        GOTO 90
353: 60     TGAP=TGAP+TAU
354:        TGAPSM=TGAPSM+TGAP
355: C
356: C      A-D DISPLACEMENT CONVERSION
357: C
358:        IDUM=NINT(1.+(.5*GPLMAX+AW(2))/GPLGI)
359:        IF(AW(4))100,105,105
```

```
100   NADA=IDUM+NARES
      GOTO 110
105   NADA=IDUM
110   CPZ=(IDUM-1)*GPLGI-.5*GPLMAX
C
C     PISTON MOTION LIMIT CHECK AND FLAG CONTROL
C
130   IF(LIMFLG)LIMFLG=.FALSE.
      IF(AW(2).GE.APZMXT)THEN
       WRITE(0,'(''0LIMIT CHECK CALLED-PISTON MAXIMUM FLAGGED'',/)')
       AW(2)=APZMAX
       AW(4)=0.
       LIMFLG=.TRUE.
      ENDIF
      IF(AW(2).LE.APZMNT)THEN
       WRITE(0,'(''0LIMIT CHECK CALLED-PISTON MINIMUM FLAGGED'',/)')
       AW(2)=APZMIN
       AW(4)=0.
       LIMFLG=.TRUE.
      ENDIF
      RETURN
      END
C
C     DERIVATIVE EQUATION EVALUATION SUBROUTINE
C
      SUBROUTINE DERIV
      IMPLICIT REAL (A-H),INTEGER (I-P),REAL (Q-Z)
      LOGICAL YAFLAG
      COMMON/CGEOM/GSA,GDA,GRV,GSVD,GBVD,GCVD,GEVD
      COMMON/CGAS/AWM,AET,ART,ACT,YBK,YSK,SR,SGAM
      COMMON/CMECH/YDC,YDM,YPC,YPM
      COMMON/CARM/YAK,YAC,YAM,ALOAD(6)
      COMMON/VPAR/AW(7),AAFT,GWV,AWP,DW(7),YAICU
      COMMON/CURR/YAI1(2000),YAI2(2000),YAFLAG
      COMMON/VCONT/NADA,CPZ,GPLGI,GPLMAX,GPLGNC
      EQUIVALENCE (AW(1),ADZ),(AW(2),APZ),(AW(3),ADV),(AW(4),APV),
     }(DW(3),ADA),(DW(4),APA)
      GEV=GEVD-GDA*ADZ
      DGEV=-GDA*ADV
      GCV=GCVD+(GDA-GSA)*ADZ-GDA*APZ
      DGCV=(GDA-GSA)*ADV-GDA*APV
      GBV=GBVD+GDA*APZ
      GSV=GSVD+GSA*ADZ
      GWV=GEV+GCV+GRV
      AWP=AWM*SR/(GEV/AET+GRV/ART+GCV/ACT)
      ABP=YBK/GBV**SGAM
      ASP=YSK/GSV**SGAM
      ADA=(GSA*(ASP-AWP)-YDC*ADV)/YDM-9.81
      DW(5)=AWP*(DGEV+DGCV)
      DW(6)=YDC*ADV**2+(YPC+YAC)*APV**2
      IF(YAFLAG)THEN
       YAICU=YAI1(NADA)
      ELSE
       YAICU=YAI2(NADA)
      ENDIF
      AAF=YAK*YAICU
      APA=((ABP-AWP)*GDA-(YPC+YAC)*APV+AAF)/(YPM+YAM)-9.81
      AAFT=AAF-YAC*APV-YAM*(9.81+APA)
      DW(7)=-AAFT*APV
      RETURN
```

```
      END
C
C     DYNAMOMETER CURRENT COMPUTATION MODULE
C
      SUBROUTINE DYNAM
      IMPLICIT REAL (A-H),INTEGER (I-P),REAL (Q-Z)
      LOGICAL YAFLAG,SIND
      COMMON/CARM/YAK,YAC,YAM,ALOAD(6)
      COMMON/CURR/YAI1(2000),YAI2(2000),YAFLAG
      COMMON/ADDR/NARES
      COMMON/TIME/TAUR,TGAP,TCALC,TGAPSM
      COMMON/STOR/SIND(2000),SVEL(2000),STFOR(2000),SACC(2000)
      COMMON/VCONT/NADA,CPZ,GPLGI,GPLMAX,GPLGNC
      FCRMAX=0.
      FERRMX=0.
      DO 10 I=1,2*NARES
      IF(SIND(I))THEN
C
      SIND(I)=.FALSE.
C
C     USER SUPPLIED LOAD DEVICE DESCRIPTION
C
      QDUM=0.
      IF(ABS(SVEL(I))-.1)30,30,35
35    QDUM=-ALOAD(4)/SVEL(I)
30    IF(ALOAD(5))45,40,45
45    SDIS=(I-1)*GPLGI-.5*GPLMAX
      QDUM=QDUM+1./(ALOAD(5)+ALOAD(6)*SDIS)
40    FD=-ALOAD(1)*(9.81+SACC(I))-ALOAD(2)*SVEL(I)-ALOAD(3)*SVEL(I)*
     }ABS(SVEL(I))+QDUM
C
C     NEGATIVE FEEDBACK CURRENT CORRECTION
C
      FCR=STFOR(I)-FD
      YAICR=FCR/YAK
      IF(I.EQ.1.OR.I.EQ.NARES.OR.I.EQ.NARES+1.OR.I.EQ.2*NARES)GOTO 20
      IF(FD)23,26,23
23    FERR=ABS(FCR/FD)
26    QDUM=ABS(FCR)
      IF(QDUM.GT.FCRMAX)FCRMAX=QDUM
      IF(FERR.GT.FERRMX)FERRMX=FERR
20    IF(YAFLAG)THEN
       YAI2(I)=YAI1(I)-YAICR
      ELSE
       YAI1(I)=YAI2(I)-YAICR
      ENDIF
C
      ENDIF
10    CONTINUE
      WRITE(6,'('' MAX FORCE ERROR='',E14.7,2X,''MAX % ERROR='',
     }F9.4)')FCRMAX,FERRMX*100.
      PAUSE
      TCALC=.014
      RETURN
      END
C
C     COMPONENT MODULE SELECTOR ROUTINE
C
      SUBROUTINE SELECT(NCOMP,NOUT,NCOMLO,NCOMHI)
      INTEGER NCOMRG(2,12)
```

```
480:        DATA NCOMRG/1,3,4,6,7,10,11,14,15,16,17,18,19,23,24,27,28,30,
481:       }31,31,32,33,34,39/
482:        GOTO(1,2,3,4,5,6,7,8,9,10,11,12)NCOMP
483: 1      WRITE(NOUT,'('' EXPANSION SPACE'')')
484:        GOTO 20
485: 2      WRITE(NOUT,'('' HEATER'')')
486:        GOTO 20
487: 3      WRITE(NOUT,'('' REGENERATOR'')')
488:        GOTO 20
489: 4      WRITE(NOUT,'('' COOLER'')')
490:        GOTO 20
491: 5      WRITE(NOUT,'('' COMPRESSION SPACE'')')
492:        GOTO 20
493: 6      WRITE(NOUT,'('' WORKING FLUID'')')
494:        GOTO 20
495: 7      WRITE(NOUT,'('' DISPLACER'')')
496:        GOTO 20
497: 8      WRITE(NOUT,'('' PISTON'')')
498:        GOTO 20
499: 9      WRITE(NOUT,'('' DYNAMOMETER ARMATURE'')')
500:        GOTO 20
501: 10     WRITE(NOUT,'('' DYNAMOMETER STATOR'')')
502:        GOTO 20
503: 11     WRITE(NOUT,'('' DISPLACEMENT TRANSDUCER'')')
504:        GOTO 20
505: 12     WRITE(NOUT,'('' USER DEFINED LOAD'')')
506: 20     WRITE(NOUT,'(1X)')
507:        NCOMLO=NCOMRG(1,NCOMP)
508:        NCOMHI=NCOMRG(2,NCOMP)
509:        RETURN
510:        END
511: C
512: C      INPUT VARIABLE LABEL DISPLAY ROUTINE
513: C
514:        SUBROUTINE DATRIT(NVLB,NOUT)
515:        INTEGER MAP(39)
516:        DATA MAP/1,2,3,4,5,6,7,8,6,9,10,11,12,6,1,2,13,14,15,16,17,
517:       }18,19,20,17,18,19,21,17,18,22,23,24,18,17,25,26,27,28/
518:        GOTO(1,2,3,4,5,6,7,8,9,10,11,12,13,14,15,16,17,18,19,20,21,22,
519:       }23,24,25,26,27,28)MAP(NVLB)
520: 1      WRITE(NOUT,'('' Midstroke volume(cm^3)'',\)')
521:        GOTO 50
522: 2      WRITE(NOUT,'('' Isothermal temperature(deg C)'',\)')
523:        GOTO 50
524: 3      WRITE(NOUT,'('' Cylinder nominal diameter(mm)'',\)')
525:        GOTO 50
526: 4      WRITE(NOUT,'('' Number of tubes'',\)')
527:        GOTO 50
528: 5      WRITE(NOUT,'('' Tube inside diameter(mm)'',\)')
529:        GOTO 50
530: 6      WRITE(NOUT,'('' Length(mm)'',\)')
531:        GOTO 50
532: 7      WRITE(NOUT,'('' Annular gap outer diameter(mm)'',\)')
533:        GOTO 50
534: 8      WRITE(NOUT,'('' Annular gap inner diameter(mm)'',\)')
535:        GOTO 50
536: 9      WRITE(NOUT,'('' Matrix porosity(%)'',\)')
537:        GOTO 50
538: 10     WRITE(NOUT,'('' Number of passages'',\)')
539:        GOTO 50
```

```
540: 11    WRITE(NOUT,'('' Passage width(mm)'',\)')
541:       GOTO 50
542: 12    WRITE(NOUT,'('' Passage depth(mm)'',\)')
543:       GOTO 50
544: 13    WRITE(NOUT,'('' Charge pressure(bar)'',\)')
545:       GOTO 50
546: 14    WRITE(NOUT,'('' Type (1 = Helium, 2 = Hydrogen, 3 = Air)'',\)')
547:       GOTO 50
548: 15    WRITE(NOUT,'('' Guiding rod diameter(mm)'',\)')
549:       GOTO 50
550: 16    WRITE(NOUT,'('' Gas spring midstroke volume(cm^3)'',\)')
551:       GOTO 50
552: 17    WRITE(NOUT,'('' Linear damping coefficient(kg/s)'',\)')
553:       GOTO 50
554: 18    WRITE(NOUT,'('' Mass(kg)'',\)')
555:       GOTO 50
556: 19    WRITE(NOUT,'('' Maximum stroke between stops(mm)'',\)')
557:       GOTO 50
558: 20    WRITE(NOUT,'('' Bounce space midstroke volume(cm^3)'',\)')
559:       GOTO 50
560: 21    WRITE(NOUT,'('' Wire length(m)'',\)')
561:       GOTO 50
562: 22    WRITE(NOUT,'('' Magnetic flux density(T)'',\)')
563:       GOTO 50
564: 23    WRITE(NOUT,'('' Resolution (1000 maximum)'',\)')
565:       GOTO 50
566: 24    WRITE(NOUT,'('' Graticule aperture(mm)'',\)')
567:       GOTO 50
568: 25    WRITE(NOUT,'('' Quadratic damping coefficient(kg/m)'',\)')
569:       GOTO 50
570: 26    WRITE(NOUT,'('' Coulombic damping coefficient(N m/s)'',\)')
571:       GOTO 50
572: 27    WRITE(NOUT,'('' Thermodynamic constant coefficient(1/N)'',\)')
573:       GOTO 50
574: 28    WRITE(NOUT,'('' Thermodynamic displacement coefficient(1/N m)'',
575:      }\)')
576: 50    WRITE(NOUT,'('' = '',\)')
577:       RETURN
578:       END
```

Sample Printout 5 - Simulation Run 9

EXPANSION SPACE

Midstroke volume(cm^3) = 64.005
Isothermal temperature(deg C) = 578.000
Cylinder nominal diameter(mm) = 56.700

HEATER

Number of tubes = 34.000
Tube inside diameter(mm) = 2.362
Length(mm) = 183.400

REGENERATOR

Annular gap outer diameter(mm) = 71.800
Annular gap inner diameter(mm) = 60.700
Length(mm) = 64.460
Matrix porosity(%) = 75.900

COOLER

Number of passages = 135.000
Passage width(mm) = .508
Passage depth(mm) = 3.760
Length(mm) = 79.200

COMPRESSION SPACE

Midstroke volume(cm^3) = 158.288
Isothermal temperature(deg C) = 40.000

WORKING FLUID

Charge pressure(bar) = 70.000
Type (1 = Helium, 2 = Hydrogen, 3 = Air) = 1.000

DISPLACER

Guiding rod diameter(mm) = 14.000
Gas spring midstroke volume(cm^3) = 31.790
Linear damping coefficient(kg/s) = 70.000
Mass(kg) = .426
Maximum stroke between stops(mm) = 40.400

PISTON

Bounce space midstroke volume(cm^3) = 20500.000
Linear damping coefficient(kg/s) = 10.000
Mass(kg) = 6.200
Maximum stroke between stops(mm) = 42.000

DYNAMOMETER ARMATURE

Wire length(m) = 35.940
Linear damping coefficient(kg/s) = .500
Mass(kg) = 2.200

DYNAMOMETER STATOR

Magnetic flux density(T) = .719

DISPLACEMENT TRANSDUCER

Resolution (1000 maximum) = 250.000
Graticule aperture(mm) = .020

USER DEFINED LOAD

Mass(kg) = 1.500
Linear damping coefficient(kg/s) = 15.000
Quadratic damping coefficient(kg/m) = 55.000
Coulombic damping coefficient(N m/s) = 20.000
Thermodynamic constant coefficient(1/N) = .050
Thermodynamic displacement coefficient(1/N m) = .001

```
CLOSURE INDICATOR=   .0086313  FREQUENCY(Hz)= 25.962  MAX CURRENT(A)=     .00
CYCLIC WORK= -.3016897E+02 DISSIPATION=  .3540081E-01 SHAFT WORK=  .1222115E+00
MAX FORCE ERROR=  .2111844E+03  MAX % ERROR= 150.0263

CLOSURE INDICATOR=   .0455218  FREQUENCY(Hz)= 27.025  MAX CURRENT(A)=    8.17
CYCLIC WORK= -.1524243E+02 DISSIPATION=  .9271904E+01 SHAFT WORK=  .2231706E+02
MAX FORCE ERROR=  .9052178E+03  MAX % ERROR=*********

CLOSURE INDICATOR=   .0132423  FREQUENCY(Hz)= 31.413  MAX CURRENT(A)=   35.03
CYCLIC WORK=  .9698518E+02 DISSIPATION=  .1396768E+02 SHAFT WORK=  .4283142E+02
MAX FORCE ERROR=  .8166060E+03  MAX % ERROR=*********

CLOSURE INDICATOR=   .0016164  FREQUENCY(Hz)= 30.828  MAX CURRENT(A)=   44.53
CYCLIC WORK=  .1169687E+03 DISSIPATION=  .1483390E+02 SHAFT WORK=  .6592047E+02
MAX FORCE ERROR=  .1762056E+03  MAX % ERROR=2080.7380

CLOSURE INDICATOR=   .0007566  FREQUENCY(Hz)= 30.887  MAX CURRENT(A)=   44.48
CYCLIC WORK=  .1185389E+03 DISSIPATION=  .1463018E+02 SHAFT WORK=  .6452023E+02
MAX FORCE ERROR=  .4982980E+02  MAX % ERROR=1693.2910

CLOSURE INDICATOR=   .0000285  FREQUENCY(Hz)= 30.941  MAX CURRENT(A)=   42.86
CYCLIC WORK=  .1179999E+03 DISSIPATION=  .1453376E+02 SHAFT WORK=  .6370761E+02
MAX FORCE ERROR=  .1360257E+02  MAX % ERROR=1296.3730

CLOSURE INDICATOR=   .0017469  FREQUENCY(Hz)= 30.892  MAX CURRENT(A)=   42.40
CYCLIC WORK=  .1143914E+03 DISSIPATION=  .1457389E+02 SHAFT WORK=  .6387058E+02
MAX FORCE ERROR=  .7572345E+01  MAX % ERROR= 161.8814

CLOSURE INDICATOR=   .0000045  FREQUENCY(Hz)= 30.932  MAX CURRENT(A)=   42.60
CYCLIC WORK=  .1183532E+03 DISSIPATION=  .1456909E+02 SHAFT WORK=  .6382315E+02
MAX FORCE ERROR=  .2019699E+01  MAX % ERROR= 179.4141

CLOSURE INDICATOR=   .0000175  FREQUENCY(Hz)= 30.933  MAX CURRENT(A)=   42.67
CYCLIC WORK=  .1183149E+03 DISSIPATION=  .1456574E+02 SHAFT WORK=  .6382067E+02
MAX FORCE ERROR=  .1138219E+01  MAX % ERROR= 129.3100

CLOSURE INDICATOR=   .0000007  FREQUENCY(Hz)= 30.934  MAX CURRENT(A)=   42.64
CYCLIC WORK=  .1182995E+03 DISSIPATION=  .1456373E+02 SHAFT WORK=  .6380711E+02
MAX FORCE ERROR=  .3040619E+00  MAX % ERROR= 237.0528

CLOSURE INDICATOR=   .0000027  FREQUENCY(Hz)= 30.934  MAX CURRENT(A)=   42.63
CYCLIC WORK=  .1183055E+03 DISSIPATION=  .1456423E+02 SHAFT WORK=  .6380752E+02
MAX FORCE ERROR=  .1665421E+00  MAX % ERROR= 827.8990

CLOSURE INDICATOR=   .0016809  FREQUENCY(Hz)= 30.887  MAX CURRENT(A)=   42.64
CYCLIC WORK=  .1144477E+03 DISSIPATION=  .1458260E+02 SHAFT WORK=  .6394683E+02
MAX FORCE ERROR=  .4647827E-01  MAX % ERROR=  76.4711

CLOSURE INDICATOR=   .0000005  FREQUENCY(Hz)= 30.934  MAX CURRENT(A)=   42.64
CYCLIC WORK=  .1183066E+03 DISSIPATION=  .1456447E+02 SHAFT WORK=  .6380947E+02
MAX FORCE ERROR=  .2541161E-01  MAX % ERROR=  14.7893

CLOSURE INDICATOR=   .0016808  FREQUENCY(Hz)= 30.887  MAX CURRENT(A)=   42.64
CYCLIC WORK=  .1144466E+03 DISSIPATION=  .1458249E+02 SHAFT WORK=  .6394652E+02
MAX FORCE ERROR=  .6805420E-02  MAX % ERROR=  20.0617

CLOSURE INDICATOR=   .0016808  FREQUENCY(Hz)= 30.887  MAX CURRENT(A)=   42.64
CYCLIC WORK=  .1144465E+03 DISSIPATION=  .1458250E+02 SHAFT WORK=  .6394655E+02
```

```
MAX FORCE ERROR=  .3524780E-02  MAX % ERROR=   3.8238

CLOSURE INDICATOR=   .0000000  FREQUENCY(Hz)= 30.934  MAX CURRENT(A)=  42.64
CYCLIC WORK=  .1183066E+03 DISSIPATION=  .1456444E+02 SHAFT WORK=  .6380922E+02
MAX FORCE ERROR=  .1144409E-02  MAX % ERROR=    .2488

CLOSURE INDICATOR=   .0016808  FREQUENCY(Hz)= 30.887  MAX CURRENT(A)=  42.64
CYCLIC WORK=  .1144468E+03 DISSIPATION=  .1458251E+02 SHAFT WORK=  .6394657E+02
MAX FORCE ERROR=  .7324219E-03  MAX % ERROR=    .5613

CLOSURE INDICATOR=   .0000001  FREQUENCY(Hz)= 30.934  MAX CURRENT(A)=  42.64
CYCLIC WORK=  .1183068E+03 DISSIPATION=  .1456445E+02 SHAFT WORK=  .6380923E+02
MAX FORCE ERROR=  .9765625E-03  MAX % ERROR=    .3287

CLOSURE INDICATOR=   .0000000  FREQUENCY(Hz)= 30.934  MAX CURRENT(A)=  42.64
CYCLIC WORK=  .1183065E+03 DISSIPATION=  .1456445E+02 SHAFT WORK=  .6380922E+02
MAX FORCE ERROR=  .6103516E-03  MAX % ERROR=    .2270

CLOSURE INDICATOR=   .0016808  FREQUENCY(Hz)= 30.887  MAX CURRENT(A)=  42.64
CYCLIC WORK=  .1144466E+03 DISSIPATION=  .1458250E+02 SHAFT WORK=  .6394657E+02
MAX FORCE ERROR=  .4882813E-03  MAX % ERROR=    .1124

CLOSURE INDICATOR=   .0000001  FREQUENCY(Hz)= 30.934  MAX CURRENT(A)=  42.64
CYCLIC WORK=  .1183066E+03 DISSIPATION=  .1456445E+02 SHAFT WORK=  .6380923E+02
MAX FORCE ERROR=  .6484985E-03  MAX % ERROR=    .0573

CLOSURE INDICATOR=   .0000001  FREQUENCY(Hz)= 30.934  MAX CURRENT(A)=  42.64
CYCLIC WORK=  .1183067E+03 DISSIPATION=  .1456445E+02 SHAFT WORK=  .6380921E+02
MAX FORCE ERROR=  .3814697E-03  MAX % ERROR=    .4963

CLOSURE INDICATOR=   .0000001  FREQUENCY(Hz)= 30.934  MAX CURRENT(A)=  42.64
CYCLIC WORK=  .1183065E+03 DISSIPATION=  .1456445E+02 SHAFT WORK=  .6380921E+02
MAX FORCE ERROR=  .6771088E-03  MAX % ERROR=    .3918

CLOSURE INDICATOR=   .0016808  FREQUENCY(Hz)= 30.887  MAX CURRENT(A)=  42.64
CYCLIC WORK=  .1144470E+03 DISSIPATION=  .1458250E+02 SHAFT WORK=  .6394657E+02
MAX FORCE ERROR=  .7324219E-03  MAX % ERROR=    .3258

CLOSURE INDICATOR=   .0016808  FREQUENCY(Hz)= 30.887  MAX CURRENT(A)=  42.64
CYCLIC WORK=  .1144467E+03 DISSIPATION=  .1458250E+02 SHAFT WORK=  .6394657E+02
MAX FORCE ERROR=  .6713867E-03  MAX % ERROR=    .3918

CLOSURE INDICATOR=   .0000001  FREQUENCY(Hz)= 30.934  MAX CURRENT(A)=  42.64
CYCLIC WORK=  .1183066E+03 DISSIPATION=  .1456445E+02 SHAFT WORK=  .6380923E+02
MAX FORCE ERROR=  .6484985E-03  MAX % ERROR=    .0573

CLOSURE INDICATOR=   .0000001  FREQUENCY(Hz)= 30.934  MAX CURRENT(A)=  42.64
CYCLIC WORK=  .1183067E+03 DISSIPATION=  .1456445E+02 SHAFT WORK=  .6380921E+02
MAX FORCE ERROR=  .4119873E-03  MAX % ERROR=    .4963
```

APPENDIX C: DIGITAL SIMULATION OF A DOUBLE ACTING INERTIA COMPRESSOR AS A LOAD FOR THE RE-1000 FPSE

The computer simulation program for a double-acting inertia compressor is presented. The compressor is designed to match the power, frequency, and stroke of the RE-1000 FPSE built by Sunpower, Inc.

The simulation is for the compressor only; the compressor housing motion is specified as appropriate for the RE-1000 FPSE.

After each simulation cycle, defined by the extreme positive housing position, tabular output is produced. Table C.1 represents the following output quantities:

- Compressor PV power,
- Gas spring PV power,
- Pressure Fourier coefficients for all spaces, and
- Position Fourier coefficients for housing, displacer, and inertia piston.

Every several cycles, depending on an input specification, graphical output is also produced. The graphical output is comprised of two plots. The first plot, given in Figure C.1, shows pressure versus piston position for the compressor and spring spaces. Actually, P_2-P_1 versus piston and P_3-P_4 versus piston are plotted. These two curves are proportional to the combined force on the housing due to the compressor spaces and the combined force on the housing due to the spring spaces. The second plot, given in Figure C.2, shows gas temperature versus piston position for each individual compressor and spring space. The graphical outputs show a full five cycles of the simulation. A few cycles are required to achieve steady state operation, which is the reason why the plots show a few stray points.

Table C.1: Double-Acting Inertia Compressor Simulation Summary

$$$

DATA FOR CYCLE NUMBER 5 BEGINNING 1.225E-01 AND ENDING 1.513E-01 HAVING DURATION 2.882E-02 SECONDS AND FREQUENCY 34.70

COMPRESSOR PV POWER* -1.490E 03 COMPRESSOR SPRING PV POWER -1.306E 02

FOURIER COSINE SERIES ICP(1) **	FOURIER SINE SERIES ICP(1)	FOURIER COSINE SERIES ICP(2) **	FOURIER SINE SERIES ICP(2)
7.4748E 05		7.4685E 05	
1.0825E 05	7.2120E 05	-9.7575E 04	-7.1828E 05
-3.8393E 05	5.9166E 04	-3.8124E 05	4.5086E 04
-1.2734E 04	-1.5253E 05	4.5552E 03	1.5259E 05
3.1383E 04	-8.5264E 03	3.4347E 04	-6.7246E 03

FOURIER COSINE SERIES ICP(3) **	FOURIER SINE SERIES ICP(3)	FOURIER COSINE SERIES ICP(4) **	FOURIER SINE SERIES ICP(4)
1.1749E 06		1.1742E 06	
1.1136E 05	-4.3469E 05	-1.1036E 05	4.3679E 05
-7.1314E 04	-4.0074E 04	-7.3735E 04	-3.5552E 04
-1.0569E 04	1.9521E 04	8.0453E 03	-2.0889E 04
4.2984E 03	2.9146E 03	5.0669E 03	1.4357E 03

FOURIER COSINE SERIES PISTON ***	FOURIER SINE SERIES PISTON	FOURIER COSINE SERIES DISPLACER ***	FOURIER SINE SERIES DISPLACER
-1.5327E-07		2.2900E-02	
-4.6348E-07	1.9994E-02	1.4286E-02	2.4651E-03
-7.9863E-07	5.7760E-08	1.0608E-07	-5.7560E-07
6.8237E-08	5.7263E-07	9.8167E-07	4.3249E-07

FOURIER COSINE SERIES ICXR ***	FOURIER SINE SERIES ICXR	FOURIER COSINE SERIES FORCE ON ICXR ****	FOURIER SINE SERIES FORCE ON ICXR
1.3400E-04		2.9315E 00	
-4.8323E-03	1.8195E-02	7.5816E 02	-5.8010E 03
-3.3474E-05	8.8986E-05	1.3201E 01	-3.0287E 01
1.2182E-05	-3.9826E-04	-6.7908E 01	5.6496E 02

NOTE:

* Power in Watts

** ICP(I) = Fourier Coefficients for Pressure Waves in Compressor Spaces (I=1,2) and Gas Spring Spaces (I=3,4). (Pascals)

*** Fourier Coefficients for Displacements for FPSE Piston (Compressor Housing), Displacer, and Compressor Piston (Meters)

**** Fourier Coefficients for Force Acting on the Compressor Piston

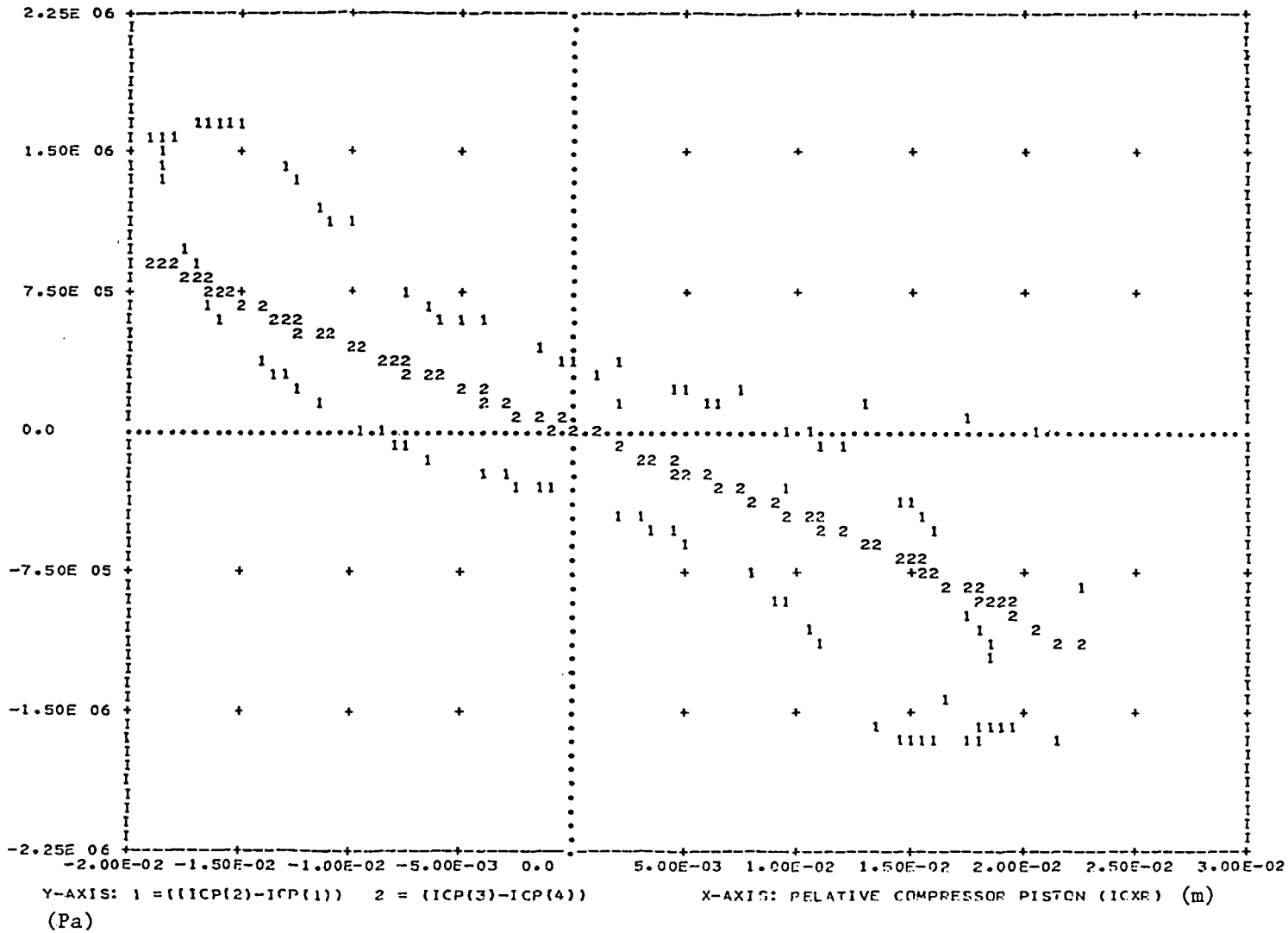

Figure C.1: Pressure versus Piston Position for Compressor Spaces and Gas Springs

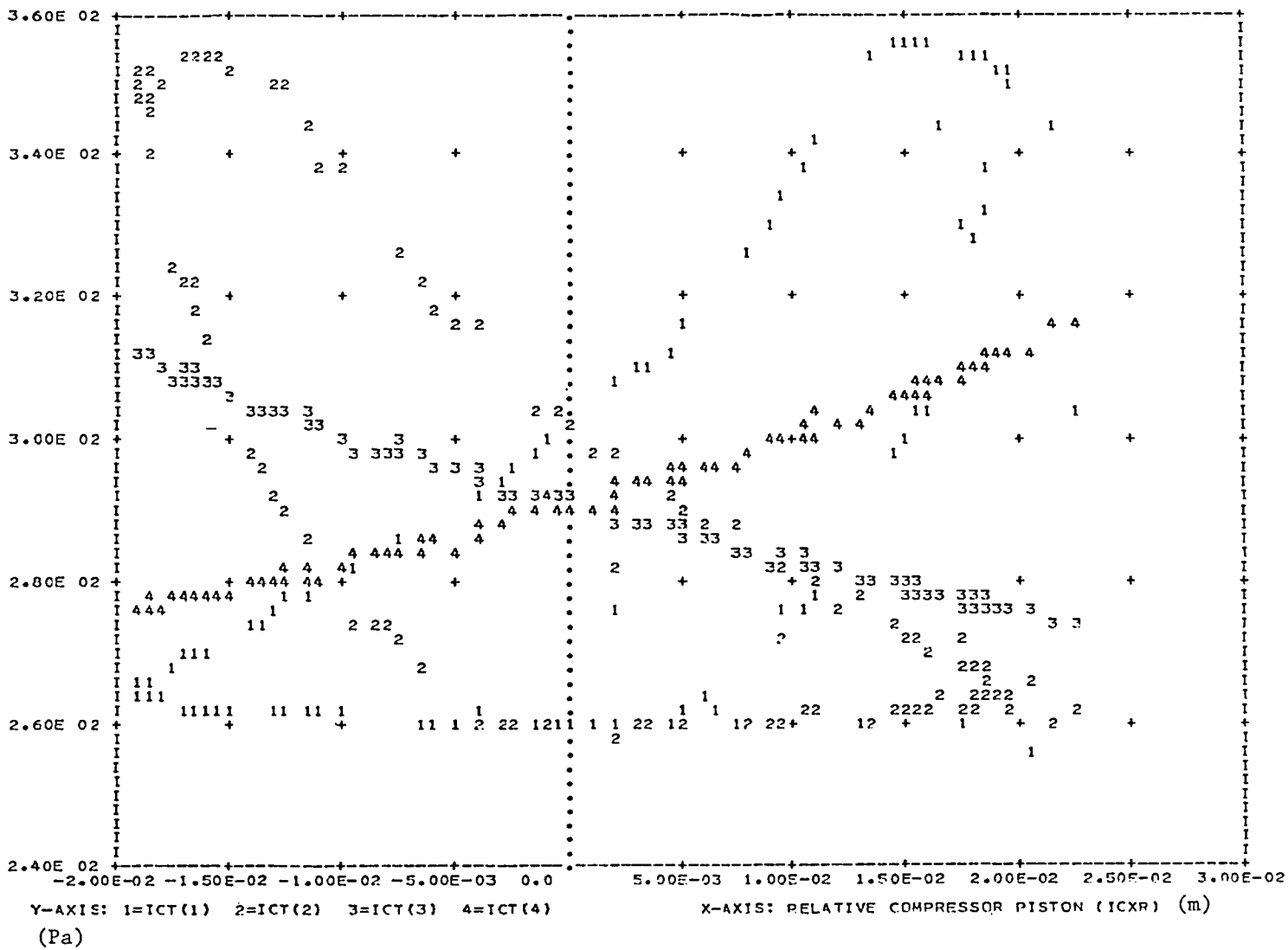

Figure C.2: Gas Temperature versus Piston Position for Compressor Spaces and Gas Springs

The listing of the computer program is given below. It includes the input data and subroutines based on the double-acting inertia compressor model described in subsection 2.4.

```
      SUBROUTINE ICSUBS                                                 ICS00010
C  THIS SUBROUTINE CONTAINS A NUMBER OF ENTRY POINTS SHARING COMMON MEM ICS00020
C  WHICH ARE REQUIRED TO DEFINE THE FREON INERTIAL COMPRESSOR MODE      ICS00030
      REAL ICR,ICCP,ICCV,ICCVR,ICCPR,ICGAM                              ICS00040
      COMMON /IC1/ ICR,ICCP,ICCV,ICCVR,ICCPR,ICGAM                      ICS00050
      REAL ICXR,ICXRD,ICP,ICDEN,ICT                                     ICS00060
      COMMON /IC2/ ICXR,ICXRD,ICP(4),ICDEN(4),ICT(4),ICNSP              ICS00070
      REAL ICVIS,ICCLCM,ICCLSP,ICHCM,ICTWCM,ICAVLV,ICGCML,ICLCML,       ICS00080
     * ICAPIS,ICASPR,ICDSPR,ICGSPL,ICWSPL,ICLSPL,ICPCON,ICPEVP,          ICS00090
     * ICTCON,ICTEVP,ICPISM                                             ICS00100
      COMMON /IC4/ ICVIS,ICCLCM,ICCLSP,ICHCM,ICTWCM,ICAVLV,ICGCML,      ICS00110
     * ICLCML,ICAPIS,ICASPR,ICDSPR,ICGSPL,ICWSPL,ICLSPL,ICPCON,ICPEVP,   ICS00120
     * ICTCON,ICTEVP,ICPISM                                             ICS00130
      COMMON /DEVICE/ NPRT,NPUN,NREAD,NTERM                             ICS00140
C                                                                       ICS00150
C                                                                       ICS00160
      ENTRY ICVALV(PSPACE,TSPACE,FLOW,FTEMP)                            ICS00170
C  CALCULATES FLOW AND FLOW TEMPERATURES (FTEMP) THROUGH MAIN CHECK VALVICS00180
C  IN PUMP CHAMBER AS  FUNCTION OF PRESSURES (PSPACE) AND              ICS00190
C  TEMPERATURE (TSPACE) OF CYLINDER SPACE                               ICS00200
C  (+ IS FLOW OUT OF SPACE)                                             ICS00210
C                                                                       ICS00220
C  INITIAL VALUES                                                       ICS00230
      FLOW = 0.0                                                        ICS00240
      FTEMP = 0.0                                                       ICS00250
C  IF CYLINDER PRESSURE LIES BETWEEN EVAP AND CONDENSOR NO FLOW         ICS00260
      IF((ICPEVP .LE. PSPACE) .AND. (PSPACE .LE. ICPCON)) GOTO 100      ICS00270
C  DEFINE CRITICAL PRESSURE RATIO FOR CHOKED FLOW                       ICS00280
      RCRIT = (2.0/(ICGAM+1.0))**(ICGAM/(ICGAM-1.0))                    ICS00290
      IF(ICPEVP .GT. PSPACE) GOTO 10                                    ICS00300
      IF(PSPACE .GT. ICPCON) GOTO 20                                    ICS00310
C  FLOW INTO SPACE FROM EVAPORATOR                                      ICS00320
10    FTEMP = ICTEVP                                                    ICS00330
      RP = AMAX1(RCRIT,PSPACE/ICPEVP)                                   ICS00340
      FLOW = -GVLV(ICPEVP,ICTEVP,RP,ICAVLV,ICGAM,ICR)                   ICS00350
      GOTO 100                                                          ICS00360
C  FLOW INTO CONDENSOR FROM SPACE                                       ICS00370
20    FTEMP = TSPACE                                                    ICS00380
      RP = AMAX1(RCRIT,ICPCON/PSPACE)                                   ICS00390
      FLOW = GVLV(PSPACE,TSPACE,RP,ICAVLV,ICGAM,ICR)                    ICS00400
100   RETURN                                                            ICS00410
C                                                                       ICS00420
C                                                                       ICS00430
      ENTRY ICLEAK(PSP1,TSP1,PSP2,TSP2,GAP,PERIM,XLEN,VREL,FLOW,FTEMP)ICS00440
C  CALCULATES FLOW (FLOW) AND TEMPERATURE (FTEMP) OF LEAK               ICS00450
C  BETWEEN SPACE 1 AT PRESSURE (PSP1) AND TEMPERATURE (TSP1)            ICS00460
C  AND SPACE 2 AT PRESSURE (PSP2) AND TEMPERATURE (TSP2)                ICS00470
C  LEAK DIMENSIONS: GAP,PERIM,XLEN                                      ICS00480
C  FLOW = FLOWP+FLOWV   WHERE: FLOWP IS DUE TO PRESSURE DROP AND        ICS00490
C  FLOWV IS DUE TO RELATIVE VELOCITY OF PISTON IN CYLINDER              ICS00500
C  VREL IS THE RELATIVE VELOCITY OF PISTON IN CYLINDER                  ICS00510
C  VREL = ICXRD WHEN SPACE 2 IS ON POSITIVE SIDE OF SPACE 1 AND         ICS00520
C  VREL = -ICXRD WHEN SPACE 2 IS ON NEGATIVE SIDE OF SPACE 1            ICS00530
C  + IS FLOW FROM SPACE 1 TO SPACE 2                                    ICS00540
      DENS = 0.5*(PSP2/TSP2+PSP1/TSP1)/ICR                              ICS00550
      FLOWP= DENS*GAP*GAP*GAP*(PSP1-PSP2)/(12.0*ICVIS*XLEN)*PERIM       ICS00560
      FLOWV= DENS*0.5*VREL*GAP*PERIM                                    ICS00570
      FLOW= FLOWP+FLOWV                                                 ICS00580
      IF (FLOW) 150,150,200                                             ICS00590
150   FTEMP= TSP2                                                       ICS00600
      RETURN                                                            ICS00610
200   FTEMP= TSP1                                                       ICS00620
      RETURN                                                            ICS00630
```

```
C
      ENTRY ICVOL(VOL,VOLD)
      DIMENSION VOL(4),VOLD(4)
C  CALCULATES VOLUMES AND DERIVATIVES OF 4 COMPRESSOR SPACES BASED
C  ON CURRENT COORDINATES IN COMMON MEMORY
      VOL(1) = ICAPIS*(ICCLCM-ICXR)
      VOL(2) = ICAPIS*(ICCLCM+ICXR)
      VOL(3) = ICASPR*(ICCLSP+ICXR)
      VOL(4) = ICASPR*(ICCLSP-ICXR)
C  CHECK FOR NEGATIVE VOLUMES
      DO 300 ICJ = 1,4
      IF(VOL(ICJ) .GT. 0.0) GOTO 300
      WRITE(NPRT,350) ICJ
350   FORMAT(' VOLUME IN COMPRESSOR SPACE ',I5,' .LE. ZERO',
     * ' EXECUTION TERMINATING')
      STOP
300   CONTINUE
      VOLD(1) = -ICAPIS*ICXRD
      VOLD(2) =  ICAPIS*ICXRD
      VOLD(3) =  ICASPR*ICXRD
      VOLD(4) = -ICASPR*ICXRD
      RETURN
C
C
      ENTRY ICQCMP(QC)
      DIMENSION QC(4)
C  CALCULATES HEAT FLUX INTO 4 SPACES.  + DENOTES HEAT INTO SPACE.
      QC(1) = ICHCM*(ICTWCM-ICT(1))
      QC(2) = ICHCM*(ICTWCM-ICT(2))
      QC(3) = 0.0
      QC(4) = 0.0
      RETURN
      END

C
C
      FUNCTION GVLV(PU,TU,RP,AV,GAMMA,R)
C  THIS FUNCTION DEFINES THE MASS FLOW RATE THROUGH AN ORIFICE OF
C  AREA AV, UPSTREAM PRESSURE PU, TEMPERATURE TU, PRESSURE RATIO RP.
C  SEE KANGPIL NOTES
      CONST = 2.0*GAMMA/((GAMMA-1.0)*R)
      GVLV= PU*AV*SQRT(CONST/TU*(RP**(2.0/GAMMA)-RP**(1.0+1.0/GAMMA)))
      RETURN
      END
```

```
      SUBROUTINE DIFFUN(N,TIME,Y,YD)
      REAL ICP,ICCP,ICCV,ICCVP,ICCPP,ICGAM,ICXRDD
      COMMON /IC1/ ICR,ICCP,ICCV,ICCVP,ICCPP,ICGAM
      REAL ICXR,ICXRD,ICP,ICDEN,ICT
      COMMON /IC2/ ICXR,ICXRD,ICP(4),ICDEN(4),ICT(4),ICNSP
      REAL ICV,ICVD,ICGFLW,ICGT,ICLFLW,ICLT,ICQ
      COMMON /IC3/ ICV(4),ICVD(4),ICGFLW(4),ICGT(4),ICLFLW(4),
     * ICLT(4),ICQ(4)
      REAL ICVIS,ICCLCM,ICCLSP,ICHCM,ICTWCM,ICAVLV,ICGCML,ICLCML,
     * ICAPIS,ICASPR,ICDSPR,ICGSPL,ICWSPL,ICLSPL,ICPCON,ICPEVP,
     * ICTCON,ICTEVP,ICPISM
      COMMON /IC4/ ICVIS,ICCLCM,ICCLSP,ICHCM,ICTWCM,ICAVLV,ICGCML,
     * ICLCML,ICAPIS,ICASPR,ICDSPR,ICGSPL,ICWSPL,ICLSPL,ICPCON,ICPEVP,
     * ICTCON,ICTEVP,ICPISM
      LOGICAL CONSTR

      COMMON /FIMO/ PNORM,DENORM,TNORM,XNORM,VNORM
      COMMON /MECH/  PISC,DISC,PISDC,DISDC
      COMMON /BFGIMO/ OMEGA,CONSTR
      COMMON /BDFGIO/ PCHG,AP,AD,CD,RHO,AP2,RP2,AP3,RP3,AD2,RD2,AD3,RD3
      COMMON /EFIOG/ CP,CV
      COMMON /DEVICE/ NPRT,NPUN,NREAD,NTERM
      DIMENSION Y(N),YD(N)
C************ADDITIONS FOR COMPRESSOR
C  TRANSLATE Y INTO COMPRESSOR VARIABLES
C
      DO 1100 ICJ=1,ICNSP
      ICP(ICJ) = Y(ICJ)*PNORM
1100  ICDEN(ICJ) = Y(ICJ+ICNSP)*DENORM
      ICXR = Y(2*ICNSP+1)*XNORM
      ICXRD = Y(2*ICNSP+2)*VNORM
C************ADDITIONS FOR COMPRESSOR
C  CALCULATE DERIVATIVES HERE
C
C  CALCULATE DERIVATIVES OF DYNAMIC VARIBLES
C  CALL CONDM TO SET PISDDC AND CYLDDC WHICH ARE NEEDED FOR
C  CALCULATION OF ICXRDD
      CALL CONDM(OMEGA,TIME)
      CALL ICDYN(ICXRDD)
      YD(2*ICNSP+1) = ICXRD/XNORM
      YD(2*ICNSP+2) = ICXRDD/VNORM
C  COMPUTE GAS TEMPERATURES
      DO 1110 ICJ=1,ICNSP
1110  ICT(ICJ) = ICP(ICJ)/(ICR*ICDEN(ICJ))
C  COMPUTE GAS FLOWS
      CALL ICVALV(ICP(1),ICT(1),ICGFLW(1),ICGT(1))
      CALL ICVALV(ICP(2),ICT(2),ICGFLW(2),ICGT(2))
      ICGFLW(3) = 0.0
      ICGFLW(4) = 0.0
      ICGT(3) = 0.0
      ICGT(4) = 0.0
C  COMPUTE LEAKAGE FLOWS:  ICLFLW(1)  GIVES FLOW 1=>3
C  ICLFLW(2) GIVES FLOW 2=>4      ICLFLW(3) GIVES FLOW 3=>4
C  ICLFLW(4) NOT USED
      CALL ICLEAK(ICP(1),ICT(1),ICP(3),ICT(3),ICGCML,SQRT(1.27*ICAPIS),
     * ICLCML,ICXRD,ICLFLW(1),ICLT(1))
      CALL ICLEAK(ICP(2),ICT(2),ICP(4),ICT(4),ICGCML,SQRT(1.27*ICAPIS),
     * ICLCML,-ICXRD,ICLFLW(2),ICLT(2))
      CALL ICLEAK(ICP(3),ICT(3),ICP(4),ICT(4),ICGSPL,ICWSPL,ICLSPL,
     * ICXRD,ICLFLW(3),ICLT(3))
C  COMPUTE VOLUMES
      CALL ICVOL(ICV,ICVD)
C  COMPUTE DERIVATIVES OF COMPRESSOR GAS DENSITY
      DO 1120 ICJ = 1,ICNSP
      IF(ICJ .EQ. 1) DMLK = ICLFLW(1)
      IF(ICJ .EQ. 2) DMLK = ICLFLW(2)
      IF(ICJ .EQ. 3) DMLK = ICLFLW(3)-ICLFLW(1)
      IF(ICJ .EQ. 4) DMLK = -ICLFLW(3)-ICLFLW(2)
1120  YD(ICJ+ICNSP) = (-ICGFLW(ICJ)-DMLK-ICDEN(ICJ)*ICVD(ICJ))
     * /(DENORM*ICV(ICJ))
      CALL ICQCMP(ICQ)

C  COMPUTE DERIVATIVES OF COMPRESSOR PRESSURES
      DO 1140 ICJ=1,ICNSP
      IF(ICJ .EQ. 1) ENTHLK =ICCP*ICLFLW(1)*ICLT(1)
      IF(ICJ .EQ. 2) ENTHLK =ICCP*ICLFLW(2)*ICLT(2)
      IF(ICJ .EQ. 3) ENTHLK =ICCP*(-ICLFLW(1)*ICLT(1)+ICLFLW(3)*ICLT(3))
      IF(ICJ .EQ. 4) ENTHLK =ICCP*(-ICLFLW(2)*ICLT(2)-ICLFLW(3)*ICLT(3))
1140  YD(ICJ) = (ICQ(ICJ)-ICCP*ICGFLW(ICJ)*ICGT(ICJ)-ENTHLK
     * -ICCPP*ICP(ICJ)*ICVD(ICJ))/(PNORM*ICCVP*ICV(ICJ))
C
      RETURN
      END
```

APPENDIX D: DESIGN CALCULATIONS

Calculations performed for the flexible connection design will be briefly described.

The geometry of the flexible connection is shown in Figures 2.10 and 2.21. The design summary including dimensional specifications is given in Table 2.4.

The following five items are of interest:

- maximum fiber stress in the thin metal strip due to bending
- buckling stress of thin flat strip
- fluid dynamic load
- dynamic stress
- temperature rise in the flexible connection.

Maximum Fiber Stress Due to Bending

The maximum fiber stress, $_f$, due to bending occurs at the outer surfaces of the bent metal strip and is calculated from [9]:

$$\sigma_f = Mt/2I \qquad \text{(D-1)}$$

where

M = Bending Moment = EI/R
E = Young's modulus for Beryllium Copper = 1.31 x 10 MPa
I = Moment of Inertia = $tb^3/12$ of the cross section
R = Radius of Curvature = 2.54 cm
t = thickness of the metal strip = 0.1 mm
b = width of the metal strip = 2.54 mm

Substituting values for M, t, and I in Equation (D-1), the maximum fiber stress, σ_f, is 258 MPa.

Buckling Stress of the Flat Strip

For a thin strip under equal uniform compression on two opposite edges, the lowest buckling stress occurs when the two opposite edges are simply supported. To be conservative, we will regard the above buckling stress as the upper limit to avoid buckling of the thin strip.

The buckling stress, σ_b, for a strip with length to width ratio of more than three is estimated from the following equation [9]:

$$\sigma_b = 3.29\ E\ (t/B)^2/(1-\nu^2) \qquad \text{(D-2)}$$

where

ν = Poisson's ratio for the metal strip = 0.27

Substituting appropriate values for E, t, b, and ν in Equation (D-2), the buckling stress, σ_b, is calculated to be 738 MPa.

Fluid Dynamic Load on the Circular Section

Uniform radial pressure, P_{buck}, that will cause the buckling of a curved flat strip with radial curvature R, and central angle 2a, and simply supported ends, is estimated from the following formula [9]:

$$P_{buck} = E\ t^3\ (\pi^2/a^2 - 1)/[12R^3\ (1 - \nu^2)], \qquad \text{(D-3)}$$

where a is $\pi/2$ in the present case.

From Equation (D-3), the buckling pressure for the circular section of the strip, P_{buck}, is 2260 Pa.

Let us estimate the maximum fluid dynamic pressure, P_{fluid}, acting on the circular section of the strip due to the reciprocating motion relative to surrounding gas. P_{fluid} is calculated from the equation below:

$$P_{fluid} = V^2 \rho /2. \qquad \text{(D-4)}$$

where

$V = \omega$ x stroke/2 = 2 x 60 x 0.025 = 9.58 m/sec,

ρ = 11.37 kg/m for helium at 13.8 MPa, 38 C.

From Equation (D-4), the maximum fluid dynamic pressure, P_{fluid}, is 524 Pa.

Since the maximum fluid dynamic pressure, P_{fluid}, only amounts to approximately one-fourth of the buckling pressure, P_{buck}, the possibility of buckling in the circular section due to fluid dynamic pressure is eliminated.

The stress caused by the fluid dynamic pressure, σ_{fluid}, will be estimated using the formula for completely circular cylinder with uniform radial pressure [9]:

$$\sigma_{fluid} = P_{fluid}\ R/t = 0.1 \text{ MPa} \qquad \text{(D-5)}$$

Dynamic Stress

The maximum stress due to the strip mass acceleration in longitudinal direction, σ_{long}, is calculated from the following formula [9]:

$$\sigma_{long} = Wa/A = 2.9 \text{ (MPa)}, \qquad \text{(D-6)}$$

where

W = Mass involved in longitudinal motion (10 cm strip)
= 2.088×10^{-4} kg

a = maximum longitudinal acceleration
= $(2\pi \times 60) \times 0.025 = 3553$ m/sec

A = Strip cross sectional area
= 0.1 mm x 2.54 mm = 2.54×10^{-7} m^2

The maximum dynamic stress due to strip mass acceleration in circumferential direction, σ_{circ}, is calculated from the following formula [9]:

$$\sigma_{circ} = \delta R^2 \omega^2 = 0.8 \text{ MPa} \tag{D-7}$$

where

δ = mass density of the strip material
= 8220 kg/m

Then, the maximum total dynamic stress, σ_{dyn}, is given by

$$\sigma_{dyn} = \sigma_{long} + \sigma_{circ} = 3.7 \text{ MPa} \tag{D-8}$$

As shown in Table 2.4, Beryllium Copper has the yield point stress of 965 MPa and endurance limit of 276 MPa. Also from Equation (D-2), the buckling stress of the flat section is calculated to be 738 MPa.

The maximum possible stress that can exist in the metal strip will be less than the sum of the maximum bending stress σ_f, total dynamic stress σ_{dyn}, and the maximum fluid dynamic stress, σ_{fluid}:

$$\sigma_{max} = \sigma_f + \sigma_{dyn} + \sigma_{fluid} = 258 + 3.7 + 0.1 \tag{D-9}$$

$$= 262 \text{ MPa}$$

The maximum stress that can possibly occur in the strip, σ_{max}, is 262 MPa, below the endurance limit of 276 MPa. σ_{max} is also well below the buckling stress of 738 MPa and the yield point of 965 MPa.

Flexible Connection Temperature Rise

First, the amount of heat dissipated in a single strip will be calculated. The resistance, R_s, of a single BeCu strip of 0.01 cm thickness, 0.254 cm width, and 15.6 cm length is given below:

$$R_s = \text{resistivity} \times \text{length/cross sectional area} \tag{D-10}$$

$$= 6.692 \times 10^{-6} (\Omega\text{-cm}) \times 15.6(\text{cm})/(0.01 \times 0.254)(\text{cm}^2)$$

$$= 4.11 \times 10^{-2} \text{ Ohms}$$

The average current based on a sinusoidal variation and the peak current of 133 A (Table 2.3) is 85 A. There are ten BeCu strips each carrying 8.5 A of average current. The average Joule heating loss in a BeCu strip, Q_s, is given below:

$$Q_s = i\ R_s = 8.5 \times 4.11 \times 10^{-2} = 3.0\ W. \qquad \text{(D-11)}$$

The heat transfer film coefficient, h, is calculated utilizing the formula for flow over submerged bodies [10]:

$$h = 0.26\ k\ Re^{0.8}\ Pr^{0.3}/D = 5.6E\text{-}03\ W/cm^2\text{-}C \qquad \text{(D-12)}$$

where

k = helium thermal conductivity at 13.8 MPa (2000 psi) and 38 C (100 F), 5×10^{-5} W/cm -C,

Re = Reynolds number, $V\rho D/\mu = 2.01 \times 10^5$

Pr = Prandtl number, 0.7

D = 3.18 cm

V = mean piston velocity at 60 Hz, 2.54 cm stroke amplitude, 610 cm/sec

ρ = helium density at 13.8 MPa and 38 C

μ = helium viscosity at 13.8 MPa and 38 C

There is a 0.0075 cm thick polyamid ribbon attached to one side of the metal strip. Therefore, there are two parallel heat transfer paths: metal strip to gas and metal-polyamid-gas. Since the metal strip is very thin, we will assume that the metal strip has a uniform temperature. The total thermal conductance, UA, between the metal strip and the surrounding gas is calculated below:

$$UA = hA + 1/(t/kA + 1/hA), \qquad \text{(D-13)}$$

$$= 4.43 \times 10^{-2}\ W/C$$

h = heat transfer film coefficient, 5.6×10^{-3} W/cm^2-C,

A = heat transfer surface area = 4.0 cm^2,

t = thickness of the polyamid ribbon = 0.0075 cm, and

k = thermal conductivity of the polyamid ribbon, 1.731×10^{-3} W/cm-C

The strip temperature rise, ΔT, above the surrounding gas temperature is calculated below:

$$\Delta T = Q_s/UA = 3.0/4.43 \times 10^{-2} = 68\ C \qquad \text{(D-14)}$$

INTERNAL DISTRIBUTION

1. R. S. Carlsmith
2-12. F. C. Chen
13. F. A. Creswick
14. J. L. Crowley
15. N. Domingo
16. P. D. Fairchild
17. S. K. Fischer
18. W. Fulkerson
19. S. M. Gillis, Consultant
20. F. P. Griffin
21. F. R. Kalhammer, Consultant
22. M. A. Kuliasha
23. T. R. LaPorte, Consultant
24. M. Lessen, Consultant
25. J. W. Michel
26. R. E. Minturn
27. R. W. Murphy
28. G. T. Privon
29. A. C. Schaffhauser
30. R. A. Stevens
31. C. D. West
32. W. H. Williams, Consultant
33-34. Central Research Library
35. Document Reference Section
36. Laboratory Records - RC
37-38. Laboratory Records
39. ORNL Patent Section

EXTERNAL DISTRIBUTION

40. William Beale, Sunpower, Inc., 6 Byard Road, Athens, OH 45701
41. Glendon M. Benson, Energy Research and Generation, Inc., Lowell & 57th Street, Oakland, CA 94608
42. Don Beremand, NASA-Lewis Research Center, Mail Stop 500-215, 21000 Brookpark Rd. Cleveland, OH 44135
43. James M. Calm, Project Manager, Heat Pump Development, Electric Power Res. Inst., 3412 Hillview Avenue, Palo Alto, CA 94303
44. Stig C. Carlqvist, Societe ECA, 17, avenue du Chateau, 92190 Meudon-Bellevue, France
45. W. S. Chiu, Systems Engineering, General Electric Company, P.O. Box 527, King of Prussia, PA 19406
46. M. Clinch, Gas Research Institute, 8600 W. Bryn Mawr Avenue, Chicago, IL 60631
47. J. G. Daley, Argonne National Laboratory, 9700 South Cass Avenue, Argonne, IL 60439
48. R. L. Demler, Foster-Miller Assoc., Inc., 350 2nd Ave., Waltham, MA 02154
49. G. Dochat, Mechanical Technology, Inc., 968 Albany-Shaker Rd., Latham, NY 12110
50. J. E. Dudenhoefer, NASA Lewis Research Center, Cleveland, OH 44101
51. T. Finkelstein, TCA, P.O. Box 643, Beverly Hills, CA 90213
52. R. J. Fiskum, Energy Conversion Equipment Branch, CE-112, GF-217/FORS, Department of Energy, 1000 Independence Avenue S.W., Washington, DC 20585
53. A. A. Frank, Dept. of Electrical and Computer Eng'g., University of Wisconsin-Madison, 1500 Johnson Drive, Madison, WI 53706

54. M. Fukiwake, Agency of Industrial Science and Technology, Ministry of International Trade and Industry, 1-3-1 Kasumigaseki, Chiyoda-Ku, Tokyo, Japan
55. D. R. Gedeon, Sunpower, Inc., 6 Byard St., Athens OH 45701
56. L. Goldberg, University of Minnesota, The Underground Space Center, 11 Mines and Metallurgy, 221 Church Street, SE, Minneapolis, MN 55455
57. T. J. Heames, Argonne National Laboratory, 9700 South Cass Avenue, Argonne, IL 60439
58. F. W. Hoehn, Rockwell International Corp., 6633 Canoga Avenue, Canoga Park, CA 91304
59. J. Hogan, General Electric Co., P.O. Box 8666, Philadelphia, PA 19101
60. Bob Holtz, Argonne National Laboratory, 9700 South Cass Avenue, Argonne, IL 60439
61. B. C. Hwang, Code 2722, David Taylor Naval Ship R&D Center, Annapolis Lab., Annapolis, MD 21402
62. Y. Ishizaki, Cryogenic Systems, 253-5 Yamanouchi, Kamakura 247, Japan
63. Naotsugu Isshiki, 2-29-6 Kyodo Setagayaku, Tokyo 156, Japan
64. H. S. Izawa, Northern Natural Gas Company, 2223 Dodge Street, Omaha, NE 68102
65. T. Kapus, Building Equipment Division, Department of Energy, CE-113, 1000 Independence Avenue, S.W., Washington, DC 20585
66. Prof. Nobuhide Kasagi, University of Tokyo, Dept. of Mechanical Engineering, Bunkyo-Ku, Tokyo 113, Japan
67. V. H. Larson, Cleveland State University, 1983 East 24th St., Cleveland, OH 44115
68. K. P. Lee, Aspen Systems Inc., 275 Boston Post Road, Marlborough, MA 01752
69. A. Maret, Gas Research Institute, 8600 W. Bryn Mawr Avenue, Chicago, IL 60631
70. W. Martini, Martini Engineering, 2303 Harris, Richland, WA 99352
71. G. McLennan, Argonne National Laboratory, 9700 South Cass Avenue, Argonne, IL 60439
72. R. C. Meijer, Advanced Energy Programs Dept., General Electric Company, P.O. Box 527, King of Prussia, PA 19406
73. N. P. Nightingale, Stirling Engine Systems Division, Mechanical Technology, Inc., 968 Albany-Shaker Rd., Latham, NY 12110
74. Herbert Nilsson, United Stirling AB, Box 856, S-201 80 Malmo, Sweden
75. W. Perceval, United Stirling, Inc., 211 Strand, Alexandria, VA 22314
76. W. Raldow, Dept. of New Energy Systems, Swedish Council of Building Research, Samkt Goransgatan 66, S-11233 Stockholm Sweden
77. B. Qvale, Laboratory for Energetics, The Technical Univ. of Denmark, DTH Bldg. 403, DK 2800 Lyngby, Denmark
78. C. J. Rallis, University of Witwatersrand, School of Mechanical Engineering, 1 Jan Smuts Avenue, Johannesburg 2001, South Africa
79. G. Rice, Department of Engineering, The University of Reading, Reading, Berkshire, England

80. A. Ross, Ross Enterprises, 37 West Broad Street, Suite 360, Columbus, OH 43215
81. J. D. Ryan, Energy Conversion Equipment Branch, CE-112, GF-217/FORS, Department of Energy, 1000 Independence Avenue S.W., Washington, DC 20585
82. A. Schock, Fairchild Industries, Germantown, MD 20874
83. D. J. R. Senft, Department of Mathematics/Computer Science, University of Wisconsin, River Falls, WI 54022
84. R. Shoureshi, Dept. of Mechanical Engineering, College of Engineering, Wayne State University, Detroit, MI 48202
85. J. L. Smith, Jr., Mechanical Engineering Department, Massachusetts Institute of Technology, Cambridge, MA 02139
86. J. G. Slaby, National Aeronautics and Space Administration, Lewis Research Center, Cleveland, OH 44135
87. P. F. Swenson, The East Ohio Gas Co., E. 9th Ave. at Superior, P.O. Box 5759, Cleveland, OH 44101
88. D. R. Taylor, Royal Naval Engineering College, Manadon Plymouth, Devon PL5 3AQ, England
89. W. P. Teagan, Arthur D. Little, Inc., Cambridge, MA 02140
90. R. C. Tew, NASA-Lewis Research Center, 21000 Brookpark Rd., Cleveland, OH 44135
91. L. G. Thieme, NASA-Lewis Research Center, 21000 Brookpark Rd., Cleveland, OH 44135
92. I. Urieli, Sunpower, Inc., 6 Byard St., Athens, OH 45701
93. Valerie J. Van Griethuysen, Energy Conversion Branch, Aerospace Power Division - Aero Propulsion Laboratory, Dept. of the Air Force, Wright-Patterson AFB, OH 45433
94. D. A. Vaughn, Belvoir R&D Center, Ft. Belvoir, VA 22060 ATTN: STRBE-EMP
95. G. Walker, University of Calgary, Dept. of Mechanical Engineering, 2920 24th Ave., NW, Calgary, Canada T2N1N4
96. B. P. Wang, Mechanical Engineering Department, University of Texas at Arlington, P.O. Box 19023, Arlington, TX 76019
97. M. A. White, University of Washington, Joint Center for Graduate Study, 100 Sprout Road, Richland, WA 99352
98. L. Williams, Logan Lewis Library, Research Division, Carrier Corporation, Carrier Parkway, Syracuse, NY 13221
99. L. Wright, Gas Research Institute, 8600 Bryn Mawr Avenue, Chicago, IL 60631
100. H. Yeh, School of Engineering, University of Pennsylvania, Philadelphia, PA 19104
101. Institute for Energy Analysis, ORAU-Library
102. Office of the Assistant Manager for Energy R&D, U.S. Department of Energy, Oak Ridge Operations, Oak Ridge, TN 37831
103. Energy Conservation Distribution, Oak Ridge National Laboratory, Building 9102-2, Rm. 112, Oak Ridge, TN 37831

104-354. Distribution for Category UC-95d.